Title
Spontaneous fission of the heaviest elements

Author
Lane, Michael

Publication Date
1999-05-01

LBNL-43433

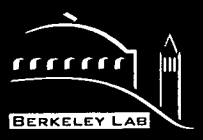

ERNEST ORLANDO LAWRENCE
BERKELEY NATIONAL LABORATORY

Spontaneous Fission of the Heaviest Elements

Michael R. Lane

Nuclear Science Division

May 1999

Ph.D. Thesis

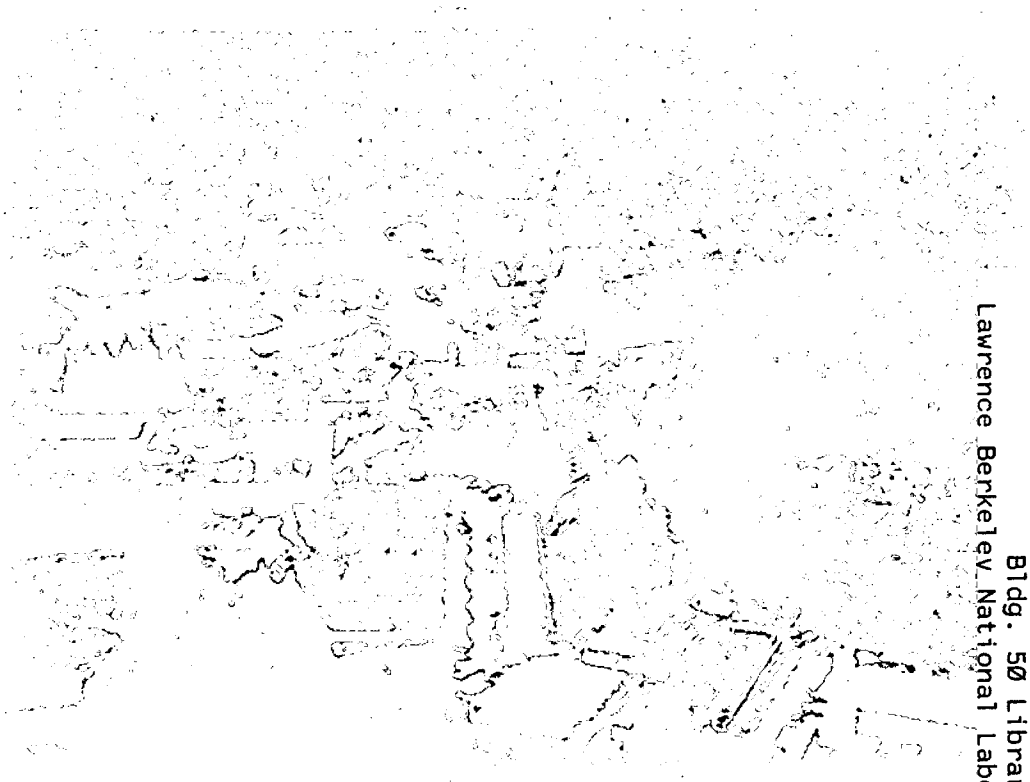

DISCLAIMER

LBNL-43433

Spontaneous Fission of the Heaviest Elements

Michael Ray Lane
Ph.D. Thesis

Department of Chemistry
University of California, Berkeley

and

Nuclear Science Division
Ernest Orlando Lawrence Berkeley National Laboratory
University of California
Berkeley, CA 94720

May 1999

This work was supported by the Director, Office of Science, Office of High Energy and Nuclear Physics, Division of High Energy Physics, of the U.S. Department of Energy under Contract No. DE-AC03-76SF00098.

Spontaneous Fission of the Heaviest Elements

by

Michael Ray Lane

A dissertation submitted in partial satisfaction of the

requirements for the degree of

Doctor of Philosophy

in

Chemistry

in the

GRADUATE DIVISION

of the

UNIVERSITY of CALIFORNIA at BERKELEY

Committee in charge:

Professor Darleane C. Hoffman, Chair
Professor Samuel S. Markowitz
Professor Stanley G. Prussin

Spring 1999

Spontaneous Fission of the Heaviest Elements

by

Michael Ray Lane

Portions of this dissertation have been previously published by the author:

M.R. Lane, K.E. Gregorich, D.M. Lee, B. Wierczinski, C.A. McGrath, M.B. Hendricks, D.A. Shaughnessy, D.A. Strellis, E.R. Sylwester, P.A. Wilk, D.C. Hoffman, "Production Cross Section of ^{261}Ha", Phys. Rev. C **58**, 3413 (1998).

M.R. Lane, K.E. Gregorich, D.M. Lee, M.F. Mohar, M. Hsu, C.D. Kacher, B. Kadkhodayan, M.P. Neu, N.J. Stoyer, E.R. Sylwester, J.C. Yang, D.C. Hoffman, "Spontaneous Fission Properties of ^{262}Rf", Phys. Rev. C **53**, 2893 (1996).

K.E. Gregorich, M.R. Lane, M.F. Mohar, D.M. Lee, C.D. Kacher, E.R. Sylwester, D.C. Hoffman, "First Confirmation of the Discovery of Element 106", Phys. Rev. Lett. **72**, 1423 (1994).

D.C. Hoffman and M.R. Lane, "Spontaneous Fission", Radiochimica Acta **70/71**, 135 (1995).

D.C. Hoffman, T.M. Hamilton, M.R. Lane, "Spontaneous Fission", Chapter 10 of *Nuclear Decay Modes*, Institute of Physics Publishing, Bristol, England (1996).

Abstract

Spontaneous Fission of the Heaviest Elements

by

Michael Ray Lane

Doctor of Philosophy in Chemistry

University of California, Berkeley

Professor Darleane C. Hoffman, Chair

Spontaneous fission (SF) is an interesting field in that it tells us so much about the structure of a nucleus. Small changes and effects brought about by both deformed and spherical shell structure are observable. Because of the stabilizing effect of shell structure, the SF-decay and alpha-decay half-lives of nuclides in the heavy element region are not decreasing as rapidly as previously anticipated. With new experimental techniques, more information can be obtained from a greater number of nuclei through the study of SF. This will enable us to understand the SF process in greater detail, which in turn will increase our understanding of the chemistry and physics of the heavy element region, and thus of chemistry itself. Such knowledge will also help in development of theoretical and empirical predictions.

Following an overview and description of the SF process, investigations of the properties of some transactinide elements are described, with an emphasis on the SF

process. Experiments on two isotopes of rutherfordium (Z=104) are performed in order to study their SF properties. The production cross section of hahnium (Z=105) is studied and measured in preparation for later experiments involving the chemistry of hahnium. The production and positive identification of element 106 is accomplished in order to confirm its discovery. This experiment allowed the original discoverers to propose a name, seaborgium, in honor of Glenn T. Seaborg.

All these experiments are performed in an attempt to increase our knowledge of nuclear structure, forces, and decay, including the stability, of the heaviest elements through the investigation of the behavior of isotopes in this region, and measurements of production reactions.

Dedication

As with everything I do in life, this is for TMH.

Acknowledgments

First and foremost, I would like to thank Darleane Hoffman, who gave me the opportunity to work in her research group starting way back in the day, during my last year of undergraduate school, and who supplied me with the encouragement to pursue this degree. I'd especially like to thank her for her saintly patience and understanding. I'd also like to thank Ken Gregorich (the brains behind the experiments) and Diana Lee, without whom none of this would be possible.

And, of course, I'd like to thank all those graduate students and post-docs with whom I've had the opportunity to work over the years: Jeb Adams, Ken Czerwinski, Todd Hamilton, Melissa Hendricks, Chris Kacher, Bobby Kadkhodayan, Steve Kreek, Carola Laue, Chris McGrath, Mike Mohar, Mary Neu, Joshua Patin, Dawn Shaughnessy, Nancy Stoyer, Dan Strellis, Eric Sylwester, Andy Türler, Birgit Wierczinski, and Philip Wilk. Although their assistance—both the intellectual *and* the cheap-monkey-labor variety—has been appreciated, I'd like to thank them more for the friendship and the fun we've had. Thanks for keeping me relatively sane.

Now, who's up for all-you-can-eat buffet in Tahoe?

Contents

List of Figures

List of Tables

1 Introduction

1.1 Early History

The investigation of modes of radioactive decay is a relatively recent science, its discovery [Bec96] occurring only a little over 100 years ago. Few sciences have had as many advancements over the past century. Experiments and theory involving the study of radioactivity and nuclear science have done as much as any field in developing and advancing physics, chemistry, astronomy, and geology, among other sciences.

Earlier scientists up to the end of the 19^{th} Century were atomists, concerned with the discovery, classification, organization, identification, separation, and behavior of the atoms: bulk studies of the properties of atoms. They were not as concerned with what it was that caused this behavior: i.e., what constituted an atom; what it was made of; what forces held it together; why it was considered to be the smallest indivisible particle in a Democritian way; what energy it possessed; if it was immutable. It wasn't until a few key discoveries at the end of the 19^{th} century and in the early 20^{th} century that atomic and nuclear physics became full-fledged sciences themselves. Atomic physics was the natural progression: the study of fundamental properties of these newly classified elements. Such experiments led directly to the discovery of radioactivity. Later, when the atomic nucleus was postulated, it sparked a new area of interest: the study of the nucleus and its fundamental properties, called "nuclear physics". Of course, when it was later

discovered that the nucleus, in turn, is composed of even more elementary particles, a new field was created called "elementary particle" or "high energy physics".

The first great discovery was that of Henri Becquerel in 1896 [Bec96]. Following in the family tradition, he had been studying the fluorescence produced from exposure of potassium uranyl sulfate, $K_2UO_2(SO_4)_2 \cdot 2H_2O$, to X-rays and ultraviolet light. After exposure to sunlight, these crystals emitted a radiation that blackened a photographic plate, even after penetrating paper. More astonishingly, he discovered that not only was the effect independent of how strong the light was, but it even worked in the dark. Furthermore, the same effect was seen in various other compounds of uranium, always with an intensity proportional to the uranium content. Pierre and Marie Sklodowska Curie continued the work, and in 1898 summarized the results and concluded that the radiation must be a property of uranium itself, unrelated to the physical form of the compound. They were the first to introduce the term "radioactivity" for the phenomenon [Cur98]. The Curies shared the 1903 Nobel Prize in Physics with Becquerel. It was later found that compounds of thorium also emitted radiation similar to that of uranium. Performing the first radiochemical separations, they discovered polonium and radium. They used the chemically separated fraction from nearly two tons of pitchblende (an ore containing ~75% U_3O_8) to isolate 0.1 g of radium chloride.

It was subsequently discovered that the intensity of the emitted radiation of radioactive substances decreased in time and that such processes result in changes in chemical properties. It was also found that when uranium X (^{234}Th) and thorium X (^{224}Ra) were separated from uranium and thorium, respectively, the newly separated X substances decayed while a new supply of the X substance grew into the parent substance

in a similar time. Also, when separated, UX and ThX emitted only beta (β^-) rays while U and Th emitted only alpha (α) rays. Based on their work, Ernest Rutherford and F. Soddy concluded that "the radioactive elements were undergoing spontaneous transformation from one chemical element into another, and that the radiation accompanied this transformation."

After J. J. Thomson's discovery of the electron in 1897 and the scattering experiments that followed, it was speculated that because the mass of electrons was so small compared to the mass of a hydrogen atom, that most of the atomic mass must be attributed to a positively charged part. This was corroborated when Rutherford performed his α-particle scattering experiments in 1911 [Rut11]. When a beam of α-particles was projected onto a thin foil, he observed large scattering angles, inconsistent with the current theory of atomic structure, Thomson's "plum pudding" model. Based on this and the experimental work of Geiger and Marsden, he concluded that the atom must be made up of a very small nucleus, which contains the positive charge and most of the mass, and of the negatively-charged electrons, which balance the charge and occupy the entirety of the atomic dimensions. This "nuclear" model of the atom paved the way for the Bohr model in 1913 and the quantum mechanics of Schrödinger and of Heisenberg in 1926.

For a long period of time, it was assumed that the nucleus of mass A and atomic number Z was made up of A protons and A-Z electrons. The A protons would account for the mass and the A-Z electrons within the nucleus would make the overall charge equal to Z. However, this created many theoretical and experimental problems that went unexplained for years. It wasn't until Chadwick's discovery of the neutron in 1932

[Cha32] that the physical picture of the atom changed from the proton-electron nucleus to the proton-neutron nucleus (Rutherford had suggested the neutron in 1920). According to this, the nucleus was made up of Z protons and A-Z neutrons, with only Z electrons balancing the charge orbiting outside the nucleus. Just as it was a common experimental practice to bombard substances with α-particles (which also led to the discovery of artificial radioactivity by Irene Joliot-Curie and Frederick Joliot in 1934), Chadwick's discovery of the neutron prompted experimentalists to begin bombarding substances with neutrons. Enrico Fermi observed that when elements were bombarded by neutrons, many of the new nuclei that are formed decay by β^- emission [Fer34]. It was postulated that this occurred because the nuclei wants to make up for the added neutron by converting one of its existing neutrons into a proton through β^- decay. This technique of increasing the atomic number of an element through neutron bombardment was used to attempt to create the first transuranic elements. In attempting to make these new elements by irradiating uranium with neutrons, Fermi, Segre and co-workers in 1934 [Fer34b] produced β^--activities that they thought were associated with a new element, element 93, or eka-rhenium. They performed a chemical separation with a precipitate of rhenium sulfide, found a 13-min activity, and suggested it was element 93. Soon after, Ida Noddack (a discoverer of rhenium) [Nod34] expressed her doubt about the assignment because of the non-specific chemistry performed and suggested that the bombarded nuclei might have been disintegrated into several larger fragments. Later, careful chemical studies by Hahn and Strassmann in 1938 [Hah39] showed that the activity was associated with barium. Additionally, more medium-mass nuclei were found. The

energy released following bombardment was over 100 MeV, more than could be explained by α-decay. This led Meitner (a former member of the team) and Frisch [Mei39] to theorize that the product nucleus is unstable after neutron capture and therefore splits, and called it nuclear fission. This spurred much more work in the theoretical as well as the experimental field. Over the next two years, Bohr and Wheeler [Boh39] proposed the liquid drop model of fission, K. A. Petrzhak and G. N. Flerov [Pet40] reported spontaneous fission (i.e., fission not induced by projectiles), and E. M. McMillan and P. A. Abelson [McM40] made the first positive identification of a transuranic element, neptunium (Z = 93). McMillan and Abelson were actually attempting to study fission when they fortuitously discovered neptunium.

The field grew and expanded at such an accelerated rate, that only 5 years later scientists were advanced enough to be able to develop and successfully detonate the first fission bomb. Since then, the study of the nucleus has continued to move forward and diversify, providing all fields of science with answers about the behavior of material at its most fundamental level.

1.2 Limits to the periodic table

The chemists of the 19th Century were able to advance their knowledge of the identity and chemical behavior of all the known elements to the point where certain common characteristics and properties among various elements were noted and established. These "periodic" properties led Mendeleev to create his famous table of the elements in 1869. The important feature of the periodic table is that Mendeleev did not order the elements according to weight, which might seem to be the most obvious choice (of course, protons or proton numbers were not known at the time). As a chemist, he ordered them according to chemical properties, aligning similar ones in columns, or periods. While this method usually corresponded with increasing atomic weights, it sometimes contradicted such ordering. Time proved him correct, although the exact reasons why it was so were not discovered until the next century.

Because not all the elements were discovered by that time, there were some "holes" in the table, intentionally left by Mendeleev for elements not yet known. One of the great triumphs of the periodic table was the subsequent discovery of these missing elements and the fact that their mass and chemical properties dictated that they did indeed belong in the spaces left for them. However, for many years there were elements not yet found on the earth and still missing from the periodic table, namely those at positions 43, 61, 85, and 87. And nothing was known about the possible existence of any elements beyond uranium ($Z = 92$). With the discoveries mentioned above (Section 1.1), it gradually came to be understood that the isotopes of these elements were too short-lived to have survived in appreciable quantities since nucleosythesis occurred in the stars,

creating the present-day elements. It wasn't that no other elements *could* exist, but rather just that they *no longer* existed. It wouldn't be long before scientists began attempting to produce these long-extinct elements in the laboratory. In 1937, element 47 became the first artificially produced element and was named technetium [Per37]. And of course, it fit in just where Mendeleev predicted. Three years later, E.M. McMillan and P.H. Abelson became the first to identify a transuranic element, neptunium, proving that there are elements beyond uranium and that there could be many more yet to be found. But how many more could be produced? Were there any limits?

Spontaneous fission (SF), the splitting apart of a nucleus, is a process that can limit the extension of the periodic table, preventing the creation of an unlimited number of new elements. To see this, we can use the binding energy formula (see Section 2.1.4), which involves terms proportional to the nuclear volume (E_{vol}), surface area (E_{sa}), Coulomb repulsion (E_{coul}), symmetry (E_{sym}), and pairing (E_{pf}).

$$B = E_{vol} - E_{sa} - E_{coul} - E_{sym} + E_{pf} \tag{1.1}$$

A spherical nucleus that stretches as it begins to undergo fission can do so while maintaining constant volume. However, the surface area increases and the Coulomb repulsion decreases, thereby altering the binding energy. Under some circumstances, the system gains energy by stretching: the more it stretches, the more energy it gains. Therefore, it will immediately undergo fission without any possibility of returning to the spherical shape. This "critical point" where a nucleus spontaneously fissions is given by

$$\frac{Z^2}{A^{1/3}} > 47 \qquad (1.2)$$

For the superheavy elements, such as $Z = 120$ with $A = 300$, $Z^2/A^{1/3} = 48$. The SF-decay half-life for such an element would be 10^{-20} s [Kra88]. In other words, the study of the nucleus could not occur because 10^{-20} s is too short for identification and detection in present-day set-ups. However, this treatment is somewhat simplified, and the condition in Equation 1.2 isn't completely accurate. It is a simplified estimation based on touching spheres, while real nuclei usually exist as deformed shapes, which would thereby decrease the Coulomb interaction.

To nuclear chemists, the limits imposed by increasingly short SF-decay half-lives for superheavy elements are not yet a major concern. What currently limits the study of heavy isotopes are (1) the low production rates and (2) the comparatively long transport, separation, and detection times at accelerators where they are produced. To effectively study an isotope, enough has to be produced to allow observation. Bulk amounts are not necessary as atom-at-a-time techniques have been developed and used [Adl93]. The production of one atom per day may be more than sufficient for discovering isotopes, but it takes one or two orders of magnitude more to be able to produce statistically significant results and conclusions about an isotope's nuclear or chemical properties. Additionally, because the isotopes are produced on-line and must be transported to some separation and/or detection device, chemical properties of directly produced isotopes with half-lives shorter than about a second cannot yet be studied, whether they decay by α-decay, β^--

decay, or SF-decay. They can perhaps be studied as a daughter product of another isotope, but that is not always possible and rarely convenient.

1.3 Importance of studies of the heaviest elements

This problem of ever decreasing half-lives of heavier elements, together with their ever decreasing production rates, might have discouraged any further study of the transactinide region of the periodic table. Few isotopes were available for study and the prospects of studying elements beyond element 106 seemed remote. However, research has continued with enthusiasm. The reason for this is that much can still be learned from the few elements which we are able to study through radiochemistry or nuclear decay measurements. In addition, current nuclear theory suggests that the current trend of decreasing total half-lives and increasing SF-decay branches will not continue as originally believed. The factor which will ultimately determine the ability to produce superheavy elements, is the idea of shell structure and an "island of stability" (see Figure 1.1). As will be discussed in more detail later, nucleons in nuclei fill energy levels analogous to the way electrons fill shells in atoms. Thus, the nucleons can similarly "complete" shells, which gives the nucleus a special energy stabilization. The numbers of nucleons needed to complete shells are known as "magic numbers". It is the prediction of nuclear theorists and the hope of experimental nuclear chemists and physicists, that element 114 will indeed possess extra stability and reverse the trend of decreasing half-lives. Additionally, because of the non-spherical shape of some nuclei, deformed shells can also exist.

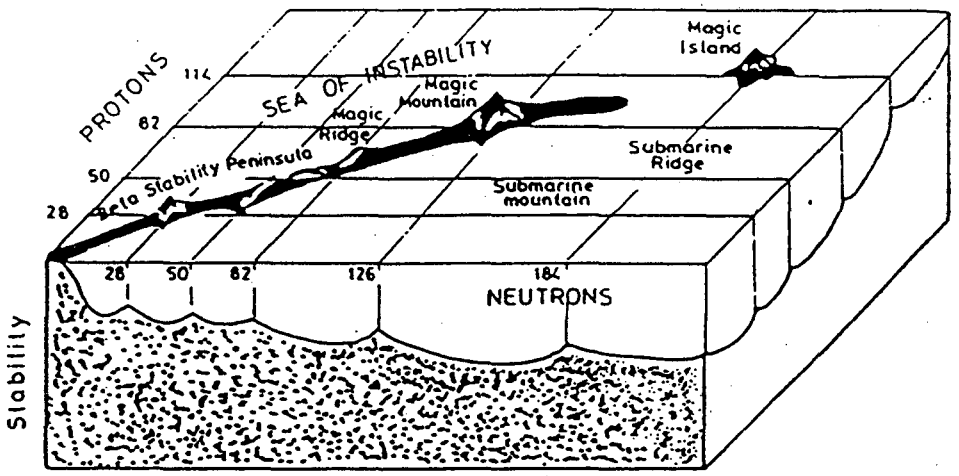

Figure 1.1: An allegorical representation of the stability of nuclei, showing a peninsula of stability and a magic island of stability in a sea of instability (from [Sea90]).

Recently, the isotopes ^{265}Sg and ^{266}Sg (Z = 106, N = 159,160) have been reported [Lou94,Laz94] to decay by α-emission with half-lives later measured to be $7.4^{+3.3}_{-2.7}$ s and 21^{+20}_{-12} s [Tür98], respectively, with upper limits for SF-decay of ≤ 35% and ≤ 82% for ^{266}Sg and ^{266}Sg, respectively. (Originally, the half-lives were inferred from Patyk and Sobiczewski [Pat91] by using the measured α-decay energy and the phenomenological formula of Viola and Seaborg [Vio66].) These relatively long half-lives (compared to extrapolated experimental half-lives) were spectacularly encouraging results for those who were hoping for a confirmation of shell stabilization. Over the past decade, the production of new elements has taken new importance with the discovery of elements up through Z = 112 [Hof96]. At the Lawrence Berkeley National Laboratory, work has started to build a gas-filled separator that will assist in the search of superheavy elements in the deformed region around Z = 108 and the spherical region around Z = 114. The Berkeley Gas-filled Separator (BGS) [Nin97] should provide access to nuclides with very low production cross sections, and would be particularly advantageous for asymmetric reactions which have a broad angular distribution, including that resulting from scattering of recoils in the target itself. This allows for thicker targets. Hot fusion reactions, such as ^{244}Pu(^{48}Ca,4n)^{288}114 can be investigated. A cross section of only 1 pb should result in the detection of nearly two events per week.

Even if the theorized positive effects of shell-stabilization turn out to be incorrect and the attempts to produce heavier elements with longer half-lives fail, research should continue. There is much to be learned from the elements that we can produce. The knowledge we gain might lead to better understanding of the nuclear properties of the

heaviest elements, perhaps establishing greater theoretical knowledge about the nucleus and atoms in general.

Many may question the relative merits of producing and studying chemical properties of isotopes with such short half-lives. The answer is, to increase our understanding of the chemistry and physics of the heavy element region and consequently of chemistry itself. One such important advancement being made thanks to work being done in the actinide and transactinide region is the observation of relativistic effects on the chemical properties of the heaviest elements [Pyk88,Per96]. With the increasing proton number of the nucleus, the velocity of the electrons in the spherically-symmetric relativistic filled orbitals $s_{½}$ and $p_{½}$ (which have a high radial distribution probability near the nucleus) must increase to remain in orbit. As these electon velocities approach c, the speed of light, there is a relativistic increase in mass of the electrons and, therefore, an even further decrease in orbital radii. These contracted orbitals will thereby screen the outer d and f orbitals from the nucleus more efficiently, causing d and f orbital expansion, a secondary effect. The electronic energy levels of the non-relativistic orbitals were already predicted to be tightly spaced. With relativistic effects, it is predicted not only that the spacings of the energy levels would be closer, but that some levels may even change order. For example, with relativistic effects, the $7p_{½}$ orbital may be lowered enough that the electron configuration of lawrencium might be $5f^{14}7p_{½}7s^2$ rather than $5f^{14}6d7s^2$ [Sea90]. Also predicted [Hyd87] is that for rutherfordium, the electronic configuration may be $7s^27p^2$ rather than the expected $6d^27s^2$ by analogy to its lighter homolog, hafnium. Similarly, hahnium might have a $7s^26d7p^2$ configuration rather than the $6d^37s^2$ configuration analogous to its lighter homolog, tantalum.

Relativistic effects can change ionization potentials, ionic/atomic radii, oxidation states, and complexing ability. Although such configurations have yet to be confirmed, recent results of experiments with isothermal gas phase chromatography has shown evidence for such effects [Tür98b].

1.4 Importance of spontaneous fission

Once again, the impetus for study of SF is the quest to understand the process in greater detail, which helps the development of theoretical and empirical predictions. One objective is to produce as many experimental results as possible in order to add to the systematics of the various properties of SF. Just as it is difficult to deduce the shape of a wavy line from two or three points on an *xy* plot, it is difficult to gain theoretical knowledge of any SF property from limited data. The greater the amount of data, the more accurately we can interpret and understand SF, from nuclear structure, to the process, to the expected resulting properties. Theoreticians can use this increased knowledge to revise and adjust their theories and equations, thereby improving their models. And, in turn, these models and predictions will help the experimentalists devise new experiments to provide yet more data.

This is particularly important in the SF field. Spontaneous fission is a complicated mode of decay. While α–decay and β–decay emit exact, known particles (a helium nucleus and an electron or positron, respectively), and therefore form expected products, SF produces a wide spectrum of products at a wide spectrum of energies. Varying numbers of neutrons can be emitted in the de-excitation of the fission fragments, which then de-excite by β–ray and γ–ray emission. Since it is these fission fragments that we detect, it is very difficult to track genetic relationships from the multitude of fission products formed. Therefore, these products tell us less about the parent. It is only through averaging and generalizing the bulk results that some knowledge may be gained.

Thus we speak of such properties as the *most probable* total kinetic energy, the *average* number of emitted neutrons, the mass yield *distribution*. There is no codification that tells us *exactly* what will happen when a nucleus fissions. However, from years of experimental research, not only are we able to understand the results in terms of our current knowledge of SF but are also able to predict what we should observe for a new isotope.

Spontaneous fission is an interesting field in that it tells us so much about the structure of a nucleus. Since SF—as opposed to induced fission—requires no external energy input, the nucleus will remain undisturbed and small changes and effects brought about by both deformed and spherical shell structure will be observable. Spontaneous fission has been found only for elements with $Z \geq 92$ (upper limits for probability of SF-decay have been made for thorium ($Z = 90$) and protactinium ($Z = 91$)). Fission induced by high-energy neutrons will tend to reduce shell effects and tells us less about the structure of the nucleus and the role shell effects play. As already mentioned (Section 1.3) and will be explored further in the next chapter, the effects of shells can have a large influence on the future of heavy element studies. This makes any information we can obtain about it from SF extremely important, and will help develop theoretical predictive models.

1.5 Scope

In this dissertation, investigations of the properties of some transactinide elements will be described, with an emphasis on the SF process. An overview of SF, from the history to a description of the process to the models to the properties of the fissioning nuclides and the fission fragments, will be discussed. In addition to experiments directly designed to study SF properties, other experiments such as investigations of production cross sections have been performed and included here that relate to the general purpose: the attempt to increase our knowledge of nuclear structure, forces, and decay, including the stability, of the heaviest elements through the investigation of the behavior of isotopes in this region, and measurements of production reactions.

2 SF Theory and Models

2.1 Basic spontaneous fission process

2.1.1 Nuclear structure

To understand the SF process, it is important to first know the composition of a nucleus and the forces involved. By a variety of methods it can be shown that the nuclear charge distribution is quite uniform. The charge is distributed evenly throughout the nucleus until it drops off dramatically (this region where it drops from 90% of its maximum value to 10% is known as the *skin thickness*). Therefore, the number of nucleons per unit volume is roughly the same for all nuclei, i.e.

$$\frac{A}{\frac{4}{3}\pi R^3} \sim \text{constant} \qquad \text{or} \qquad (2.1)$$

$$R = R_o A^{1/3} \qquad (2.2)$$

where R is the mean nuclear radius. Many experimental results show that the proportionality constant, R_o, is equal to approximately 1.2-1.3 fm. Other calculations show that the nuclear *matter* distribution is the same, within 0.1 fm, as the nuclear charge distribution, with both behaving as Equation 2.2 with R_o = 1.2-1.3 fm. Despite the fact

that most nuclei contain many more neutrons than protons, the nuclear charge and nuclear matter radii are similar. This is because the protons repel each other outward while they attract the neutrons inward to dampen and shield protons from each other.

The nucleons are arranged such that they are in the most stabile configuration, that is, with the lowest energy and greatest binding energy. Since the binding energy increases with the number of nucleons, it is most useful to observe how the binding energy *per* nucleon changes from atom to atom. Figure 2.1 plots the binding energy per nucleon against the mass number for many nuclei. It shows that there exists a maximum to the binding energy per nucleon. There is a point, at around ^{56}Fe, that the nucleons are most tightly bound: nuclei heavier and lighter are less stable. Therefore, lighter nuclei can gain stability and release energy by combining to form iron-like nuclei ("fusion"), and heavier nuclei can gain stability and release energy by splitting to form iron-like nuclei ("fission"). It is this desire to form the most energetically stable nuclei that is the driving force for heavy isotopes to fission.

2.1.2 Nuclear shape

As discussed in the section above, the nucleus has a nearly uniform distribution of protons and neutrons, a value of approximately 0.17 nucleons/fm^3 [Sea90], up to the "skin", where the density drops from 90% to 10%. The radial distribution can be characterized by the Fermi distribution

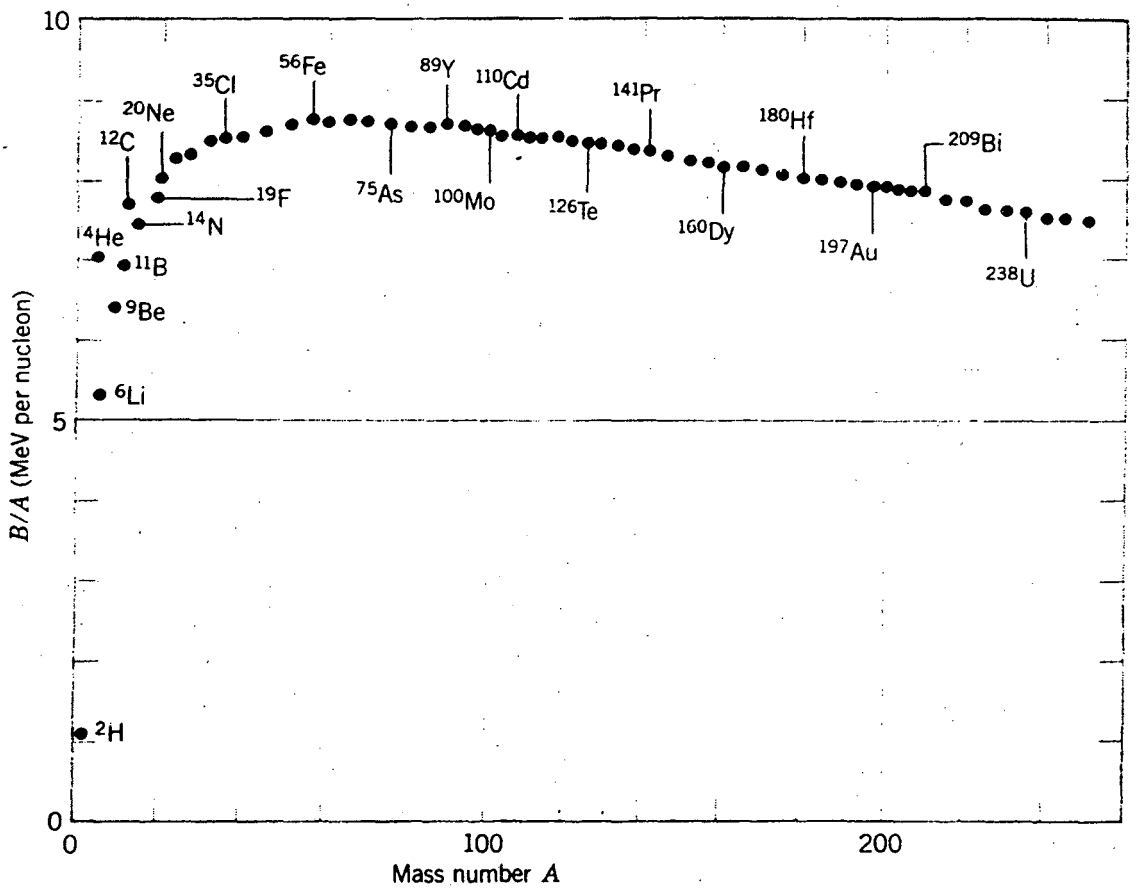

Figure 2.1: The binding energy per nucleon for nuclei with mass number A (from [Kra88]).

$$\rho(r) = \frac{\rho_o}{1+\exp\left(\frac{r-R}{a}\right)} \tag{2.3}$$

where $\rho(r)$ is the density as a function of radius r, ρ_o is the "constant" density of 0.17 nucleons/fm^3, R is given by Equation 2.2, and a is the *surface diffuseness constant*, related to the skin thickness by

$$t = 2a\ln 9 \tag{2.4}$$

A more mathematical description of the shape of a nucleus, which takes into account the non-spherical shape of heavy nuclei, can be given by using the deformation parameters, β_l, and the spherical harmonic functions, Y_{l0}:

$$R(\theta) = c[1 + \beta_2 Y_{20}(\theta) + \beta_4 Y_{40}(\theta)] \tag{2.5}$$

where c is a experimentally-determined parameter, and the spherical harmonic functions (with associated Legendre polynomials) are given by

$$Y_{20}(\theta) = \sqrt{\frac{5}{4\pi}}\frac{\left(3\cos^2\theta - 1\right)}{2} \quad \text{and}$$

$$Y_{40}(\theta) = \sqrt{\frac{9}{4\pi}}\frac{\left(35\cos^4\theta - 30\cos^2\theta + 3\right)}{8} \tag{2.6}$$

For typical transuranium nuclei, β_2 ranges from 0.23 to 0.29 and β_4 ranges from –0.1 to +0.1 [Bem73,Zum84], and the axis ratio is 1.3:1.

2.1.3 Fission barriers

The impetus for SF is the energetic preference for nuclei to be more stable, or more tightly bound. If ^{238}U, for example, divided into two symmetric ^{119}Pd fragments, Figure 2.1 can be used to illustrate this preference. The binding energy (BE) of a heavy nucleus around the ^{238}U region is about 7.6 MeV/nucleon. The BE of a nucleus near ^{119}Pd is about 8.5 MeV/nucleon. Therefore, the total BE goes from 238 x (–7.6) = –1809 MeV to 2 x 119 x (–8.5) = –2023 MeV. Clearly, fission into 2 smaller fragments is energetically favorable. About 80% of this extra 214 MeV appears in the products as kinetic energy brought about by Coulomb repulsion; the rest is dissipated as radiated energy in the form of neutrons, γ-rays, or β^-–decay, as discussed in the Section 2.1.7.

What, then, prevents heavy nuclei from instantaneously fissioning to attain this preferred state? What holds them together? Inside the parent nucleus (^{238}U, using our current example), the nucleons may arrange themselves and exist momentarily as two ^{119}Pd nuclei *within* the nucleus. If they exist as two spheres just touching at their surface, then we can use Equation 2.2 to find that the Coulomb barrier is

$$V = \frac{Z_1 Z_2 e^2}{4\pi\varepsilon_o R} \tag{2.7}$$

$$V = (1.44\ \text{MeV·fm})(\frac{46^2}{12.2\text{fm}}) = 250\ \text{MeV}$$

Therefore, even though the two Pd nuclei have 214 MeV of potential energy, they are in a potential well of 250 MeV. Using more realistic fragmentation and calculations, the Coulomb barrier is actually only about 6 or 7 MeV above the excess energy that would be gained from fission. Spontaneous fission is made possible by this close matching between the Coulomb barrier and the energy release in fission. Figure 2.2 shows the energy of a nucleus as a function of the separation of the fragment centers. It also shows the barrier, or activation energy, needed to fission. This energy difference is small enough that these two fragments could quantum mechanically tunnel through this barrier. This process will of course be slow and depend on the height of this barrier. If a nucleus were formed by a reaction such that its excitation energy is *above* the barrier, prompt fission would occur, and neutron or proton emission will compete. For nuclei that have a fission barrier that is too high to spontaneously fission, they could be *induced* to fission by supplying an amount of energy equal to the difference needed to get the nucleus above the barrier. This is called the *activation energy* and the type of fission that takes place is called *induced fission*, as opposed to *spontaneous* fission.

As will be discussed later, although it was theoretically predicted that the fragment mass-yield distributions of SF should be symmetrical, the observed actinide SF-decay activities showed decidedly asymmetrical distributions. Because the actinide region has double-humped fission barriers, it was decided that the two features were related to each other. The second fission barrier must somehow be responsible for the

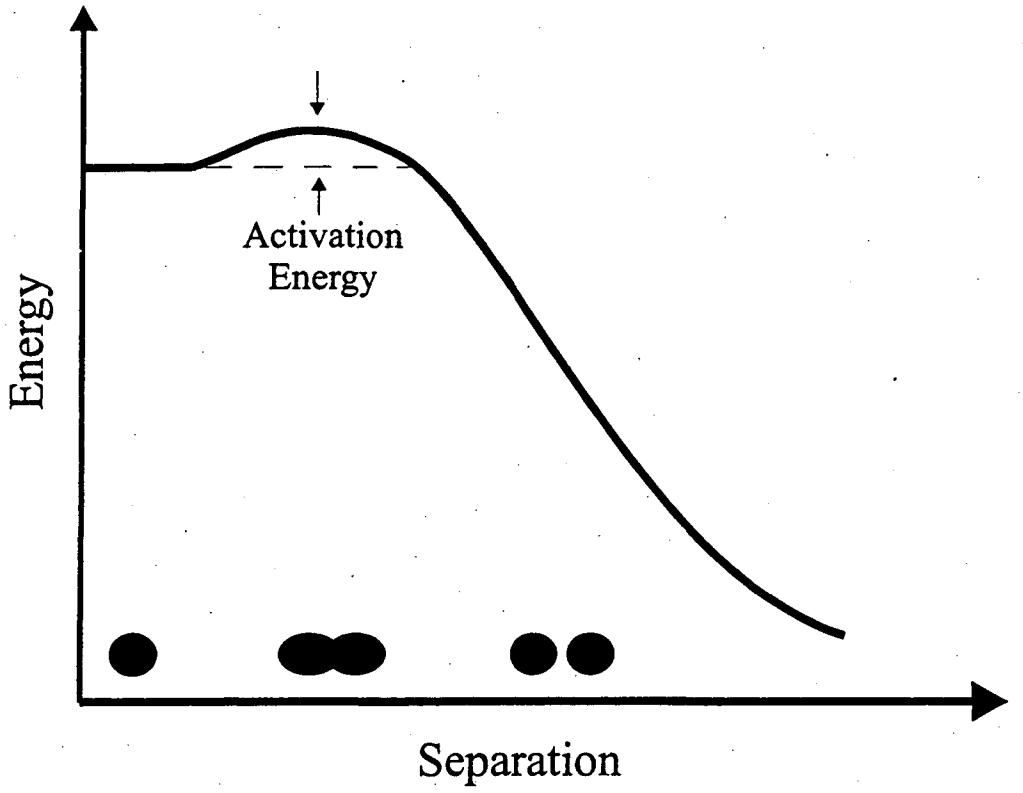

Figure 2.2: A schematic illustrating the fission barrier. At the bottom are representative shapes during the process.

observed mass asymmetry. This can be observed by seeing how the double-humped fission barriers arise.

The top of Figure 2.3 shows the most important part of Figure 2.2, that is, the top of the fission barrier. The shape shown is what is expected from a simple macroscopic model (i.e., does not include shell effects). As Z^2/A increases, the height of the barrier decreases and the maximum shifts toward lower deformations. However, to accurately describe the fission barrier, microscopic effects must be taken into account. Therefore, a shell correction must be applied as shown in the middle part of Figure 2.3.

The oscillating nature of the shell correction comes from the theory that the properties of a nucleus are dictated by the properties of the single odd particle. As nuclei become deformed, the non-spherical potential that results causes the angular momentum of a single particle state to no longer be constant. However, its projection on the axis of symmetry is constant, which causes the state to split up into separate levels. Because all these once-constant angular momentum states split up as the nucleus deforms, the levels cross each other and complicate the order of filling for nucleons. The splitting of these states and their ordering were investigated by S. G. Nilsson and the diagrams that result are called Nilsson diagrams. One of these is shown in Figure 2.4. It shows the ordering of single particle states as a function of deformation, ε. A particle in one state will move up and down in energy as the nucleus deforms. When level crossings occur, the particle will take the path of lowest energy, sometimes transferring to another state. Such transfers are shown by the solid line. This rising and falling of energy is what causes the shape of the shell correction in the figure.

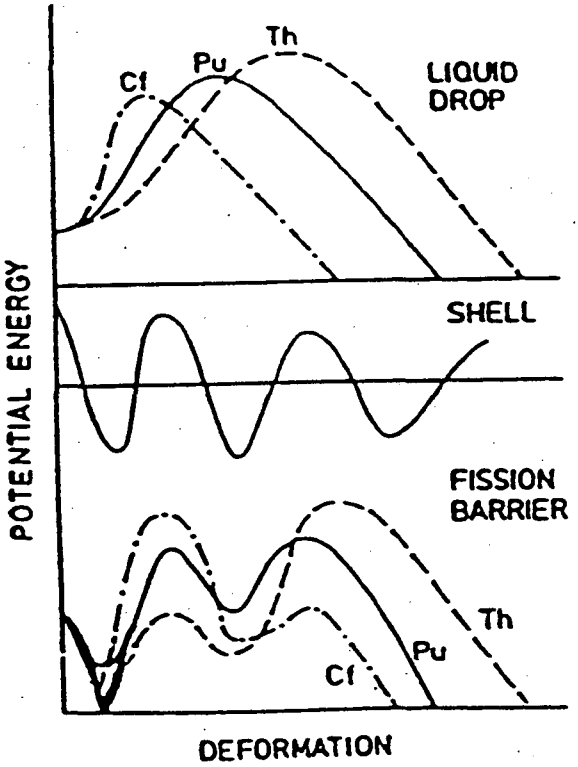

Figure 2.3: The top portion shows the macroscopic liquid drop fission barrier for Th, Pu, and Cf. Plotted is the potential energy as a function of deformation. The middle portion shows the microscopic shell correction. The bottom portion shows the total fission barrier after applying this correction (from [Bri82]).

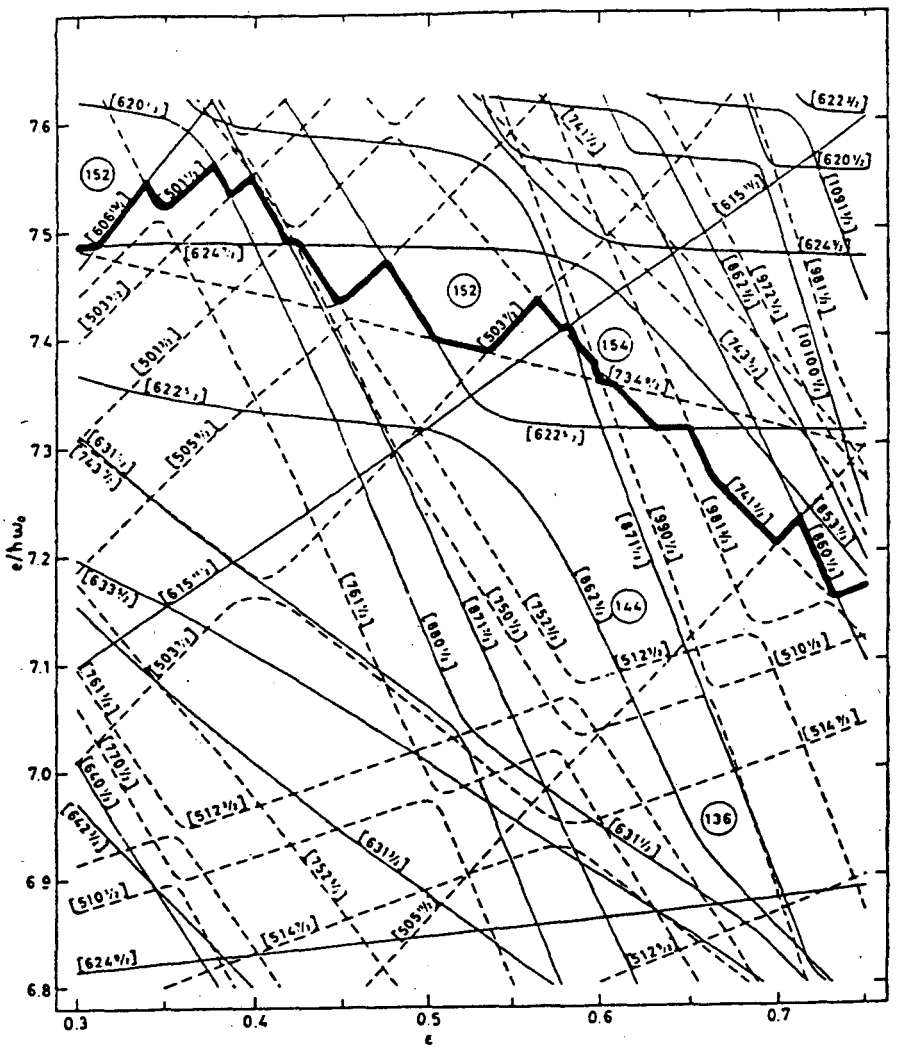

Figure 2.4: Nilsson diagram, showing energy levels as a function of deformation ε. Also shown is the lowest energy level the 152nd neutron would occupy at various stages of deformation (from [Nil69,Van73]).

When this is applied to the potential at the top of Figure 2.3, the resulting total fission barriers develop a double-hump shape, as shown at the bottom of the figure. Although shell effects are generally small compared to the total potential of a nucleus, their effects can be great since the area at the top of the barrier is extremely sensitive to changes in energy. The first (inner) barrier arises from the macroscopic barrier, while the second (outer) barrier arises from shell structure. The inner barrier gives rise to symmetric deformations. However, as the nucleus passes across the outer barrier, mass asymmetric shapes are preferred. This is because of the tendency—brought about by shell structure—of a nucleus to split into a light and heavy fragment, one of which prefers to be near the stable, doubly magic nucleus ^{132}Sn (with closed shells at $Z = 50$ and $N = 82$). It is therefore because of this second barrier that asymmetric mass-yield distributions result.

2.1.4 Nuclear mass

As a first attempt to develop a model that would account for the shape and features of the binding energy curve (Figure 2.1), successive terms are introduced to produce the binding energy equation:

$$B = a_v A - a_s A^{2/3} - a_c \frac{Z(Z-1)}{A^{1/3}} - a_{sym} \frac{(A-2Z)^2}{A} + \delta \qquad (2.8)$$

where δ is given by

$$\begin{array}{ll} +a_p A^{-3/4} & \text{when } Z \text{ and } N \text{ even} \\ 0 & \text{when } A \text{ odd} \\ -a_p A^{-3/4} & \text{when } Z \text{ and } N \text{ odd} \end{array} \qquad (2.9)$$

Equation 2.8 replicates fairly well the experimental data discussed in Section 2.1.1. It includes contributions from two different models: the first three terms come from the liquid-drop model (which treats collective features of nuclei similar to those of a drop of liquid), and the last two terms are refinements that considers the special nature of nuclei.

The first term accounts for the number of nucleons—the greater the mass, the greater the contribution to the binding energy—and is proportional to the volume. However, the equation overestimates the binding energy because the nucleons at the surface are not as tightly bound as interior nucleons. Therefore, they contribute less to the total binding energy. We must subtract a term taking into account this surface area, which is proportional to R^2, or $A^{2/3}$ (Equation 2.2). The binding energy is also decreased by the destabilizing effect of proton-proton repulsion, which is proportional to $Z(Z-1)/R$, since each proton repels all other protons.

Corrections and refinements must be made to this simple liquid-drop treatment. Since the nucleus is made up of fermions (protons and neutrons), Fermi-Dirac Statistics tell us that no two of them may have the same quantum numbers. In other words, they cannot occupy the same states/energy levels. Since for heavy nuclei $N > Z$, neutrons occupy higher states in the potential well than do protons, and therefore they have a lower average binding energy. The liquid-drop model treats neutrons and protons

equally and assumes their binding energies are the same. The fourth term, then, takes into account the neutron-proton asymmetry and is proportional to the neutron excess.

We must also take into account the empirical observation that there are very few nuclei found in nature with both odd Z and odd N. Conversely, there are a multitude of nuclei with even Z and N. Evidently, a nuclear system does not favor having both an unpaired proton and an unpaired neutron. The last term, then, takes into account this pairing force.

Equation 2.8 can also be used to derive the mass of an isotope

$$M(Z,A) = Zm\left({}^{1}\mathrm{H}\right) + Nm_n - \frac{B(Z,A)}{c^2} \tag{2.10}$$

which is simply the sum of the mass of the hydrogen atoms and the mass of the neutrons along with a term to take into account the extra stability caused by the binding force of the nucleons. This is known as the *semiempirical mass formula*. Over the years, as new knowledge is gained through experimental research, nuclear theoreticians have been able to modify, expand, and improve this equation to produce models of extreme accuracy (see Section 2.2). Each new discovery in the laboratory is used as a test for these models and provides motivation for further improvement of our understanding of the nucleus.

2.1.5 Nuclear forces

The force that holds nucleons together is for the most part a central force that depends only on distance between the charge centers (however, there is a very small

noncentral term, called the *tensor potential*). It must be greater than Coulomb forces at short distances to overcome the strong proton-proton repulsion in the nucleus. However, the range of its effects is very short and is only an intra-nuclear force: that is, there is no nuclear force interaction between two nuclei in adjacent atoms. The force is strongly spin dependent, but it is charge symmetric. In other words, the proton-proton interaction is of the same magnitude as the neutron-neutron interaction. It is also nearly charge independent, which means the proton-neutron force is nearly the same as the proton-proton and neutron-neutron force. Lastly, the nuclear force has a repulsive term. This term is needed to keep a fixed distance between nucleons.

2.1.6 Fissionability

Calculating fission properties such as fission barriers requires the knowledge of the masses involved. Mass is given by Equation 2.10, with the most interesting term being the binding energy, Equation 2.8, which is made up of separate energy terms involving volume, surface area, Coulomb repulsion, symmetry, and pairing. Now consider a spherical nucleus that begins to undergo fission. It stretches and distorts, and can do so while conserving volume. However, the surface area increases, which increases the surface energy term of Equation 2.8, and the Coulomb repulsion decreases, which decreases the Coulomb energy term. The symmetry and pairing energy terms, of course, remain unchanged. The binding energy will be dynamically altered by only the surface area and Coulomb repulsion as it stretched. Quantitatively, consider the ellipsoid

produced having a volume $\frac{4}{3}\pi ab^2$, with semimajor axis a and semiminor axis b. The relationship between these axes and the radius, R, of the sphere, is given by the equations

$$a = R(1+\varepsilon) \tag{2.11}$$

$$b = R(1+\varepsilon)^{-1/2} \tag{2.12}$$

where the eccentricity of the ellipsoid ε (the quadrupole distortion parameter) is related to the deformation parameter, β_2, by the equation

$$\varepsilon = \beta_2 \sqrt{\frac{5}{4\pi}} \tag{2.13}$$

For small distortions, the surface area can be shown to be increased by a factor of $(1+\frac{2}{5}\varepsilon^2)$, with a corresponding increase in the surface energy term (E_{sa}) of Equation 1.1. The Coulomb energy term (E_{coul}) can be shown to decrease by a factor of $(1-\frac{1}{5}\varepsilon^2)$. Therefore, the energies will be given by

$$E_{sa} = E_{sa}^{o}\left(1+\frac{2}{5}\varepsilon^2\right) \qquad \text{and}$$

$$E_{coul} = E_{coul}^{o}\left(1-\frac{1}{5}\varepsilon^2\right) \tag{2.14}$$

where E^o_{sa} and E^o_{coul} are the surface and Coulomb energies of an undistorted sphere. So the difference in binding energy of a stretched nucleus (with eccentricity ε) and a spherical unperturbed nucleus ($\varepsilon = 0$) is

$$\Delta B = B(\varepsilon) - B(\varepsilon = 0) \tag{2.15}$$

$$= \left(-\frac{2}{5} E^o_{sa} + \frac{1}{5} E^o_{coul} \right) \varepsilon^2 \tag{2.16}$$

If the Coulomb term is larger than the surface term, the energy difference will be positive, meaning the system gains stability by stretching: the more it stretches, the more stable it becomes. Therefore, it will immediately undergo fission without any possibility of returning to the spherical shape. The "critical point" is when the change in binding energy (Equation 2.16) becomes zero. At this point

$$\frac{E^o_{coul}}{2E^o_{sa}} = 1 \tag{2.17}$$

Values larger than 1 will make the nucleus even more "fissionable". Therefore, the term

$$\frac{E^o_{coul}}{2E^o_{sa}} \tag{2.18}$$

is called the fissionability parameter, χ. Substituting values for these terms yields

$$\chi = \left(\frac{a_c}{2a_s}\right)\left(\frac{Z^2}{A}\right) \quad \text{or} \tag{2.19}$$

$$\chi = \left(Z^2/A\right) \Big/ \left(Z^2/A\right)_{crit} \tag{2.20}$$

where $\left(Z^2/A\right)_{crit}$ is the reciprocal of $\left(a_c/2a_s\right)$. The value of $\left(Z^2/A\right)_{crit}$ is given by [Sea90]

$$\left(Z^2/A\right)_{crit} = 50.883\left[1 - 1.7826\left(\frac{N-Z}{A}\right)^2\right] \tag{2.21}$$

Therefore, the higher the value of Equation 2.20, the more fissionable the nucleus will be.

2.1.7 Timescale

A ground state deformed nucleus will deform further and reach an excited transition state, called the *saddle point configuration*. As this requires passing over an activation energy barrier, this is the rate-determining step for fission. The lifetime of this state is approximately 10^{-15} s and is dependent on the excitation energy. Within 10^{-20} s, the neck ruptures, forming two highly deformed fragments. At this *scission point*, the fragments do not yet have high kinetic energy. The high Coulomb repulsion will, within 10^{-20} s, accelerate these fragments to 90% of their final kinetic energy. As this happens,

the potential energy of deformation is converted to internal excitation energy as the fragments contract to more spherical shapes. The fragments de-excite through emission of neutron(s). First, at around 10^{-14} to 10^{-15} s, neutrons are evaporated (see Figure 2.5). Then, at around 10^{-12} s to 1μs, gamma (γ) rays are emitted. Finally on a millisecond or greater timescale, β^--decay of neutron-rich fragments to more stable species occurs.

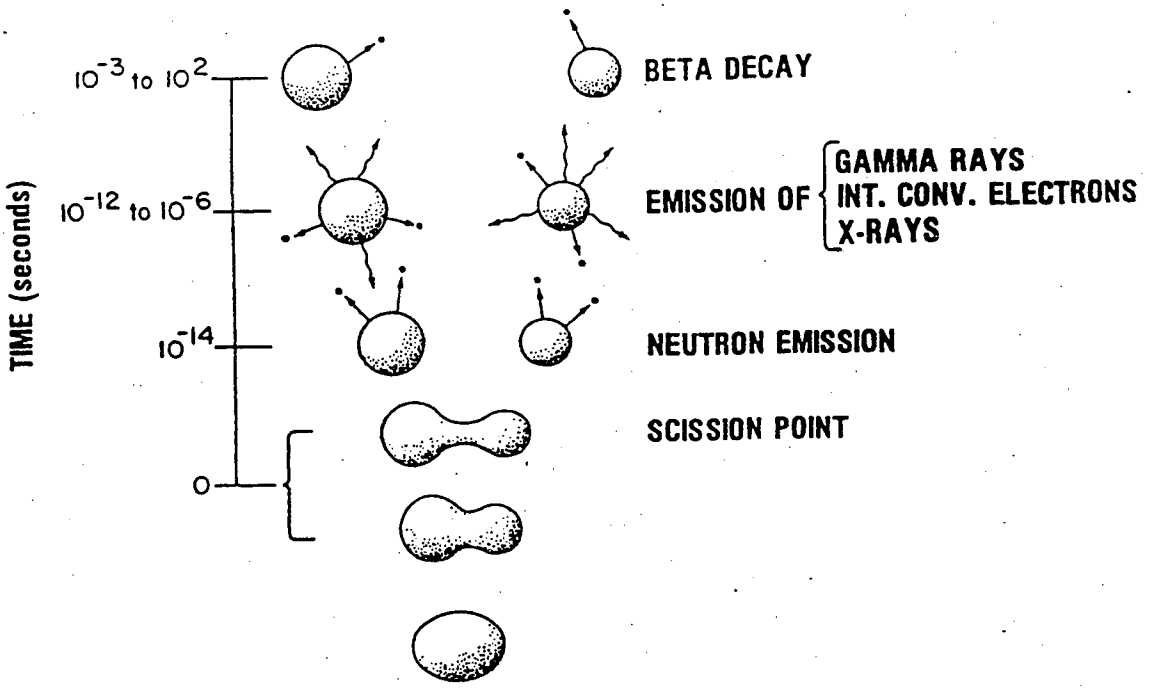

Figure 2.5: A schematic showing the timescale of the spontaneous fission process.

2.2 Nuclear models

Many models have been used to describe the nucleus and its SF-decay and α-decay properties in the superheavy element region. By "superheavy", it is meant the heavy elements that exist solely due to shell effects. Two subsets of superheavy elements are differentiated: the deformed superheavy nuclei and the spherical superheavy nuclei. The former are nuclei situated near the nucleus ^{270}Hs, which has the predicted closed deformed shells at $Z = 108$ and $N = 162$ [Smo95b]. This doubly magic deformed nucleus has been predicted to exhibit enhanced stability toward SF-decay and α-decay [Smo97]. Although this nucleus has yet to be synthesized, results of the LLNL-Dubna collaboration on ^{265,266}Sg seem to corroborate this suggestion [Lou94,Laz94]. The spherical superheavy nuclei are situated near the nucleus ^{298}114, which has the predicted closed spherical shells at $Z = 114$ and $N = 184$ [Sob66]. (Some models, however, predict a larger magic proton number at $Z = 126$ [Cwi96], or predict that the true island of stability for superheavy spherical nuclei is shifted down toward elements 110 through 112 [Wu96].) The SF-decay and α-decay properties are, of course, expected to exhibit enhanced stability in this region.

Properties of the heaviest nuclei have been studied by fully microscopic methods, such as Hartree-Fock calculations and other variations [Ber96,Lal96,Cwi96]. However, this approach is exceedingly difficult. Much simpler is the macroscopic-microscopic method [Str67]. In this method, a simple potential model is used to represent the smooth, average properties of nuclei, and then a single-particle correction is applied to take into

account shell structure. Theoretical results predicting the ground-state properties of heavy nuclei—such as mass, deformation, and half-lives—have been obtained using this approach and those calculations of Smolanczuk, Sobiczewski, Skalski, et al. have been especially successful in predicting these properties. Their theoretical modeling of the heavy and superheavy elements has been more accurate than other methods of calculation. It would be instructive to examine how the calculations are performed, which predict the shape and structure of nuclei and describe the dynamics of fission. Also given will be the results these calculations predict.

The vast majority of superheavy nuclei are expected to be both axially symmetric (along the axis of elongation as the fragments separate) and reflection symmetric (where the plane of symmetry is orthogonal to the axis of elongation at the neck between fragments). Only for a few of the heaviest isotopes of elements 104-110 does reflection asymmetry become important [Smo97]. Similarly, axially asymmetric shapes are unimportant for most nuclei in the superheavy region [Smo97].

Because the properties of these nuclei depend greatly on small details in shape, a large deformation space is required in order to accurately describe both the equilibrium shapes and the shape changes as they tunnel through fission barriers (or, to be more exact, move along the potential energy surface). Older calculations [Bar81] used simpler two-dimensional deformation spaces (considering only the quadrupole (β_2) and octupole (β_3) multipolarities) to describe the shape of nuclei, similar to Equation 2.5. We must include higher order spherical harmonics $Y_{\lambda 0}(\theta)$ (and associated Legendre polynomials) and larger deformation spaces. Therefore, a four-dimensional deformational space is

used: β_λ, λ = 2, 4, 6, 8. Generalizing Equation 2.5 to include higher components of deformation yields

$$R(\theta) = R_o(\beta_\lambda)\left[1 + \sum_\lambda \beta_\lambda Y_{\lambda 0}(\theta)\right] \tag{2.22}$$

Odd-multipolarity states are ignored, because, as stated above, reflection asymmetry is unimportant in this region (although very important in lighter nuclei such as the actinides). For the few superheavy nuclei that *are* affected by reflection asymmetry, the larger space λ = 2, 3, 4, 5, 6, 7, 8 is used. Axial asymmetry is also ignored, so only the "axially symmetric" spherical harmonics $Y_{\lambda 0}$ are used. Figure 2.6 shows contour maps of the equilibrium deformations. The values of the deformations (given by the contour lines) are plotted as a function of Z and N. The values are those at which the potential energy is minimized in the β_λ degrees of freedom. The largest effects are, of course, in the quadrupole multipolarity. It is roughly constant throughout most of the region, quickly decreasing towards the edges as it approaches the doubly magic, spherical nuclei ^{208}Pb and ^{298}114. The higher multipolarity components are of much smaller magnitude and play less of an important role in determining nuclear properties, but still must be considered for an accurate description. The theoretical shapes of these nuclei are plotted in Figure 2.7.

The potential energy of a nucleus is calculated using the macroscopic-microscopic method. For the calculations performed by Smolanczuk [Smo95b,Smo97],

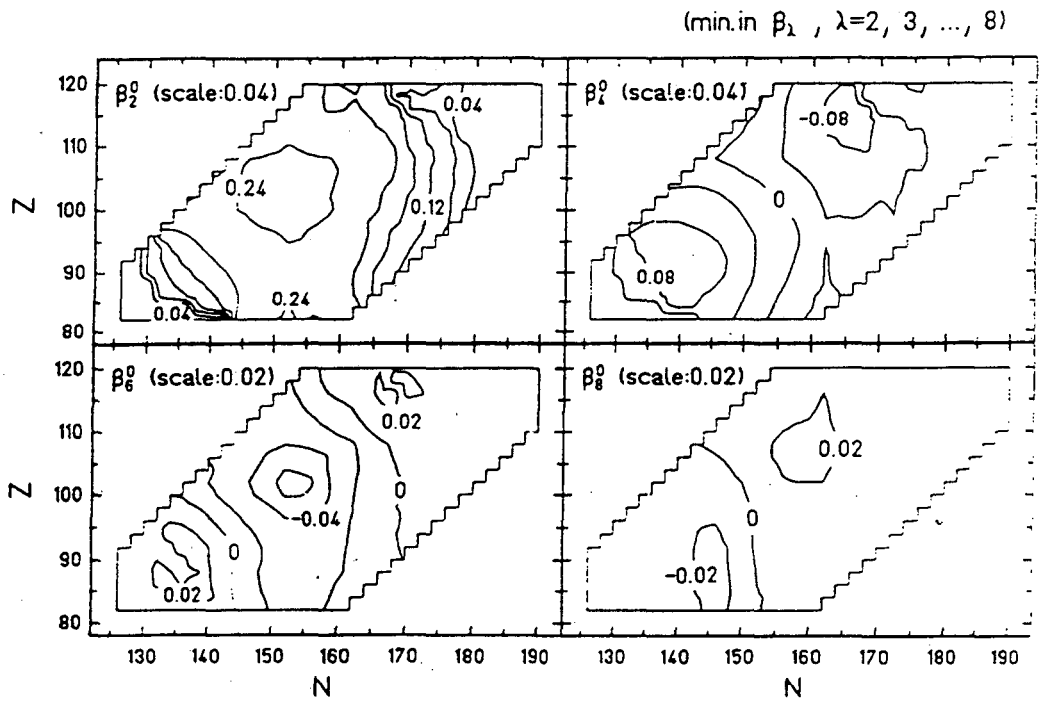

Figure 2.6: Contour maps of the equilibrium deformations β_λ^0, λ=2,4,6,8, plotted as functions of proton Z and neutron N numbers. The energy of a nucleus is minimized in the β_λ degrees of freedom. (From [Sob97, Smo95])

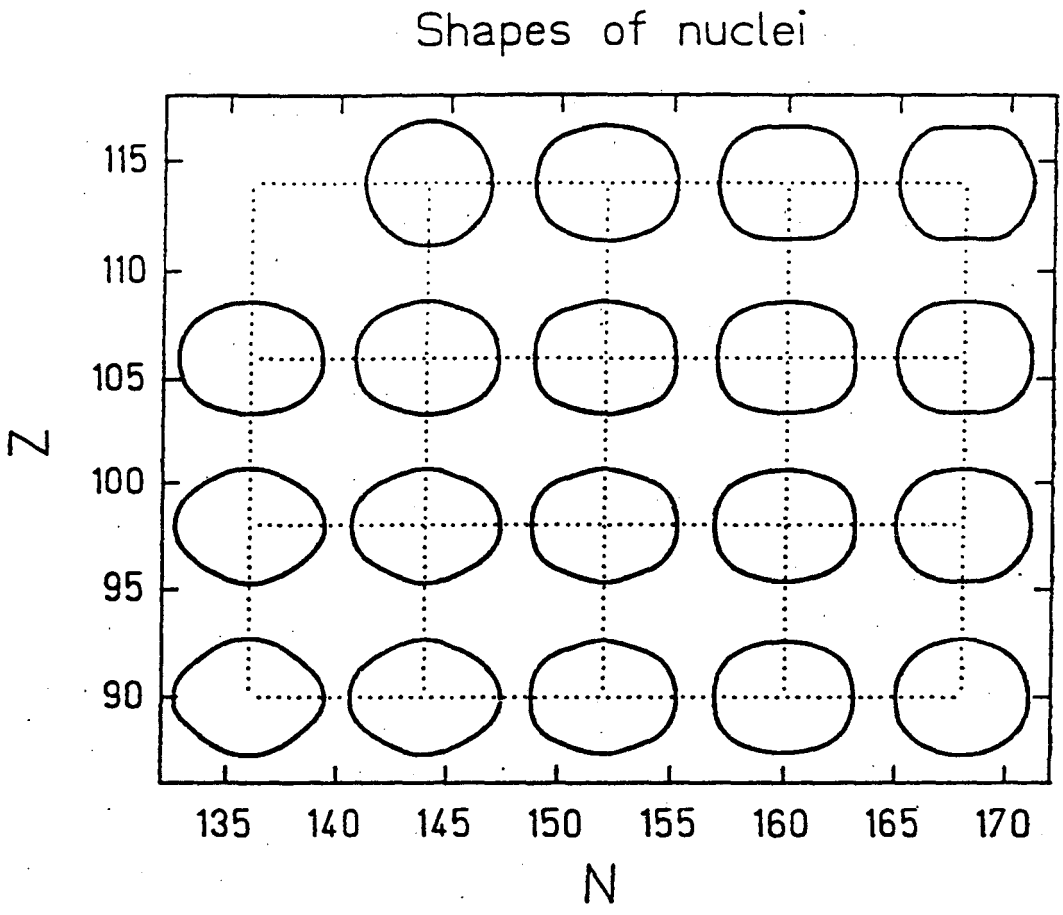

Figure 2.7: The shapes of nuclei for various Z and N combinations. (From [Sob97])

the Yukawa-plus-exponential model [Kra79] is used for the macroscopic part, and the microscopic part is obtained by the Strutinsky shell correction method, based on a Woods-Saxon single-particle potential [Cwi87], with the residual pairing interaction taken into account by the BCS approximation [Bar57]. The potential energy is calculated for each nucleus, without averaging.

The importance of the microscopic correction is shown in Figure 2.8, which shows the macroscopic barriers to fission (i.e., those that don't include shell effects) for ^{264}Hs. Plotted is the ground-state energy of the nucleus as a function of the deformation parameter β_2. The barriers were obtained using the liquid-drop model and the Yukawa-plus-exponential model (dotted and dashed lines, respectively). Also shown (solid line) is the barrier obtained by the macroscopic-microscopic method, which includes a correction for shell effects. As can be seen, only after shell structure is taken into account does there exist a barrier to fission, which is what allows the nucleus to exist.

The shell stabilization energy is shown in Figure 2.9, plotted as a function of Z and N (once again calculated with the energy minimized in the β degrees of freedom). The shell stabilization energy is defined as the difference between the total potential energy for the equilibrium shape (taking into account deformity) and the macroscopic part of the potential energy for the spherical shape. Thus, it represents the gain in energy (stabilization) brought about by its shell structure. The values indicated on the contour lines represent this shell correction energy (in MeV) for differing values of Z and N (plotted on the ordinate and abscissa, respectively). The difference between neighboring lines is 1 MeV. The values are obtained by minimization of the energy in the β_λ degrees

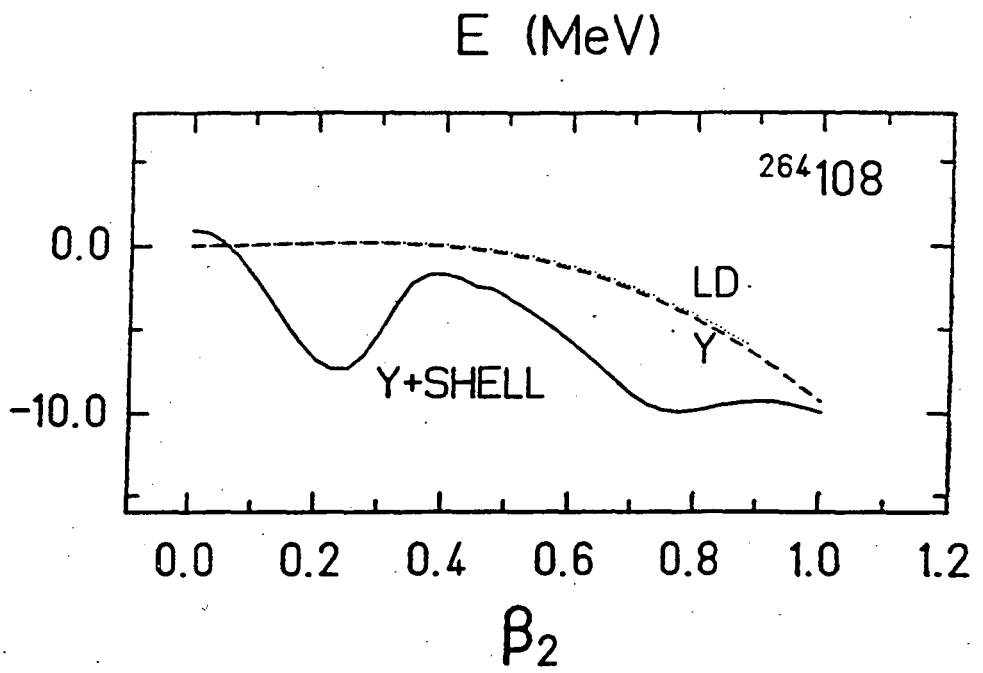

Figure 2.8: Total fission barrier (Y + SHELL) and its macroscopic part obtained by Yukawa-plus-exponential (dashed line) and by the liquid-drop (dotted line) models, for ^{264}108. (From [Pat89])

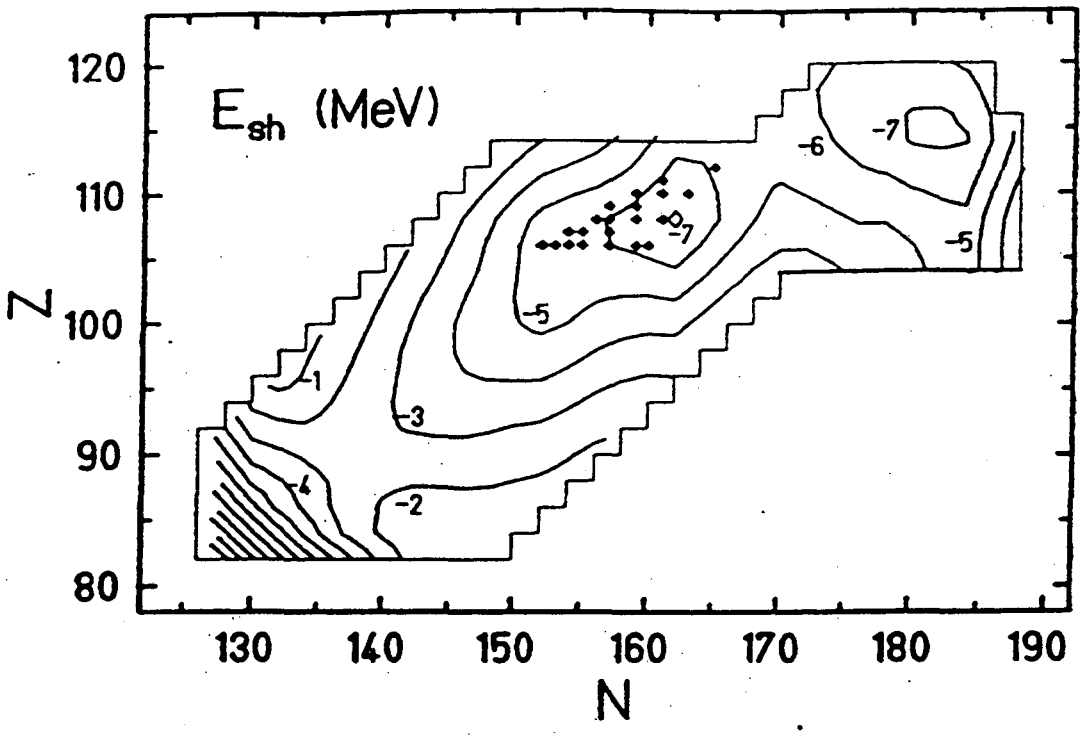

Figure 2.9: Contour map of the shell correction, E_{sh}. The heaviest nuclides synthesized up to now are denoted by crosses. The energy of a nucleus is minimized in the β_λ degrees of freedom. (From [Sob97, Smo95])

of freedom. Three minima appear. The first is at the doubly magic spherical ^{208}Pb (E_{sh} ~ 14 MeV); the second near the doubly magic deformed ^{270}108 (E_{sh} ~ 7 MeV); the third at the doubly magic spherical ^{298}114 (E_{sh} ~ 7 MeV). The plotted points indicate known nuclei. As can be seen, these nuclei gain between 5 and 7 MeV in stability from the shell effects. Also, this figure reveals that there is no longer just an "island of stability" (see Figure 1.1) around the spherical nuclei ^{298}114, but more of a "peninsula of stability" that stretches further than previously thought [Sob87].

Shown in Figure 2.10 is the dynamical fission barrier (see below) for even-even nuclei as a function of Z and N. The symbols represent nuclei experimentally synthesized. Because the main contribution to the fission barrier is the shell correction energy, details of this figure are similar to those of Figure 2.9. The barriers in the deformed region are actually larger than those in the spherical region. However, the spherical nuclei barriers are broader.

The shell correction energy greatly affects the SF-decay half-lives, as shown in Figure 2.11. Plotted are the experimental and theoretical SF-decay partial half-lives, where the theoretical half-lives are calculated by a macroscopic (Yukawa-plus-exponential [Kra79]) model (i.e., no microscopic terms used). Thus, the difference between the values is a measure of the shell effects. As can be seen, these effects can cause as much of an effect as 15 orders of magnitude (for the case of ^{260}Sg) in the SF-decay half-life. Clearly, many of these nuclei could never exist without the stabilizing influence of shell effects.

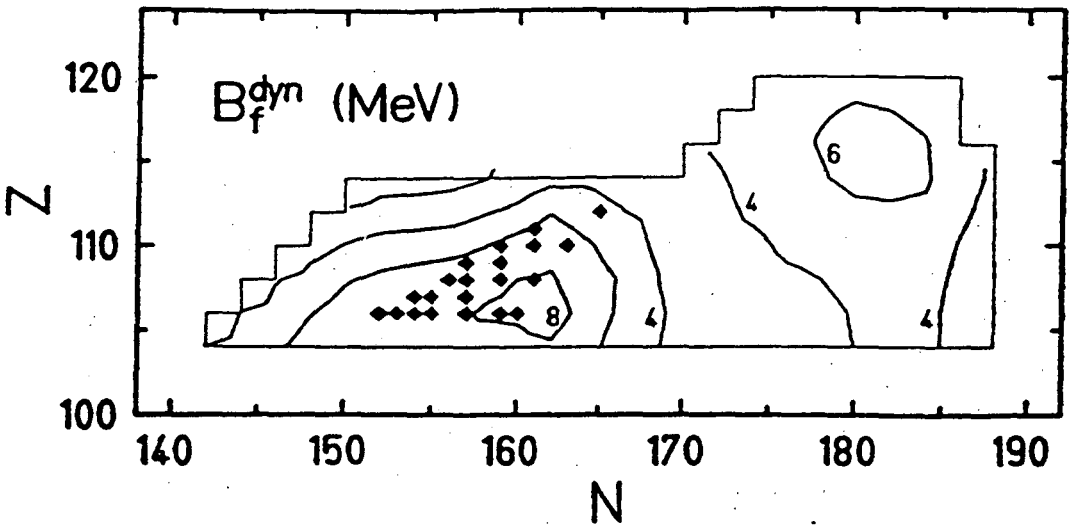

Figure 2.10: Contour map of the dynamical fission barriers for elements 104-120. Symbols represent experimentally-synthesized isotopes (from [Smo97]).

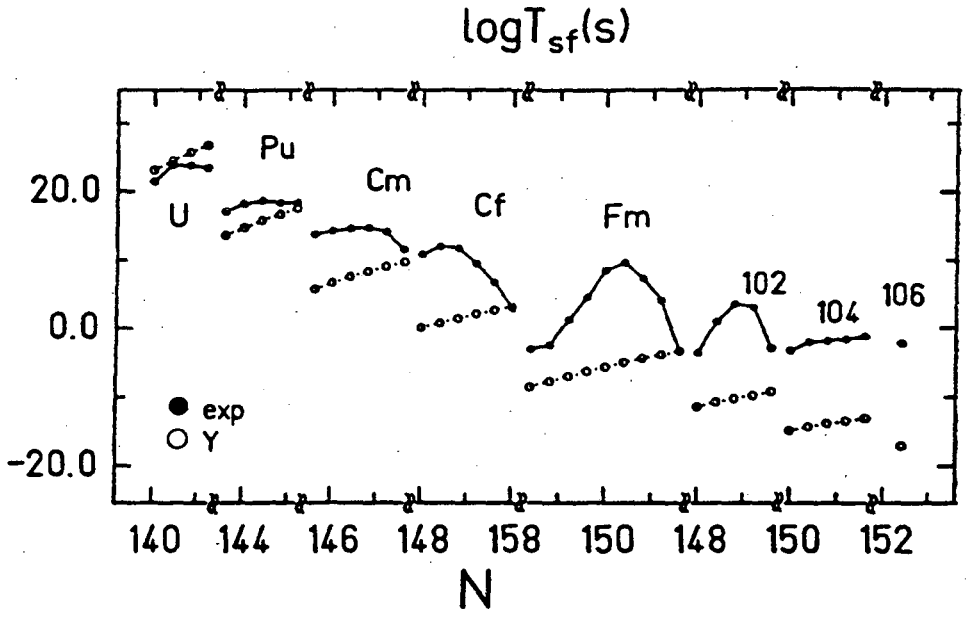

Figure 2.11: Logarithm of spontaneous-fission half-lives T_{sf}. (exp) denotes experimentally determined values. (Y) denotes macroscopically-calculated theoretical values. (From [Pat89])

Spontaneous fission decay half-lives are calculated using the formula

$$T_{sf} = T_o P^{-1} \tag{2.23}$$

In this equation, P is the probability of barrier penetration by the nucleus and T_o is the half-life when $P = 1$. T_o is calculated by

$$T_o = 2\pi \ln 2 / \omega_o \tag{2.24}$$

where ω_o is the frequency corresponding to the zero point energy of the nucleus. The probability in Equation 2.23 is obtained by the WKB (Wentzel-Kramers-Brillouin) approximation

$$P = \left[1 + e^{2S(L)}\right]^{-1} \tag{2.25}$$

where $S(L)$ is the action integral along a one-dimensional trajectory L in a multidimensional deformation space

$$S(L) = \int_{s1}^{s2} \left\{ \frac{2}{\hbar^2} B_L(S)\left[E_L(S) - E_o\right] \right\}^{1/2} ds \tag{2.26}$$

$E_L(s)$ is the potential energy at a position s along the trajectory L, $B_L(s)$ is the effective inertia at position s, E_0 is the equilibrium potential energy of the fissioning nucleus, and points s_1 and s_2 are the entrance and exit positions. The effective inertia $B_L(s)$, which describes a nucleus' resistance to shape changes, is given by

$$B_L(s) = \sum_{ij} B_{\alpha i \alpha j}(s) \frac{d\alpha_i}{ds} \frac{d\alpha_j}{ds} \tag{2.27}$$

where α_i and α_j are the deformation parameters β_λ, and $B_{\alpha i \alpha j}$ is the inertia (mass) tensor

$$B_{\alpha i \alpha j} = 2\hbar^2 \sum_{\nu\nu'} \frac{\langle \nu | \partial H / \partial \alpha_i | \nu' \rangle \langle \nu | \partial H / \partial \alpha_j | \nu' \rangle}{(E_\nu + E_{\nu'})^3} (u_\nu \upsilon_{\nu'} + u_{\nu'} \upsilon_\nu)^2 + P^{ij} \tag{2.28}$$

which describes the inertia with respect to its deformation. In this equation, H is the Hamiltonian, u_ν and υ_ν are the BCS variational parameters, and E_ν is the quasiparticle energy corresponding to the single-particle state $|\nu\rangle$. P_{ij} describes the effect of collective motion on the pairing interaction.

The determination of the fission path (trajectory) is done dynamically. This means that they are calculated along a trajectory, L_{dyn}, for which the action integral (Equation 2.26) is minimal (i.e., the path of least action), with the inertia tensor (Equation 2.28) taken into account. Calculations can be simplified by noting that the higher multipolarity deformations β_6 and β_8 are small and change very little along the fission

path (see Figure 2.6), thereby not affecting the effective inertia. Because of this, the four-dimensional space used is $\{ \beta_2, \beta_4, \beta_6^m, \beta_8^m \}$ in which β_6^m and β_8^m are values of β_6 and β_8 at which the potential energy is minimized at each point (β_2,β_4).

Figure 2.12 shows the potential energy surface and the dynamical trajectory, L_{dyn}, of ^{266}Sg as it undergoes fission. The potential energy surface plot gives values of the potential energy at various stages of deformation, β_2 and β_4, as the nucleus undergoes fission. This figure gives a more realistic representation of the barrier toward fission than the simple one-dimensional plot in Figure 2.2. It shows what path (i.e., what types of deformations) the nucleus must undergo to fission and what shape the fission fragments will have. The dynamical path tends to be straight with a small slope with respect to the β_2 axis, a result of requiring the minimization of the action integral, and thus the effective inertia. For comparison, the path, L_{stat}, obtained by performing the calculations in a static way is shown in Figure 2.12. Static calculations use a phenomenological formula for the inertia function, which has free parameters to fit to experimental data. Also, they do not take into account the shell structure of the nucleus, as they are in dynamical calculations using Equation 2.28. While the static method follows the path of lowest potential energy, this requires a large effective inertia and large action integral. The barriers can be seen with respect to β_2 in Figure 2.13. The dynamical path has a larger fission barrier and is of a different shape than that of the static path. Because small differences in fission barriers greatly affect half-lives, different treatments of the calculations clearly will give drastically different predictions for these values.

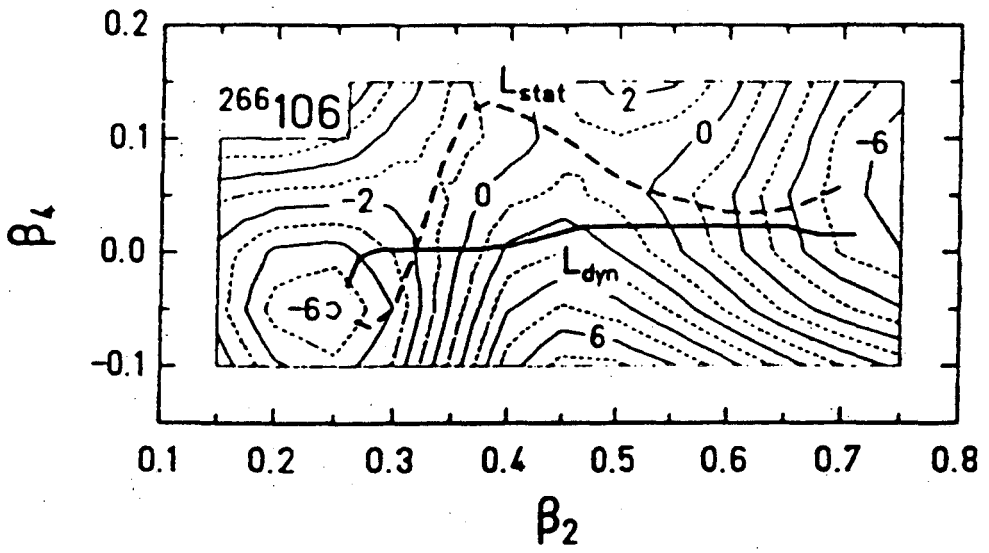

Figure 2.12: Contour map of the potential energy (in MeV) calculated as a function of the deformations β_2 and β_4, for the nucleus ^{266}Sg. At each point (β_2, β_4), the energy is minimized in the β_6 and β_8 degrees of freedom. The energy difference between neighboring solid lines is 2 MeV. Dynamical, L_{dyn}, and statical, L_{stat}, fission trajectories are shown. (From [Smo95b])

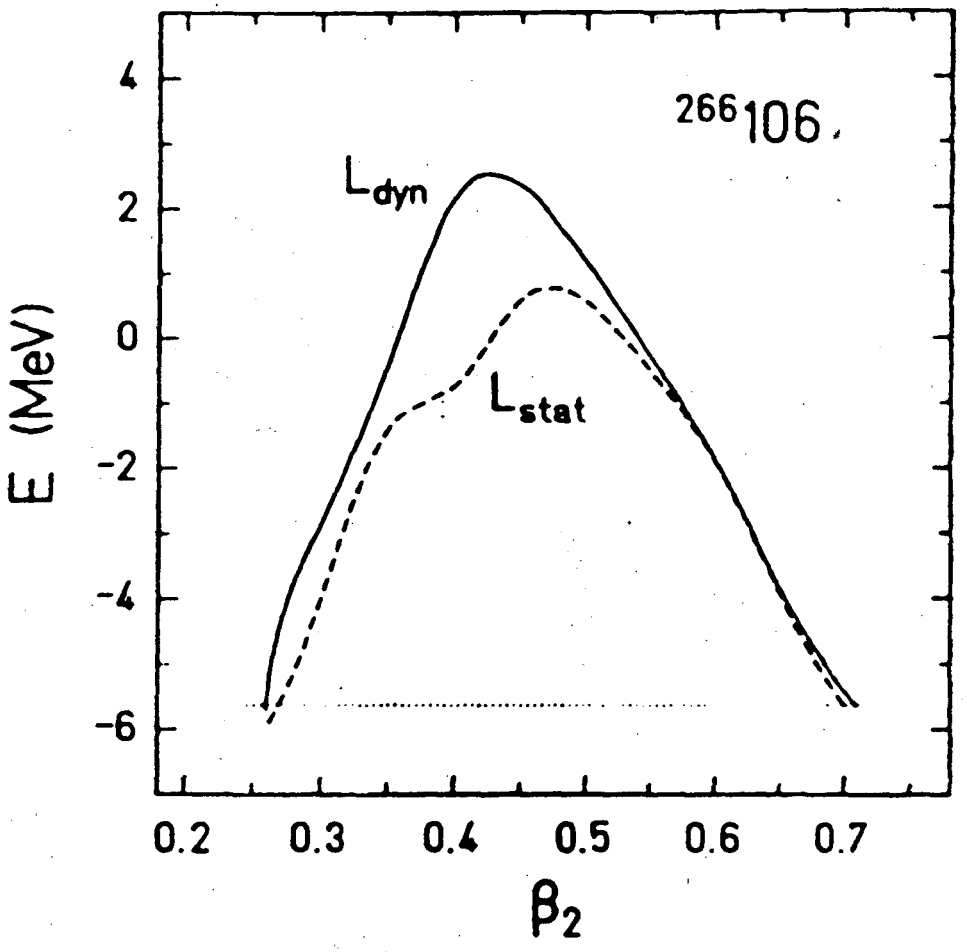

Figure 2.13: Shape of the potential-energy barrier for ^{266}Sg calculated along the dynamical and statical fission trajectories. (From [Smo95b])

The theoretical and experimental (where available) half-lives of deformed and spherical superheavy nuclei are plotted in Figure 2.14. The partial α-decay half-lives are calculated using the phenomenological formula of Viola and Seaborg [Vio66] using readjusted parameters recently determined [Smo95,Smo96]. The partial SF-decay half-lives are analyzed in a dynamical way, with the inertia (mass) tensor taken into account [Smo97]. As can be seen, there is evidence for the closed deformed shell effect at N = 162 (and also to a lesser extent at N = 152 for Z = 104 and 106), in addition to the obvious closed spherical shell at N = 184. The more pronounced peak caused by the N = 184 shell is because of the broader fission barriers and larger effective inertia of these spherical nuclei. Also, it is shown that SF is more sensitive to shell effects than is α-decay. This causes most of the isotopes beyond Z = 104 to be more stable toward SF-decay than toward α-decay, and to have SF-decay half-lives that increase more rapidly compared to α-decay half-lives.

Plotted in Figure 2.15 are the theoretically-calculated half-lives [Smo95] along with the experimentally measured half-lives recently determined for isotopes of Element 110 [Hof95d,Hof95e,Ghi95,Laz96]. Although the experimental half-lives are all odd-A nuclei (while the theoretical values calculated are even-even), they illustrate a few important points. First, the prediction that the SF-decay half-lives would be much longer is corroborated by the fact that only α-decay and no SF was observed in the experiments. Evidently, the total decay is governed by α-decay. Second, the deformed shell at N = 162 is hinted at by the experimental values, which mirror the shape of the curve predicted

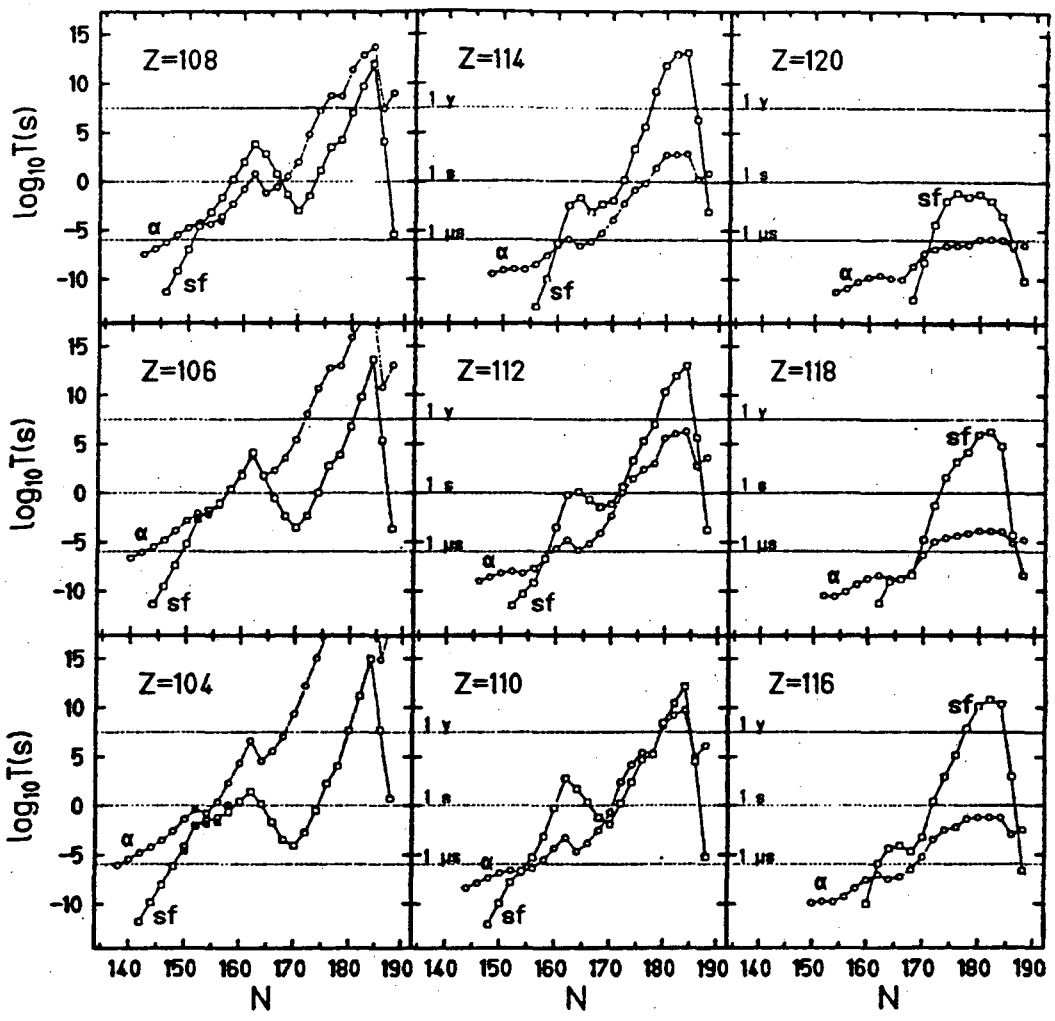

Figure 2.14: Logarithms of the theoretical spontaneous-fission (sf) and alpha-decay (α) half-lives calculated as function of the neutron number *N*, for the elements 104-120. Available experimental values are also shown (filled symbols). The lower horizontal dashed line indicates about the lowest half-life (1 μs) of a nucleus that can be detected in a present-day set-up. (From [Smo97])

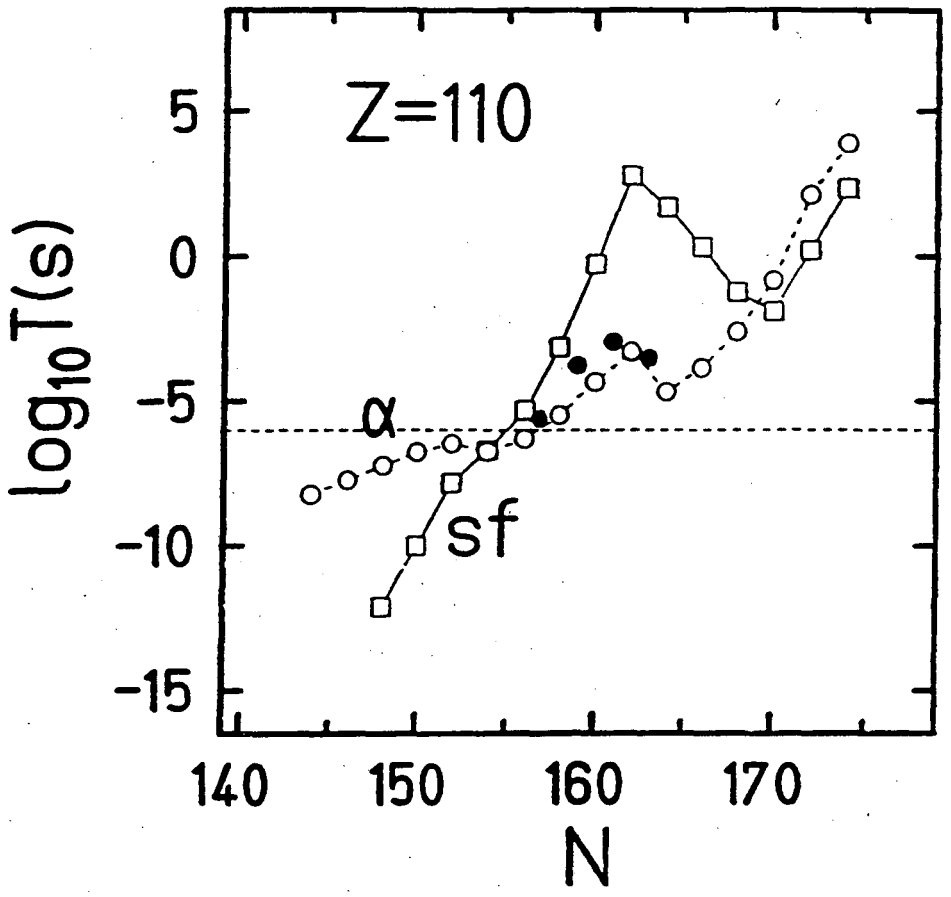

Figure 2.15: Comparison between theoretically-predicted (open circles) and experimentally-measured (filled circles) α-decay half-lives, for isotopes of the element 110. (From [Sob97])

by the calculations. And third, these experimental half-lives, while generally agreeing with predictions, give an indication of the stabilizing effect of the odd-nucleon on SF-decay half-lives. For example, the value obtained for the α-decay of $^{267}110$ is approximately equivalent to the value predicted for the SF-decay half-life of $^{267}110$. However, because no SF-decay was observed, the odd particle must cause a longer partial SF-decay half-life, due to the hindrances involved.

3 SF properties

Although SF was discovered in 1940 as a natural mode of decay of ^{238}U with a partial SF-decay half-life of nearly 10^{16} years, detailed studies of SF properties were not conducted until higher Z elements with shorter SF-decay half-lives were synthesized. The availability of 2.6-y ^{252}Cf, which has a high specific activity, in milligram quantities during the 1960's, stimulated numerous detailed measurements of the mass, charge, and kinetic energies of the fission fragments. Such studies have been extended to numerous isotopes of still heavier elements as they have been synthesized at accelerators and techniques have been developed for measuring ever shorter half-lives. The 1992 and 1995 reviews by Hoffman, Hamilton, and Lane [Hof95,Hof95b] tabulated all of the SF-decay half-lives and the various properties of the fission fragments that were reported up to that time. Many other reviews of SF and low-energy (induced) fission have been published [von69,Hof74,Hof89b,Hof89c,Hul90,Wag91,Hof95] since the late 1960's. The total number of SF activities reported as of 1999 is still about 135.

3.1 Half-lives

3.1.1 Nuclides with even proton and neutron numbers

The total half-lives and partial SF-decay half-lives of spontaneously fissioning nuclei are given in Appendix A. The partial SF-decay half-lives of even Z-even N (e-e)

nuclei in their ground states are plotted vs. neutron number in Figure 3.1. Although the half-lives generally decrease with increasing atomic number, Z, there is an overlapping of half-life values so that it is very difficult to identify a new SF activity based on half-life alone. The extra stability observed for $N = 152$ beginning around curium (96) extends through nobelium (102), but seems to have been "washed out" for elements heavier than rutherfordium (104). This change has been discussed in detail in [Hof95b,Hof89c,Hul90,Wag91] and has been attributed not only to destabilization of the $N = 152$ subshell, but to the lowering of the energy of the second barrier to fission (see [Poe95]) below the ground-state energy. However, recent reports [Lou94,Laz94] of longer than expected α-decay and SF-decay half-lives in the region of elements greater than or equal to 104 and near $N = 162$ have been interpreted as a result of the predicted deformed shells [Cwi89, Pat91, Pat91b, Cwi92, Sob94, Sob94b, Smo95b,Smo97] in the region of $N = 162$ and $Z = 108$. For example, the e-e isotope, ^{266}Sg ($Z = 106$), was reported [Tür98] to decay primarily by α-particle emission with an estimated half-life of ~21 s, rather than by SF with a few millisecond half-life as might otherwise have been expected.

The SF-decay half-lives calculated for both the superheavy deformed nuclei and the superheavy spherical nuclei are shown in Figure 3.2 [Smo95b,Smo97]. As seen in the figure, the predicted SF-decay half-lives increase as a function of neutron number up to the deformed subshell at $N = 162$ followed by a decrease to about $N = 170$; then another increase in half-life up to the spherical closed shell at $N = 184$, followed by another decrease. Figure 2.14 shows the logarithm of the predicted SF-decay half-lives

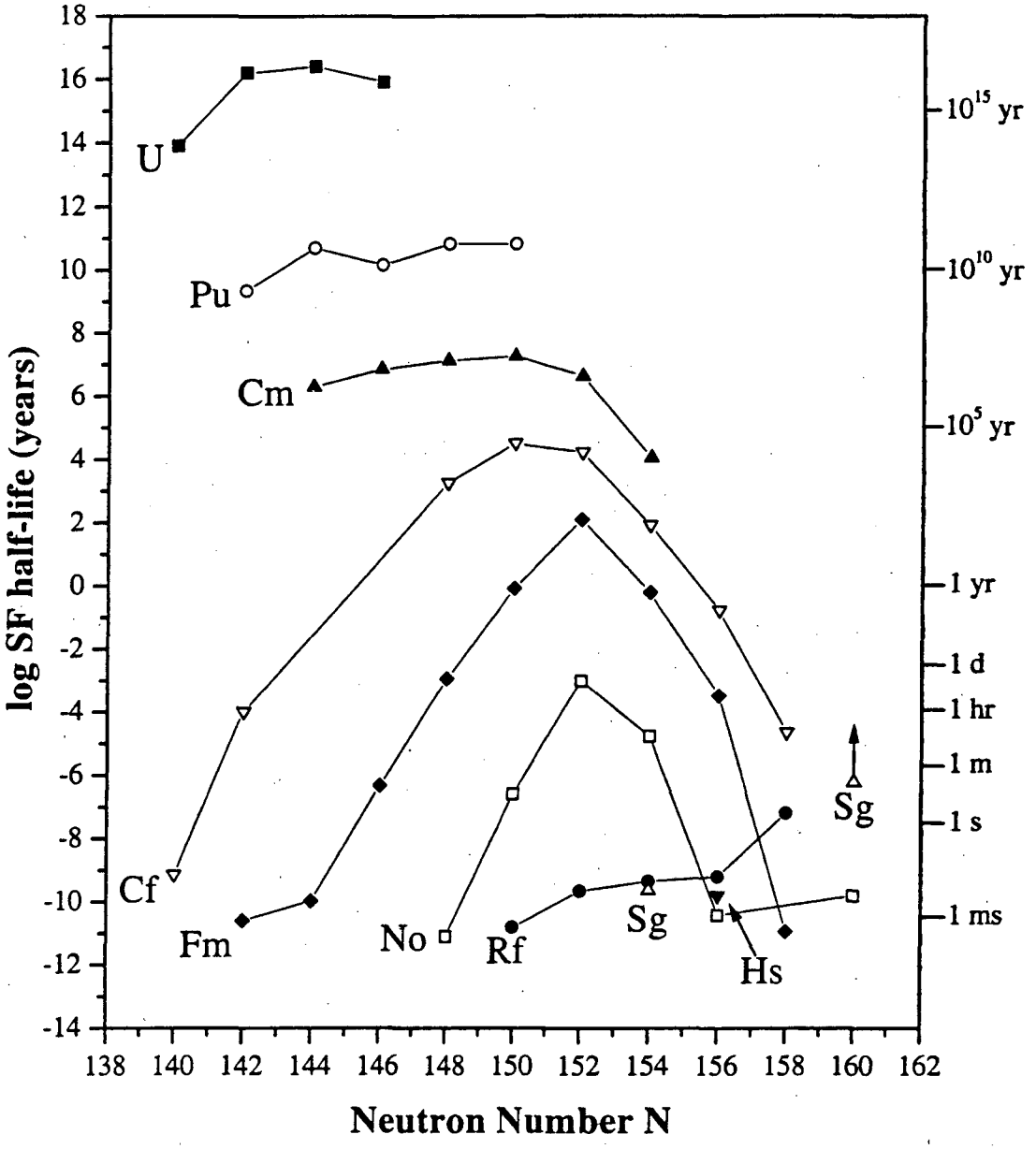

Figure 3.1: Logarithms of SF half-lives of e-e nuclei plotted vs. neutron number. Arrows are used to indicate lower limits. (Data from [Hof95] and [Hof95b])

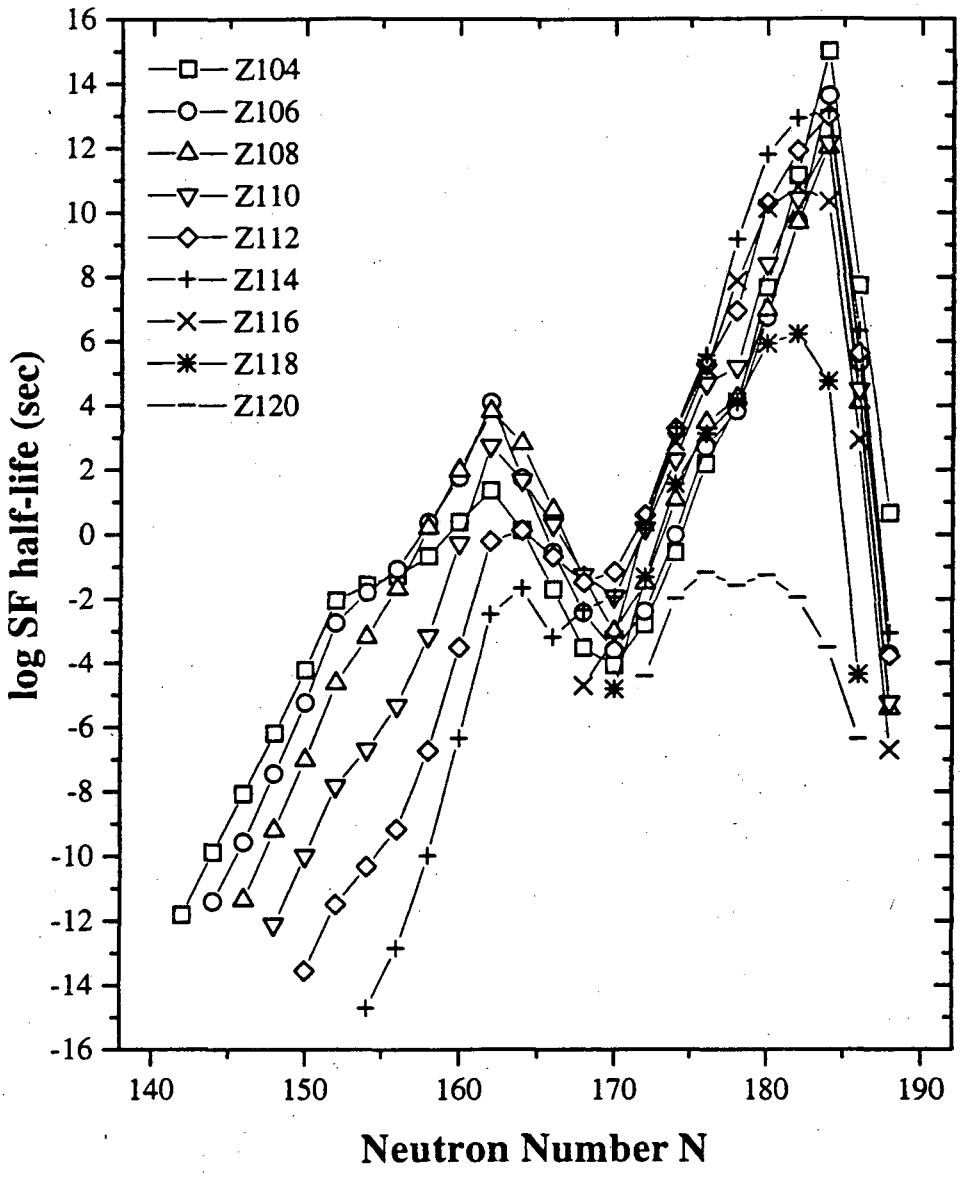

Figure 3.2: Logarithms of the theoretical SF half-lives for even-Z elements 104 through 120 as a function of even neutron number 142 through 188. (Data from [Smo95b,Smo97])

together with the predicted α-decay half-lives for the e-e isotopes of elements 104 through 120. For element 104 the longest predicted SF-decay half-life (~23 s) in the deformed region occurs at $N = 162$ which is still several orders of magnitude shorter than the predicted α-decay half-life. Thus SF would dominate and determine the half-lives of these nuclides. At higher neutron numbers, approaching the spherical $N = 184$ shell, the nucleus becomes quite stable toward SF, and the α-decay half-lives, less affected by shell structure, become ten to fifteen orders of magnitude longer compared to the SF-decay half-lives. However, these neutron-rich nuclei are far from the region of β-stability. At element 106, SF should not dominate until $N > 164$, and at element 108, SF should not dominate until $N > 166$. For $Z = 110$, 112, and 114, the α-decay half-lives are predicted to be microseconds to milliseconds until about $N = 172$ when they reach about a second and are increasing. Since the SF-decay and α-decay half-lives are calculated to be comparable, it seems likely that these isotopes will have appreciable SF-decay branches and half-lives long enough to permit study if they can be produced in reasonable yields. For $Z = 116$, 118, 120, α-decay dominates for almost all values of N, though there are some isotopes in the microsecond range that may compete by SF-decay. However, SF-decay half-lives of seconds or more may be expected for many odd isotopes of these elements because of the hindrances to fission caused by odd-particle effects (see next section), and thus should allow study of still heavier isotopes.

Because of the extreme sensitivity to details of the height and shape of the fission barrier (or barriers), calculation of SF-decay half-lives is extremely difficult. Furthermore, the barriers may be dependent on the exact route in the potential energy

surface that the nucleus follows en route to fission. Shell effects are of prime importance in stabilization of the heavy element isotopes toward decay by SF and must be included in any realistic calculation of half-lives.

3.1.2 Nuclides with odd-proton and/or odd-neutron numbers

The half-lives for e-o (even *Z*-odd *N*), o-e (odd *Z*-even *N*) and o-o (odd *Z*-odd *N*) nuclides are plotted in Figure 3.3. It is extremely difficult to obtain measurements for the o-o isotopes because often they decay by electron-capture to e-e nuclides which decay via SF with very short half-lives; unless SF in coincidence with the characteristic X-rays of the parent is measured it is nearly impossible to tell which isotope is spontaneously fissioning. In order to assess the effects on SF associated with odd nucleons—caused by the specialization energy arising from the conservation of spin and parity of the odd particles during fission—we define the SF hindrance factor (HF). The experimentally observed HFs for the SF-decay of odd proton or neutron nuclides are calculated relative to the SF-decay half-lives of their adjacent e-e neighbors as follows (if the half-life of only one e-e neighbor is known, it is used in the calculation):

- For odd *Z* and even *N*, o-e, (odd *A*):

$$HF = T_{1/2}({}^{A}Z)/[T_{1/2}({}^{A-1}Z\text{-}1) \times T_{1/2}({}^{A+1}Z\text{+}1)]^{1/2}$$

- Similarly, for even *Z* and odd *N*, e-o, (odd *A*):

$$HF = T_{1/2}({}^{A}Z)/[T_{1/2}({}^{A-1}Z) \times T_{1/2}({}^{A+1}Z)]^{1/2}$$

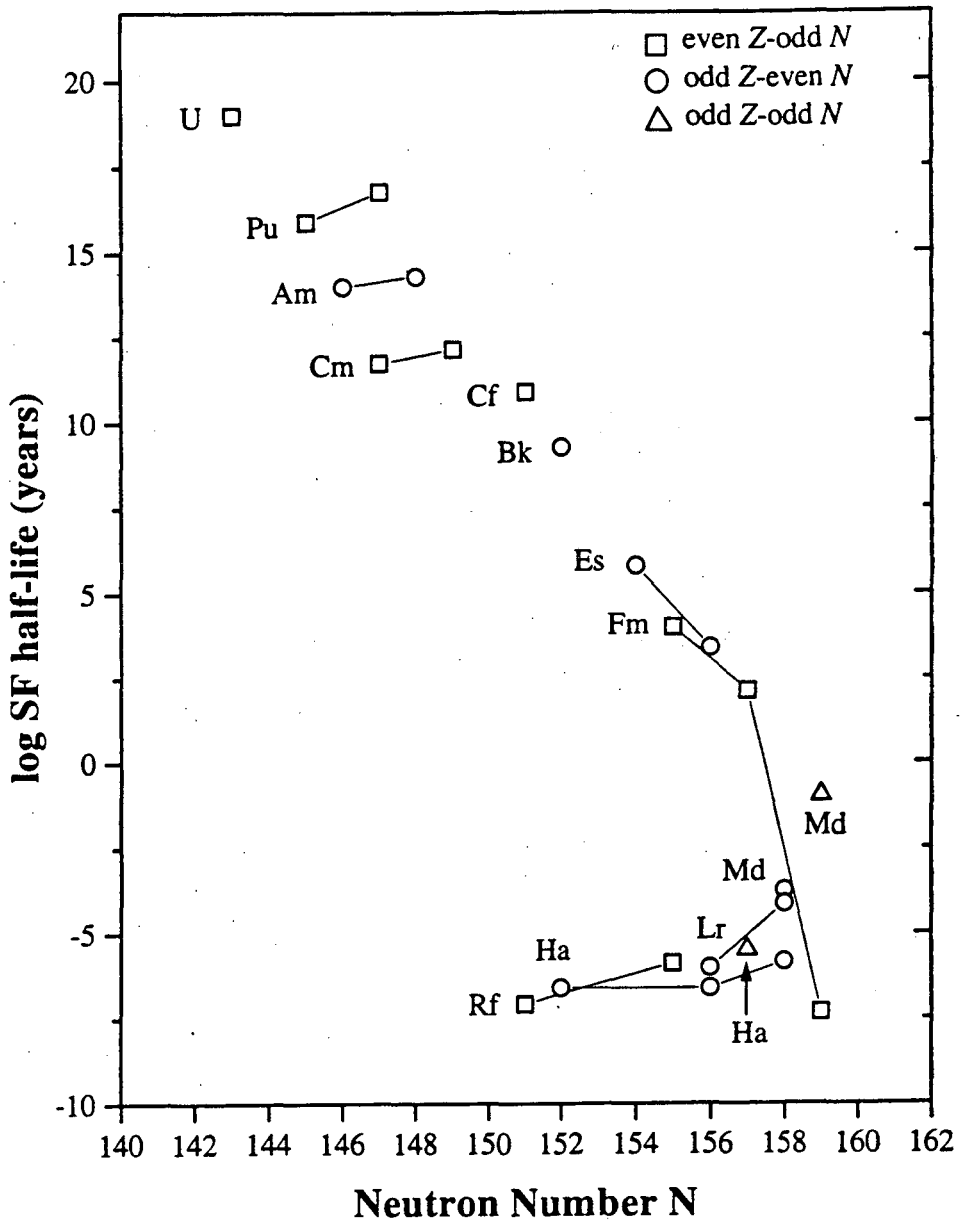

Figure 3.3: Logarithms of SF half-lives of e-o, o-e, and o-o nuclei plotted vs. neutron number. Lower limit values are not included. (Data from [Hof95])

In recent reviews [Hof89c,Wag91] of half-life data and systematics, it was pointed out that HFs have long been known to be associated with the SF-decay of nuclides having an odd number of protons or neutrons compared to those of their e-e neighbors. This makes the theoretical calculations of their half-lives even more difficult than for the e-e nuclei.

The logarithms of the HFs calculated for the known SF-decay partial half-lives of o-e and e-o isotopes are plotted in Figure 3.4 as a function of odd Z and odd N. New values (not just lower limits) for proton HFs for ^{259}Lr, ^{261}Lr, and ^{263}Ha (N = 156 and 158) have been obtained since the 1989 reviews and seem to be consistent with the previously measured values for Z = 103 and 105. They actually seem to show that the HF's are larger than the earlier limit values. In general, the logs of the HF's for actual measurements (not just limit values) are about 5 for both odd protons and neutrons, but for some of the high spin states such as N = 157 [9/2$^+$(615)] and Z = 101 [7/2$^-$(514)], the HF's are much larger.

It has been postulated that the HF's for o-o nuclei are the product of the odd proton and odd neutron HF's which would result in log HF's of the order of 10, if the log HF's average about 5. Now that a revised lower limit for the partial SF-decay half-life for the o-o nuclide ^{258}Md and new values for ^{258}Lr, ^{262}Lr, ^{262}Ha, ^{262}107, and ^{266}109 have been obtained, they can be compared with this estimate. The ^{258}Md shows log HFs of $\geq$ 7.1 relative to its e-e neighbors ^{256}Fm and ^{258}No. ^{258}Lr (> 78 sec) shows log HFs of > 4.7 and > 3.7 relative to its e-e neighbors ^{258}No and ^{258}Rf. However, ^{258}Md and ^{258}Lr might instead decay by EC and the SF observed is actually from the decay of their respective

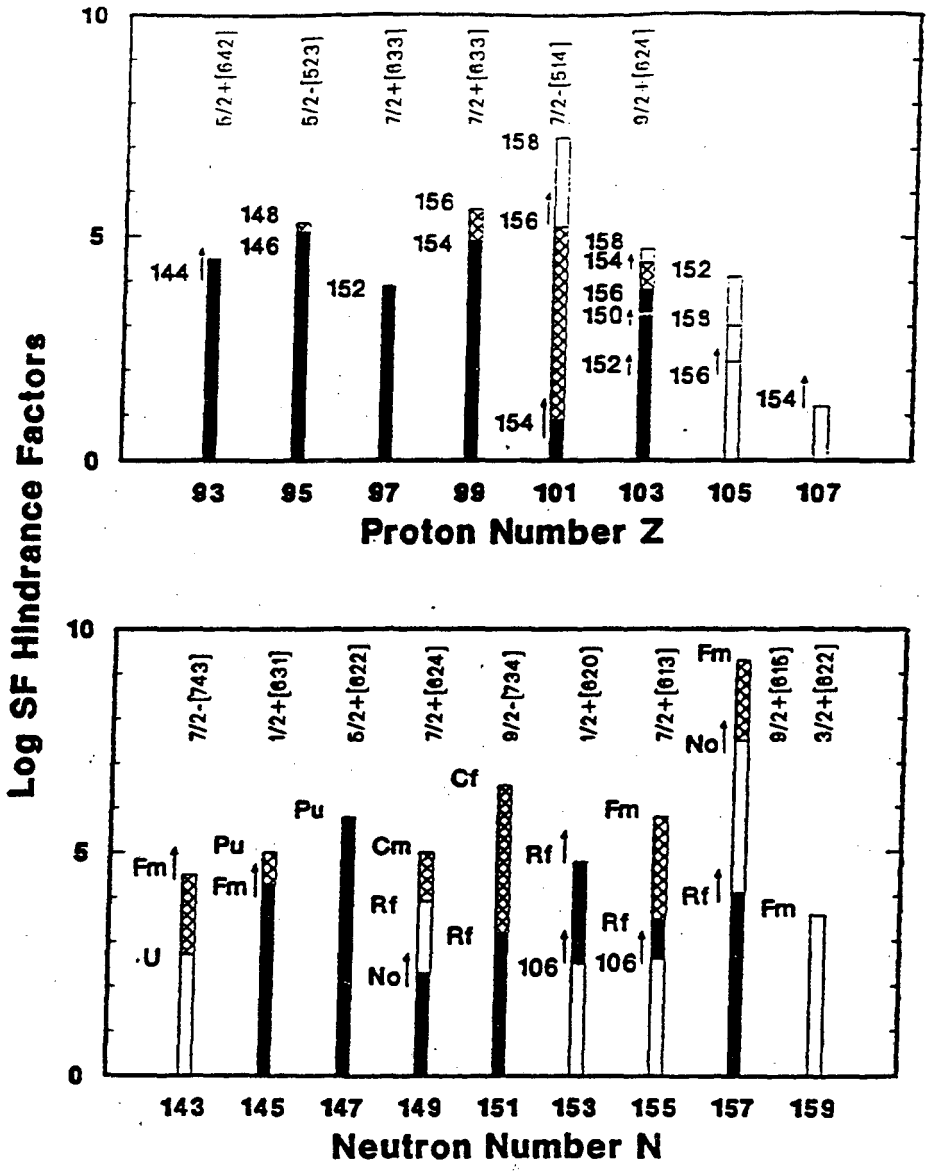

Figure 3.4: Logarithms of SF hindrance factors (HF) for odd-neutron and odd-proton nuclides. Lower limit values are indicated by arrows. An open bar indicates that the HF was calculated relative to only one e-e neighbor. A filled or hacked bar indicates that the HF was calculated relative to two e-e neighbors.

EC daughters, ^{258}Fm and ^{258}No. No hindrance can be calculated relative to its e-e neighbor ^{256}No whose SF-decay partial half-life of 550 sec is actually longer than the lower limit value of > 78 sec for ^{258}Lr. The unusual stability of the e-e isotope ^{256}No can be attributed to the stabilizing influence of the deformed N = 152 subshell which has disappeared by Z = 104 (see Figure 3.1) and may actually no longer be a stabilizing influence in Lr (Z = 103) either.

Lougheed et al. [Moo92] have calculated the HF for the o-o nuclides ^{260}Md as 9 x 10^9 (log HF ≈ 10) from their estimates of a hindrance of 3.6 x 10^6 (log HF = 6.6) for the odd proton (101) in ^{259}Md and 2.4 x 10^3 (log HF = 3.4) for the odd neutron (159) based on the hindrance from ^{259}Fm. They propose assignments of 7/2$^-$[514] for the 101st proton in ^{260,259}Md and 3/2$^+$[622] for the 159th neutron in both ^{259}Fm and ^{260}Md. These are very close to the values given by Hoffman [Hof89c] and in Figure 3.4 for Z = 101 and N = 159, respectively. The lower log HF of 3.4 for the 159th neutron, 3/2$^+$[622], is consistent with the hypothesis that there is less hindrance associated with the lower spin states. However, ^{262}Ha (102 sec) exhibits log HFs of only 3.3 and 3.7 relative to ^{260}104 and ^{262}104, whereas based on a log HF of about 3 for the 105th proton (see Figure 3.4) and > 4 to 7.4 for the 157th neutron in Rf, No, and Fm, a log HF of 7 or more might have been expected.

With odd-particle effects, the SF-decay partial half-lives can be greatly increased. While this makes study of the SF of odd-Z and/or odd-A nuclei more difficult than that of even-even nuclei, it has the beneficial effect of stabilizing the superheavy elements toward decay by SF, thereby making study of the heaviest elements possible.

3.1.3 Isomeric states

Spontaneous fission of isomeric states of actinide nuclei has been discussed by Baran and Lojewski [Bar87]. They calculated SF-decay half-lives of K-isomeric states on the basis of the microscopic-macroscopic method for an isomeric state assumed to be a 2-quasiparticle excited state with high angular momentum. They performed calculations for e-e nuclei with $96 < Z < 110$ and $144 < N < 158$ and found that the SF-decay half-life may be comparable to that of the SF-decay half-life of the ground state. They found for $Z \geq 104$ that the SF-decay half-lives of the isomers and ground states may be comparable, provided the spin of the K-isomer is sufficient to prevent it from decaying by other processes. The recent assignment [Lan96] of a 2.1-s SF activity to ^{262}Rf which already has a $\approx$ 50 ms SF activity assigned to it [Hof74] could be a case in point. Reasonable neutron and proton single-particle assignments for this nuclide could give a two-quasiparticle K-isomeric state with 9+ or 10-. It is important to investigate whether or not this phenomenon can occur as there is the possibility that measured half-lives assumed to be that of the ground state could actually be the half-lives of isomeric states, which would affect the interpretation of shell effects in these heavy nuclides [Gre94].

3.2 Properties of the fission fragments

A knowledge of the masses, atomic numbers, kinetic energies, and deformation energies of the individual fragments at scission, as well as their deexcitation modes, is necessary for understanding the SF process itself. Detailed studies have been performed in order to help understand the SF process and aid in developing and testing predictive theoretical models. An early comprehensive review of these properties for SF and low-energy fission was made in 1974 by Hoffman and Hoffman [Hof74]. The book on nuclear fission by Vandenbosch and Huizenga [Van73] and a recent review of the nuclear fission process [Wag91] contain more detailed information on the nuclear fission process in general. Recent reviews of SF [Hof80b,Hof89c,Hul90] have tended to concentrate on the SF properties of the heavier isotopes because of the interest in the dramatic change in properties which occurs in the region of the heavy Fm isotopes. In this region, a change of only one or two neutrons results in a dramatic change from asymmetric mass division with "normal" total kinetic energy (TKE) to narrowly symmetric mass division with very high TKE approaching the Q-value for fission.

The SF process is unique in that no energy is put into the nucleus before fission occurs which makes it much more sensitive than induced fission to the effects of relatively small changes in the nuclear structure and shell effects in both the fissioning nucleus and the resulting fragments. The total energy released in binary fission, E_f, is simply the energy equivalent (or Q-value) of the difference in mass of the fissioning nucleus and the masses of the two resulting fission fragments. There is, of course, a wide distribution of Q-values for SF of a given nuclide because of the multitude of different

mass and charge divisions that are possible. The energy of fission is divided between the kinetic energy, E_k, and the excitation or deformation energy, E_x, of the two resulting fission fragments. This fragment excitation energy can be subsequently dissipated by prompt neutron and/or photon emission. From measurements of the kinetic energies, masses, and atomic numbers of the primary fragments, the excitation energy of the fragments can be deduced. E_x can also be inferred from measurements of the total numbers and energy distributions of both the prompt neutrons and γ-rays emitted from the fragments, but these are generally not available for the heaviest isotopes which have small production cross sections and short half-lives. Average or most probable values derived from the distributions for all of these quantities are usually tabulated. As the TKE of the primary fragments approaches the Q-value for the reaction, there can be very little excitation (or deformation) energy in the fragments and consequently fewer neutrons or photons can be emitted.

3.2.1 Fragment mass, atomic number, and kinetic-energy distributions

Properties of mass and TKE distributions for SF are given in Appendix B. Early measurements of fragment mass-yield distributions from both SF and neutron-induced fission were obtained by radiochemical and mass spectrometric methods and were summarized by von Gunten [von69] in 1969. Although such measurements have perfect Z and A resolution they suffer from the fact that the distributions of the fragments after neutron emission are measured and the distributions at scission must be inferred after correction for these processes. In addition, time-of-flight and kinetic-energy

measurements have been performed for SF of ^{252}Cf and some lighter nuclides, but for the shorter-lived trans-Cf isotopes, most of the information about kinetic-energy and mass-yield distributions has been derived from measurements of coincident fission fragments with solid-state (SS) detectors. Again, distributions after prompt neutron emission are obtained, and corrections must be applied for prompt neutron emission unless neutrons in coincidence with the fragments can be measured. Since only the kinetic energy of the fragments is measured, the masses are obtained by conservation of momentum and kinetic energy: the ratio of the kinetic energies of the heavy fragment and light fragment is inversely proportional to the ratio of their masses. Therefore, the mass of the fissioning nucleus must be assumed, unless there is positive identification of its mass by some other method. Furthermore, the mass resolution of the SS detectors is not as good as with the other methods, but determination of major features and the most probable values of the mass and kinetic-energy distributions can be made. On-line systems using rotating wheels to collect short-lived SF nuclides on thin foils and move them between pairs of SS detectors for measurement have been devised [Hof80,Dou84,Hul86] and have furnished much information on mass and kinetic-energy distributions. Other methods such as gas-filled detection systems [Boi84] have been proposed, but are extremely difficult to implement for short-lived nuclides with low production yields which must be studied in nearly "on-line" experiments at the accelerators where they are produced.

Fission is often characterized according to the fission fragment mass yield plotted as a function of fragment mass as being "symmetric" or "asymmetric". Fission into two nearly equal-mass fragments is called symmetric while fission into two unequal mass fragments is called asymmetric. A distribution of different mass splits around the most

probable one has been found for all cases studied so far, but the widths of the mass peaks can vary widely. A schematic representation of mass-yield distributions (all normalized to fragment yield of 200%) for the SF of some heavy trans-Bk isotopes is given in Figure 3.5. Most of these distributions have been derived from SS measurements of the kinetic energies of coincident fragments. From such data, the masses are obtained via the conservation of momentum relationship, $M_1V_1 = M_2V_2$, by assuming the mass of the fissioning nucleus and a prompt neutron emission distribution for the fragments.

Prior to 1971 it was commonly believed that all SF resulted in asymmetric division, but with the discovery [Bal71] of enhanced yields for symmetric mass division of ^{257}Fm, there was a renaissance of interest in SF of the heaviest isotopes. It was subsequently found [Hof80c,Hul80] that ^{258}Fm and ^{259}Fm exhibited narrowly symmetric mass distributions. Measurements for still higher Z isotopes also showed symmetric mass division, but some had rather large full widths at half maximum (FWHM). Measurements for four No isotopes have now been made and they exhibit a similar trend toward symmetry with increasing mass although ^{262}No does not appear to have quite as narrow a distribution as ^{258,259}Fm.

It is interesting to compare the progression from asymmetric to symmetric mass distribution with increasing neutron number for Fm (Z = 100), No (Z = 102) and Rf (Z = 104) isotopes. The change from an asymmetric to symmetric mass distribution in No between N = 154 and 156 is not as abrupt as for Fm between N = 157 and 158, nor does the mass distribution become as narrowly symmetric even at N = 160 as it is for Fm at N = 159. Perhaps this is because the symmetric fragments for No cannot both have the Z = 50 closed shell configuration. It would be extremely interesting to measure the

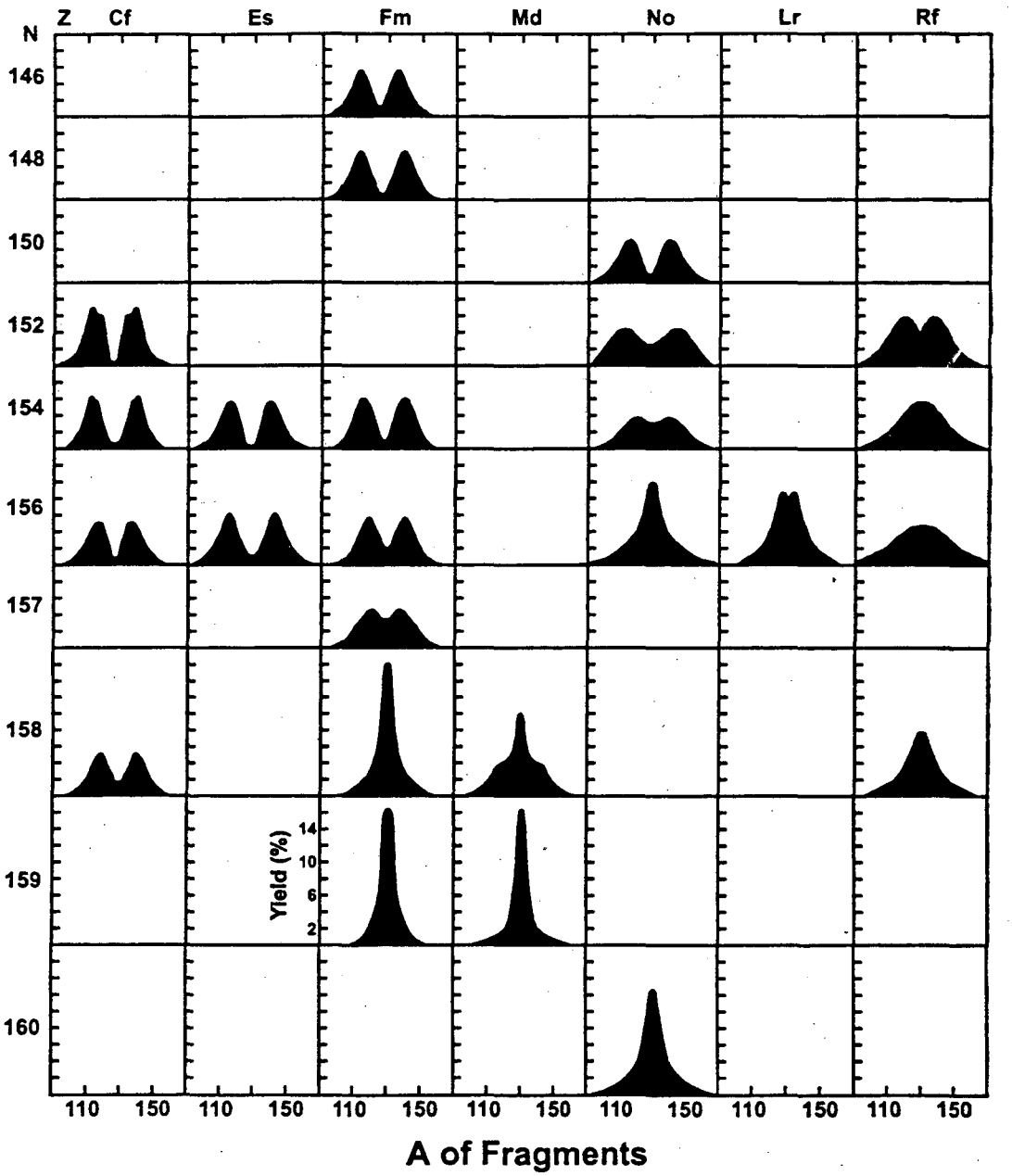

Figure 3.5: Schematic representation of all known mass-yield distributions (normalized to 200% fission fragment yield) for SF of trans-Bk isotopes.

distributions for ^{260}No and ^{261}No, the N = 158 and 159 isotopes. The data for Rf are not as complete, but Hulet [Hul94] postulated on the basis of the data for the N = 152, 154, and 156 isotopes of Rf that, because of the disappearance of the second barrier to fission, these isotopes exhibit "liquid-drop model" (LDM) type fission with broadly symmetric mass distributions and TKE distributions with only one component, close to empirical TKE fits based on the liquid-drop model. This can be seen in Figure 2.3 in Section 2.1.3. Compared to thorium, the heavier californium has a reduced second barrier. It has been theorized that the second barrier to fission should disappear completely for fermium isotopes above mass 260 and for all isotopes of rutherfordium [Ran76]. This will mark a return to liquid-drop type fission with a broadly symmetric mass division. However, our recent measurements of ^{262}Rf (N = 158) [Lan96] show a rather narrow, symmetric mass peak with "wings", not unlike the mass distribution observed for the transition nucleus ^{259}Md which also has 158 neutrons. In order to ascertain whether or not the properties of the Rf isotopes are being determined by disappearance of the second fission barrier, it is especially important to make measurements for the decay of ^{263}Rf to see if its mass distribution becomes more narrowly symmetric or exhibits the broad distribution characteristic of LDM type fission and whether its TKE becomes higher or is consistent with LDM fission.

Very little information is available for the odd-proton nuclides and additional measurements for Lr (Z = 103) would be most helpful. Although ^{261}Lr ($t_{1/2}$ = 39 m) and ^{262}Lr ($t_{1/2}$ = 216 m) are known [Lou87,Lou89] and can be produced by transfer reactions between ^{254}Es and heavy ions such as ^{18}O and ^{22}Ne, their fission properties have not

been measured because ^{262}Lr decays primarily via electron-capture (EC) to 5-ms ^{262}No which spontaneously fissions and masks the SF properties of both ^{261}Lr and ^{262}Lr. An upper limit of 10% was estimated [Lou87] for the SF-decay branch of ^{262}Lr.

The TKE distributions also showed unexpected changes and Figure 3.6 shows a plot of the average or most probable TKE's for SF as a function of $Z^2/A^{1/3}$. Anomalously high values that approach the fission Q-values are observed for ^{258}Fm, ^{259}Fm, and ^{259}Md. The very high TKE's and the narrowly symmetric mass distributions observed for these isotopes have been explained on the basis of symmetric division into two fragments with configurations close to doubly magic, spherical ^{132}Sn. Coulomb repulsion would be near maximum for touching spheres, leading to much higher TKE's than "normal".

Total kinetic-energy distributions for some trans-Es isotopes are given in Figure 3.7. It shows that many of the distributions, e.g., those for ^{258}Fm, ^{259,260}Md, and ^{258,262}No cannot be easily fit with a single Gaussian. Hulet and others [Hul86,Hul89] have fit the distributions for these isotopes with two Gaussians; one centered around 235 MeV and the other on 200 MeV. They called this "bimodal" symmetric fission, postulating that one symmetric mode leads to nearly spherical fragments with anomalously high TKE caused by the higher Coulomb repulsion, and the other leads to elongated fragments with lower TKE caused by LDM type fission in which the second fission barrier has disappeared. The early data for the "transition" nucleus ^{257}Fm, which give a most probable TKE of about 200 MeV, also show a small shoulder on the high-energy side. The range of TKE's for symmetric mass division of ^{257}Fm is extremely large, and may indicate shapes ranging from nearly spherical with TKE's approaching the

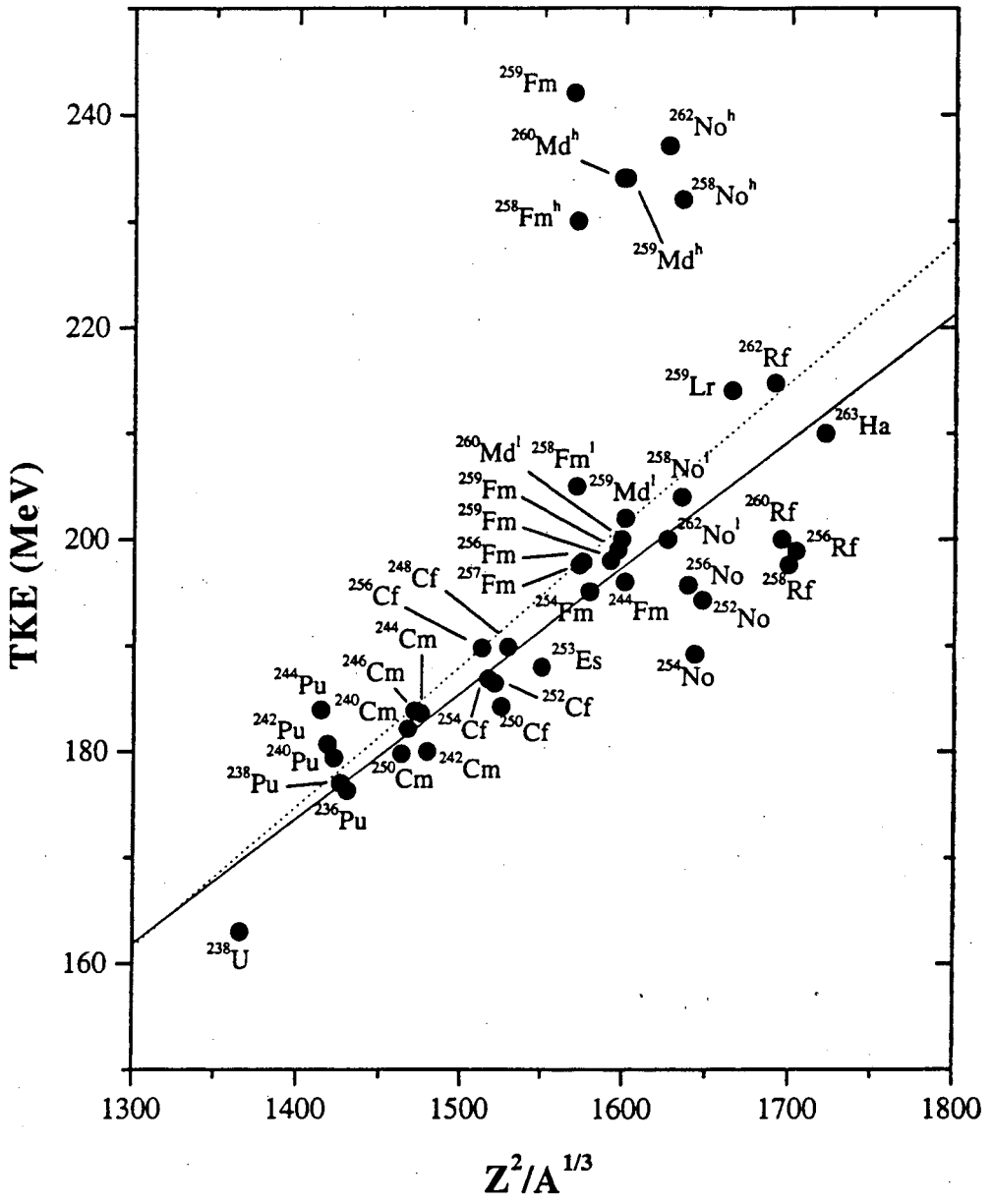

Figure 3.6: Average or most probable TKE vs. $Z^2/A^{1/3}$. The solid line is the linear fit of Viola et al. [Vio85] and the dashed line is the linear fit of Unik et al. [Uni74]. Data are from [Hof95] and [Hof95b] and have been corrected to the new Weissenberger parameters [Wei86] as discussed in [Hof95].

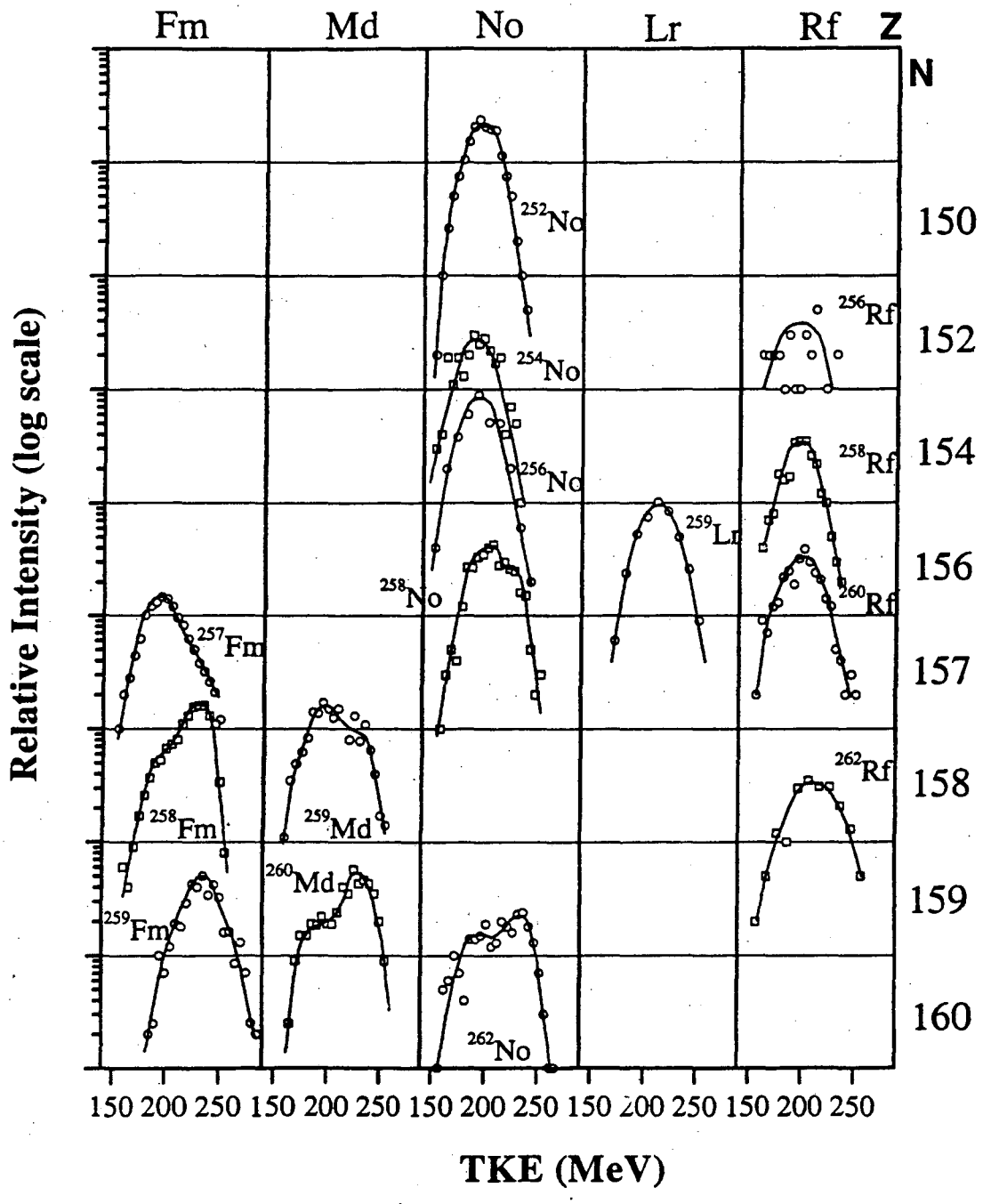

Figure 3.7: TKE distributions for SF of some trans-Es isotopes.

Q-value to deformed shapes with low TKE, and perhaps combinations of spherical and elongated shapes, which might be dubbed multimodal. However, several "transition" nuclei such as ^{256}No, ^{259}Lr, as well as ^{262}Rf show more or less symmetric TKE distributions with no evidence for more than one component and their mass distributions range from symmetric and asymmetric in ^{256}No to broadly symmetric in ^{259}Lr to narrowly symmetric with asymmetric "wings" in ^{262}Rf. These features can be seen more clearly in the contour plots shown in Figure 3.8. The fragments from these transition nuclides may show not just "bimodal" fission consisting of two compact (spherical) or two deformed fragments, but combinations [Wag91] including one compact fragment and one deformed fragment (with different deformations) as discussed in the scission-point model of Wilkins et al. [Wil76]. Thus, because of the extremely large variances of the TKE values for symmetric mass division, we should perhaps speak of "multimodal" [Hof89], rather than bimodal fission and a variety of combinations of different shapes, depending on the shell structure in the fissioning systems, could be involved.

Cwiok et al. [Cwi89] have explained bimodal fission in terms of calculations based on the macroscopic-microscopic model. The contour plot of Figure 3.9 shows the potential energy of ^{258}Fm as a function of β_2 and β_4 deformations, where the potential energy is minimized in the β_3, β_5, and β_6 degrees of freedom and the fission trajectory is calculated statically. Two paths for fission result: one giving rise to compact, reflection symmetric shapes (L_1) while the other leads to much more elongated shapes which are not necessarily reflection symmetric (L_2). The half-life for each mode will be the same because—since there is no barrier after the bifurcation point *D*—the paths have the same

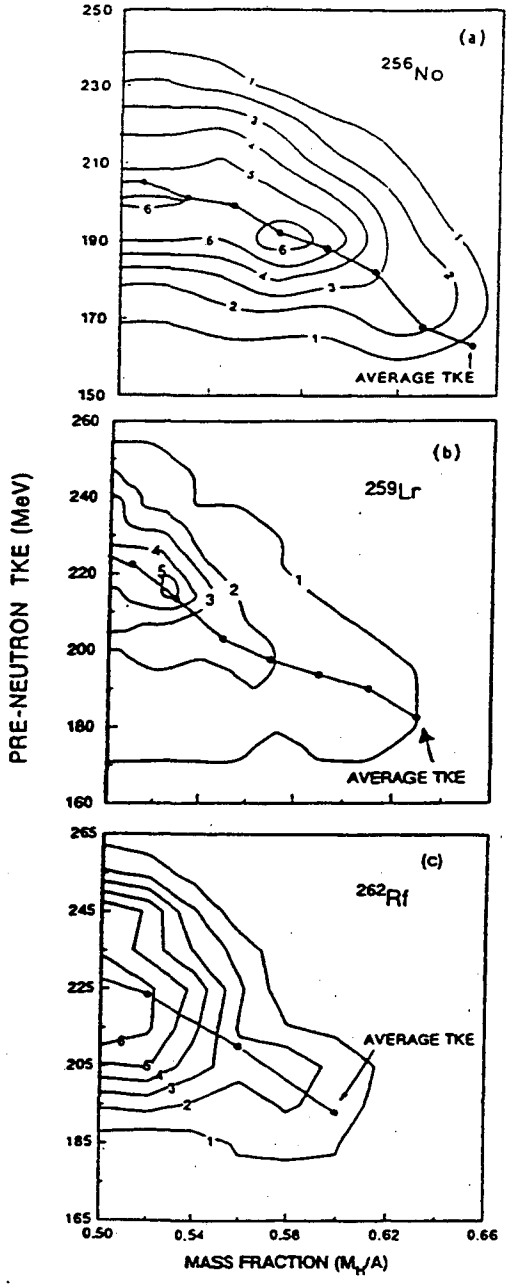

Figure 3.8: Contour plots of pre-neutron-emission TKE vs. mass fraction. The connected points represent average TKE as a function of mass fraction. (a) ^{256}No. The contours indicate equal numbers of events based on data groupings of 20 MeV X 0.04 units of mass fraction. Contours labeled 1 through 6 represent 10 through 60 events, respectively. (b) ^{259}Lr. Data are in groupings of 10 MeV X 0.02 units of mass fraction. Contours labeled 1 through 5 represent 10 through 50 events, respectively. (c) ^{262}Rf. Data are in groupings of 10 MeV X 0.02 units of mass fraction. Contours labeled 1 through 5 represent 4 through 24 events, respectively. (From [Hof95] and [Lan96])

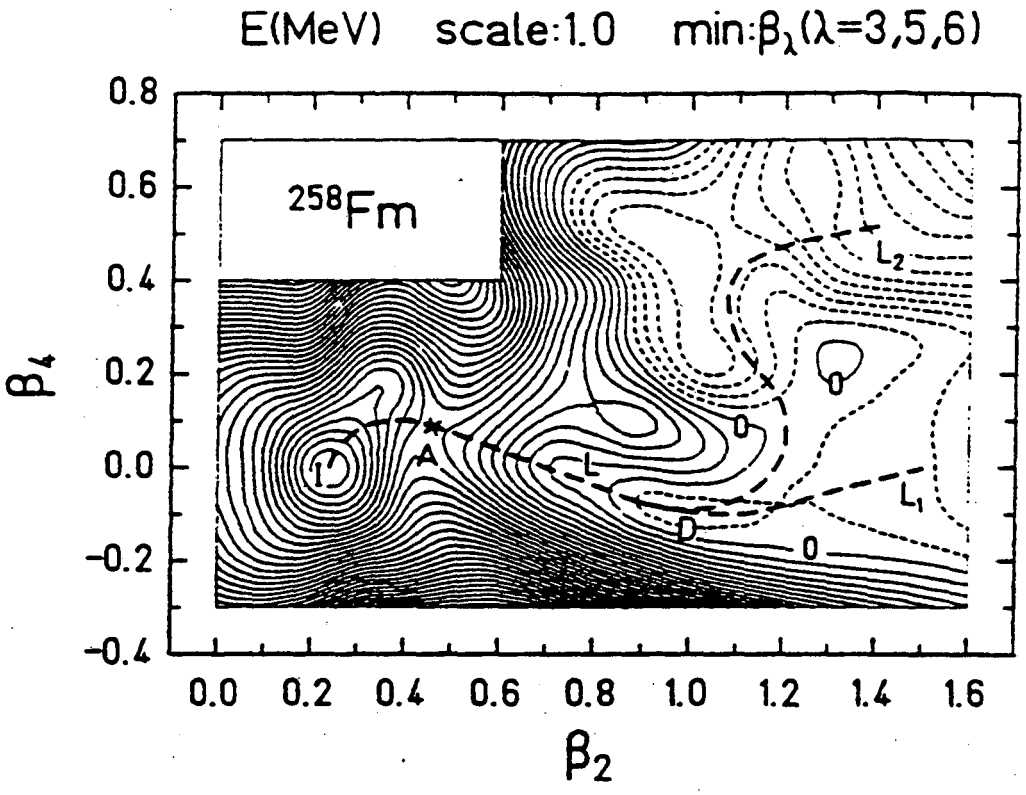

Figure 3.9: Contour map of the potential energy of ^{258}Fm as a function of the deformation parameters β_2 and β_4. The energy is minimized at each point in the deformations β_3, β_5, and β_6. Also shown is the fission trajectory *L*. (From [Cwi89])

fission barrier. The trajectories for the two modes are shown, with the predicted shapes along the paths, in Figure 3.10. This result is consistent with the observation [Hul89] of both high and low TKE fission in ^{258}Fm with nearly equal intensities. High-TKE fission will be observed for those compact fragments appearing due to path L_1. Low-TKE fission will be observed for those elongated fragments appearing due to path L_2.

Unlike the superheavy elements (see Section 2.2), calculations of the fission trajectory of actinides depend greatly on reflection asymmetric shapes. If only reflection symmetric shapes are included in the calculation above for ^{258}Fm, then the fission proceeds only to the compact shape valley, as shown in Figure 3.11. The path to the elongated fission fragments is blocked by a high ridge: a second barrier. It would appear that a similar calculation, which takes into account reflection asymmetric shapes and also includes dynamical effects in the fission process following the barrier, might give paths resulting in the variety of asymmetric and symmetric fragments with different deformations as indicated by the experimental results for the transition nuclei ^{256}No, ^{259}Lr, and ^{262}Rf.

The effects of neutron shells and fission channels in the SF of the even-even Pu isotopes 236, 238, 240, 242, and 244 have been carefully investigated by Wagemans et al. [Wag89,Dem95]. They have found rapidly varying fission fragment mass and kinetic energy distributions with the change of only a few neutrons. These were initially interpreted in the frame of the static scission-point model [Wil76] as arising from the changing relative importance of the $N = 82$ spherical fragment and the $N = 87$ deformed fragment shells and their combination with the $Z = 50$ spherical shell. More recently,

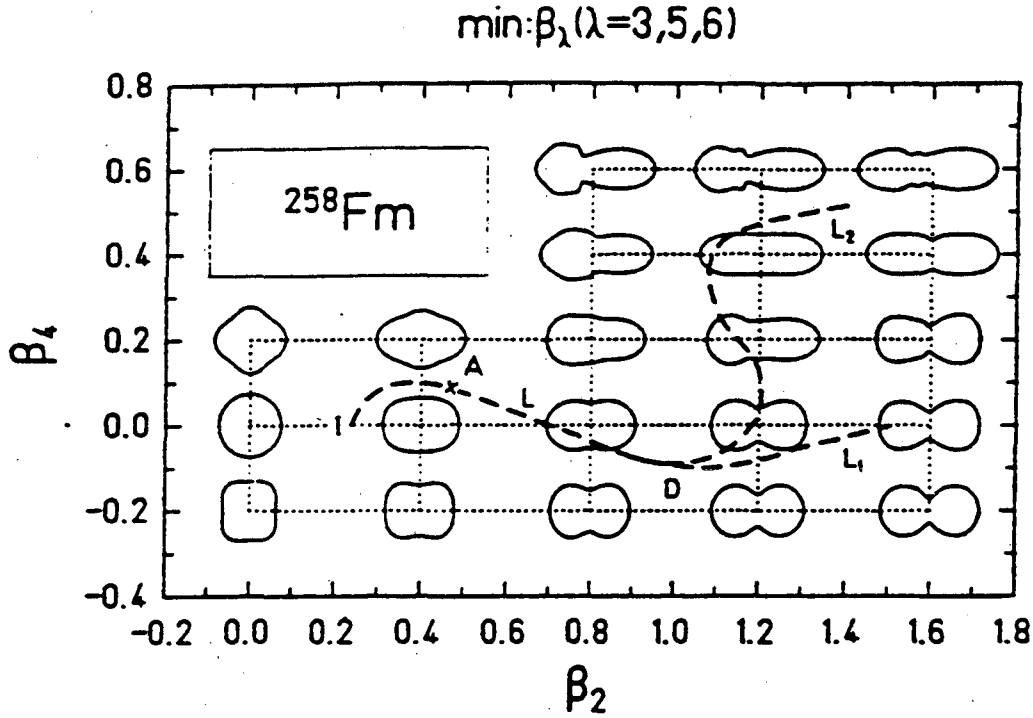

Figure 3.10: Similar to Figure 3.9, but showing the resulting shapes of the nucleus ^{258}Fm along the fission trajectory. (From [Cwi89])

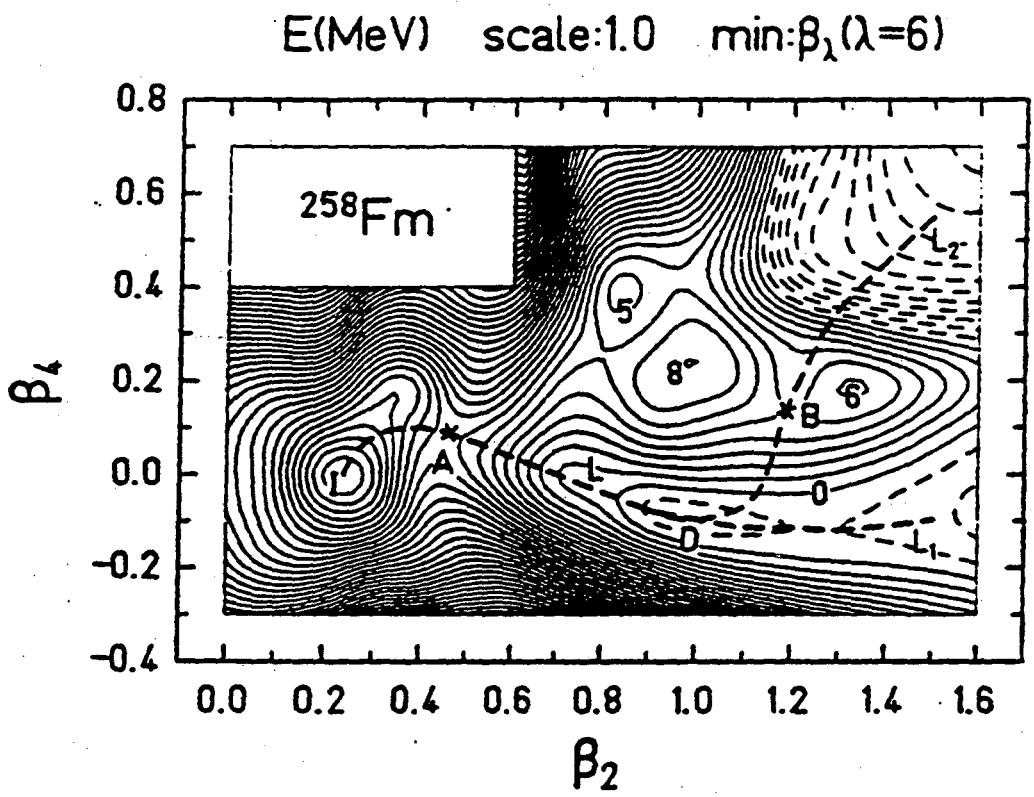

Figure 3.11: Similar to Figure 3.9, but where the calculations use only reflection symmetric deformations β_2, β_4, and β_6. (From [Cwi89])

these results have been interpreted in terms of the fission channel model of Brosa and coworkers [Bro83,Bro90] and the relative fragment yields have been correlated in detail with this multimodal, random neck rupture model. In this model the potential-energy surface as a function of the deformation is calculated for the fissioning nucleus from ground state to scission. The pre-scission configuration is allowed to rupture in a random manner according to Rayleigh instabilities [Ray78]. A filament of liquid remains stable as long as the wavelength of a perturbing vibration along the filament's axis stays smaller than the filament's circumference. However, if the wavelength grows longer, the vibrations increase without limit and finally disrupts the filament. The potential energy of the nucleus is calculated as a function of its nuclear deformation that is parameterized in terms of the half-length of the pre-scission shape, its neck radius and the position at which the neck ruptures. This gives rise to a number of different fission barriers which correspond to certain pathways within the calculated potential energy surface. These different pathways or channels give rise to different fragment mass and energy distributions, etc., and six different fission channels (three asymmetric channels called Standard I, II, and III, superasymmetric, superlong, and supershort) have been predicted for ^{252}Cf.

Essentially all of the information concerning charge division in SF is based on measurements of ^{252}Cf. Wahl [Wah88] has comprehensively evaluated the data for SF of ^{252}Cf and thermal neutron-induced fission of ^{233}U, ^{235}U, and ^{239}Pu, and derived parameters for empirical models which describe charge dispersion for constant mass number and mass number dispersion for constant atomic number. The element yields as

a function of atomic number that he has obtained for ^{252}Cf (SF) are given in Figure 3.12. The plotted points and the line are calculated from differing models, the Z_p and the A'_p model, respectively (see [Wah88]). Although he notes the preference for formation of fragments with Z = 50 because of the effect of the 50-proton shell in the fragments, he also points out that the maximum fragment yields occur at higher Z values of 52, 54, 56, and at the 82-neutron shell and above.

3.2.2 Prompt neutron emission

For most spontaneously fissioning nuclei, only the average number of prompt neutrons emitted per fission, $\bar{\nu}_T$, is known (see Appendix C). In some cases, the neutron multiplicity distributions (average number of neutrons emitted as a function of fragment mass) are also known and it was early shown that these multiplicity distributions could be fit by a Gaussian distribution [Ter59] with a variance, σ^2_ν = 1.17 for the thermal neutron-induced fission [Hof80b] of ^{235}U. As measurements were made for SF of ^{252}Cf and other heavy actinide isotopes, larger values of the variance were measured, reaching a value of about 4 for ^{252}No. The values of $\bar{\nu}_T$ are plotted in Figure 3.13 as a function of the mass number of the fissioning nucleus. In general, they increase with the proton number of the fissioning nuclide, and for trans-Pu nuclides, they increase with mass for a given Z. At Fm this trend is reversed and the average neutron emission is actually lower for ^{256}Fm and ^{257}Fm than for ^{254}Fm. This is because of the increased yield of symmetric mass division with high TKE, which means there is less energy left for prompt neutron and photon emission from the fragments. However, caution must be exercised in comparing

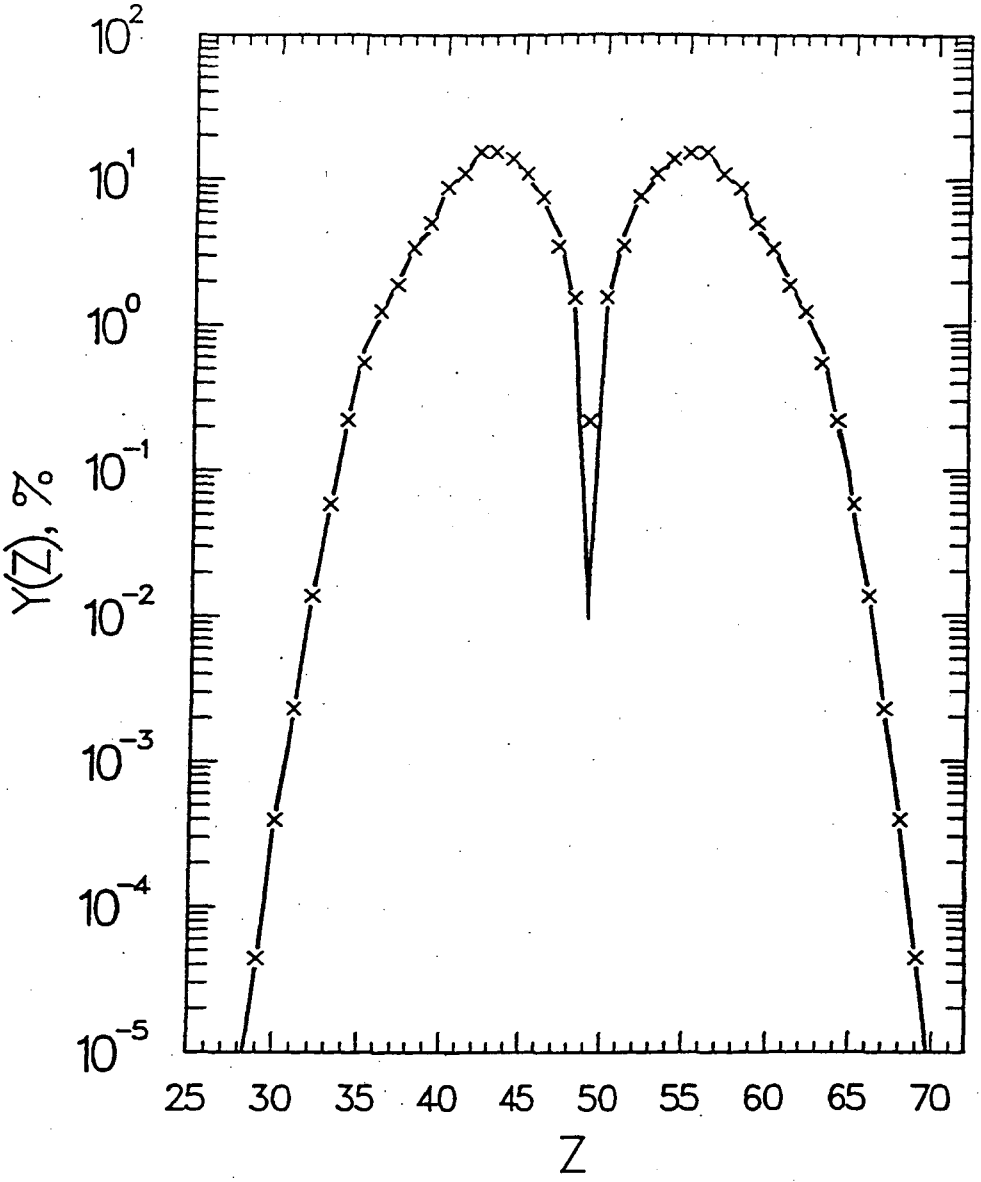

Figure 3.12: Element yield, $Y(Z)$, vs. atomic number for the spontaneous fission of ^{252}Cf. (From [Wah88])

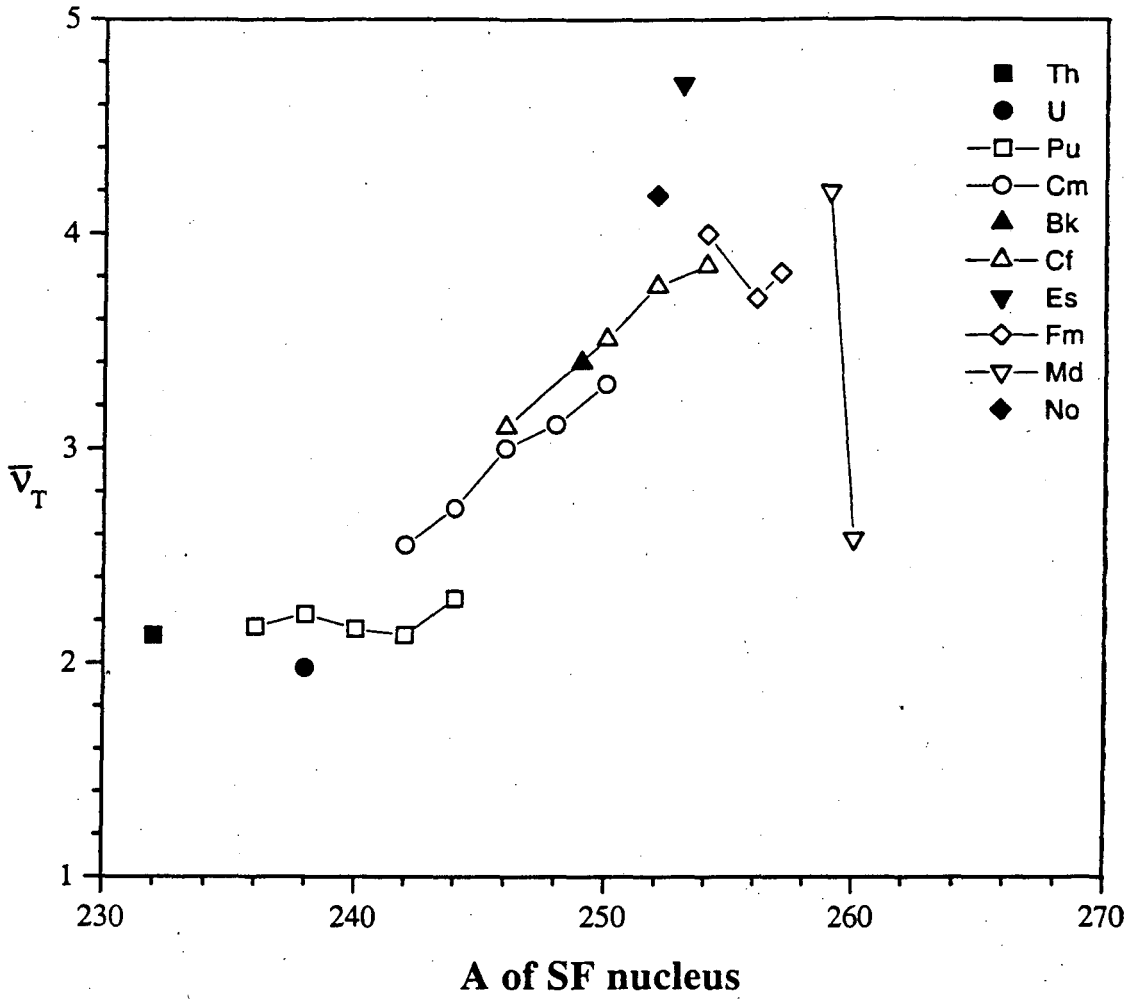

Figure 3.13: Average total neutron emission per fission, $\overline{\nu}_T$, as a function of A of the spontaneously fissioning nucleus. (Data from [Hof95] and [Ter87])

the TKE distributions because of the potential differences in the energy resolution of different systems and the observation that many of these cannot be fit by a single Gaussian component.

In the case of ^{259}Fm and ^{260}Md, whose most probable TKEs approach the Q-values for fission, it would be expected that prompt neutron emission from the symmetric, near-spherical fragments must also be very low. This was experimentally verified for ^{260}Md, which has a much more abundant high-energy component than does ^{257}Fm, by Wild et al. [Wil90] who measured a value of 2.58 for the average neutron emission from the fragments.

Early measurements [Hof80d] showed that the neutron multiplicities vary greatly for these isotopes as a function of mass split and TKE. For example, for ^{252}Cf the average neutron emission for the most symmetric mass splits was found to range from 2.1 for the highest TKE (210-220 MeV) events to 5.9 for the lowest TKE (150-170) events; for the most asymmetric events, the range was from 1.7 for TKE from 190 to 210 MeV to 4.8 for TKE from 150 to 170 MeV, although the overall $\bar{\nu}_T$ was measured to be 3.735 with a variance of 1.55. For the most symmetric events from ^{257}Fm, $\bar{\nu}_T$ ranged from only 1.1 for TKE > 240 MeV (close to the Q-value for fission) to 4.9 for TKE from 160 to 180 while the average neutron emission over all mass splits and TKEs was 3.8 with a variance of 2.5. These data could probably now be interpreted on the basis of Brosa's multimodal model.

Recently, Van Aarle et al. [van94] performed similar measurements for ^{252}Cf of the neutrons emitted from the fragments as a function of fragment mass and kinetic

energy. From an investigation of the correlations between the neutron multiplicity and the TKE of the fission event, they derived SF parameters in order to search for the six different fission channels predicted by Brosa et al. [Bro90] and found evidence for all channels, although the intensity of the superasymmetric mode was only 0.3%. They also derived schematic pre-scission configurations for these various modes, including the number of neutrons emitted from the light and heavy fragments.

Because information about neutron emission as a function of fragment mass is not generally available for SF, various methods for use in correcting radiochemical data and SS measurements to pre-neutron emission values have been devised and fuller discussions of neutron emission and energy spectra are given in [Hof89b,Wag91].

As discussed earlier, a knowledge of prompt neutron emission as a function of fragment mass for each fissioning system is required in order to obtain primary fragment (pre-neutron emission) mass-yield distributions from radiochemical or kinetic-energy measurements of the fission fragments. However, very little information of this type exists except for SF of ^{252}Cf. From an evaluation of the experimental data obtained from a variety of methods for the average number of neutrons emitted by the fragments from ^{252}Cf and thermal neutron-induced fission of ^{233}U, ^{235}U, and ^{239}Pu, Wahl [Wah88] has derived a function which gives reasonable agreement with the experimental values. He plots the average number of prompt neutrons $\bar{\nu}_f$ emitted by fission fragments with mass number A_f before prompt-neutron emission vs. $A = A_f - \bar{\nu}_f$, the average fragment mass number after prompt-neutron emission (see Figure 3.14). In other words, the graph gives the average number of prompt neutrons emitted to form fission products with mass

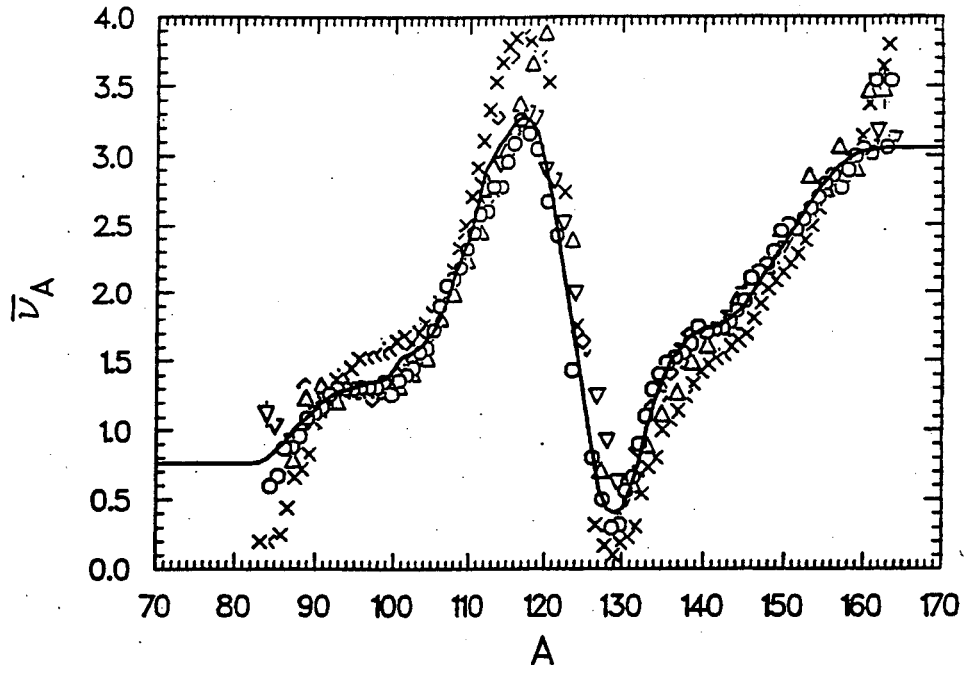

Figure 3.14: The solid line is a plot of the function, $\bar{\nu}_A$, derived by Wahl [Wah88], of the average number of prompt neutrons emitted to form fission products with mass number A for SF of ^{252}Cf. Also plotted are experimental values for ^{252}Cf of the average number of neutrons emitted by fragments, $\bar{\nu}_f$. Symbols represent different experimental results. (From [Wah88])

number A. These typical "saw-tooth" $\bar{\nu}_A$ functions can be related to variation with mass number of the fragment excitation energy (related to fragment deformation at scission).

The existence of even-odd proton effects on the $\bar{\nu}_A$ distribution for ^{252}Cf with excitation energy has been reinvestigated [Wal87] and observed to increase as fragment excitation energy decreases. Recent measurements for ^{252}Cf of neutron multiplicity distributions from the individual fission fragments [Alk88], and of the numbers of neutrons [Alk88b] emitted as a function of the mass and TKE of the fragments, have provided information on properties of the fragments immediately after separation and on the process of deexcitation of the excited fragments, and the distribution of excitation energy between the fragments. Measurements [Bud88] of the correlations between neutron emission, and fragment angle, mass, and kinetic energy have shown isotropic neutron emission in the c.m. system over the whole fission neutron energy range, permitting the conclusion that fission neutrons are emitted from the fully accelerated fragments and that the scission neutron component is much smaller than the previously assumed 15-20%. (Other studies [Bat88,See88] of the anisotropy of prompt neutron emission put limits of only 3 to 5% for the contributions of scission neutrons.) The mass range for $\bar{\nu}_A$ was extended beyond previous measurements and revealed two new "sawteeth" near masses 80 and 176.

3.2.3 Prompt gamma-ray emission

As discussed earlier, the excitation energy of the fission fragments can be dissipated by emission of γ-rays as well as neutrons. This phenomenon has been even less

well investigated than neutron emission although it can give information concerning the deformation of the fragments and the configuration at scission. Most studies have been of ^{252}Cf but the SF of ^{238}U, ^{240}Pu, and ^{244}Cm have also been investigated. Measurements show that about 80% of the γ-rays are emitted within 10^{-10} sec after fission and 11% of those from ^{252}Cf are emitted within 10^{-13} sec after fission. A significant fraction is emitted with a mean lifetime of 10^{-14} sec, which suggests that a competition between neutron and γ–ray emission may exist. Gamma-ray multiplicity measurements for ^{252}Cf were found to follow a double-Poisson distribution with a mean of about 10 γ-rays per SF. The total γ-ray energy per SF of ^{252}Cf was found to be 6.7 to 9 MeV, in agreement with calculations from both the statistical model for γ-rays in competition with neutrons and with a liquid-drop model. No satisfactory model had been found to fit the higher-energy region (4 to 16 MeV) of the γ-energy spectrum. Investigations of the anisotropy of γ-ray emission indicated that the excess emission along the fission axis (the axis of elongation as the fragments separate) is caused by large fragment spins aligned perpendicular to the fission axis.

Glässel et al. [Glä89] measured γ-ray energies and multiplicities and neutron multiplicities of ^{252}Cf together with the mass and kinetic energy of the fission fragments. The neutron multiplicity as a function of TKE is quite linear, but the slopes show a definite mass dependence. They found the total γ-ray multiplicity for both fragments to vary by only about 10%, with lower multiplicity for symmetric and very asymmetric mass splits. Most of this variation was from energies below 0.8 MeV. Their unfolded data for the γ-ray yield of individual fragments exhibited a rather flat behavior, unlike

earlier measurements, which resemble the neutron "sawtooth" function. They believe the earlier data were incorrect because the accuracy of the absolute mass scale was inadequate. They also found a high-energy component in the γ–ray spectra in the vicinity of symmetric fission. They investigated the competition of neutron and γ-ray emission in the life-time ranges of 10^{-13} to 10^{-14} sec and a rather linear, negative correlation with a decrease of 0.02 emitted neutrons per total γ-ray multiplicity for both fragments, independent of the excitation energy range. This gives the first evidence of neutron–γ competition in the last steps of deexcitation.

Varma et al. [Var91] measured the mean and standard deviation of the prompt γ-ray multiplicity distribution as a function of the charge ratio of the fission fragment pairs of ^{252}Cf. Their results show a small odd-even effect (larger values for even *Z*) as a function of the fragment charge ratio while the results of Glässel et al. [Glä89] for the mean multiplicity as a function of the mass of the emitting fragments is nearly structureless.

Although Kasagi et al. [Kas89], from measurements of γ-rays with energies up to 160 MeV, reported evidence for very high-energy γ-rays from the SF of ^{252}Cf, other investigators [Pok90,Luk91] found no evidence for this. Pokotilovskii [Pok90] examined γ-ray emission in the 20 to 160 MeV range and set upper limits of approximately 10^{-8} to 10^{-10} photons/MeV over the energy range from 20 to 120 MeV, more than an order of magnitude lower than reported. Luke et al. [Luk91] also set upper limits at the level of 10^{-9} to 10^{-8} photon/MeV for the emission of γ-rays with energies above 30 MeV.

Clearly, as seen by the multitude of products emitted at widely varying energies, SF is a complicated subject. This makes the study of SF more intriguing, as there is still a lot more to learn about it, especially in regards to predictive modeling.

4 Experimental

In this chapter, the experimental setup and procedures will be described. Five experiments have been performed. Two isotopes of rutherfordium, ^{259}Rf and ^{262}Rf, have been produced in order to study their SF properties. The production cross section of an isotope of hahnium, ^{261}Ha, was studied in two separate experiments, using two different target/beam combinations. Element 106 was produced and studied in order to confirm its original discovery in 1974. All the experiments used the same basic experimental setup, as described below.

4.1 Production of isotopes

The isotopes used for these experiments are produced using the Lawrence Berkeley National Laboratory 88-Inch Cyclotron, which is a sector-focused cyclotron capable of generating relatively large beam currents of many different ions, ranging from ions of hydrogen to uranium. When using radioactive targets, a fast-closing "slammer valve" is used to ensure that the 88-Inch Cyclotron is protected from contamination with target material in the case of a catastrophic target failure. During these irradiations, the pressure inside the beam line between the accelerator and the target system is continuously monitored. In the event of a vacuum failure, the "slammer valve" simply seals the beam line between the target system and the cyclotron, isolating the cyclotron.

A "beam wobbler" [Moo83] is also used to spread the beam intensity over the entire target area to prevent local overheating in the target. Without a wobbler, the beam could burn a hole in the target.

4.2 Reaction chamber and gas transport

For each experiment, the chosen beam passes through a collimator, a 1.8-mg/cm^2 to 2.4-mg/cm^2 HAVAR entrance window, 0.3 mg/cm^2 N_2 cooling gas, and the beryllium target backing before entering the target material (refer to Figure 4.1). The beam is then terminated in a beam stop. A Faraday cup at the beam stop measures the current and the integral beam dose is recorded. The targets, being radioactive, required a HAVAR foil as an entrance window to isolate the targets from the rest of the cyclotron. The collimator and beam stop are composed of graphite to reduce neutron production and make the irradiation area less hazardous to the experimenter. The reaction products recoil and are thermalized in the recoil chamber by helium at a pressure of 1.3 bar.

The reaction products are then attached to KCl aerosols contained in flowing helium gas (3.0 to 4.0 l/min) and are swept out of the reaction chamber through a 1.4-mm to 1.6-mm i.d. teflon capillary tube to the vacuum chamber of our MG rotating wheel system [Hof80] (described next section) located 7 m away. The KCl-seeded helium gas is obtained by passing a He stream over KCl heated in an oven, which is maintained at 640 °C. The transport efficiency is approximately 74 to 86%.

Details specific to each experiment will be given in Chapter 5.

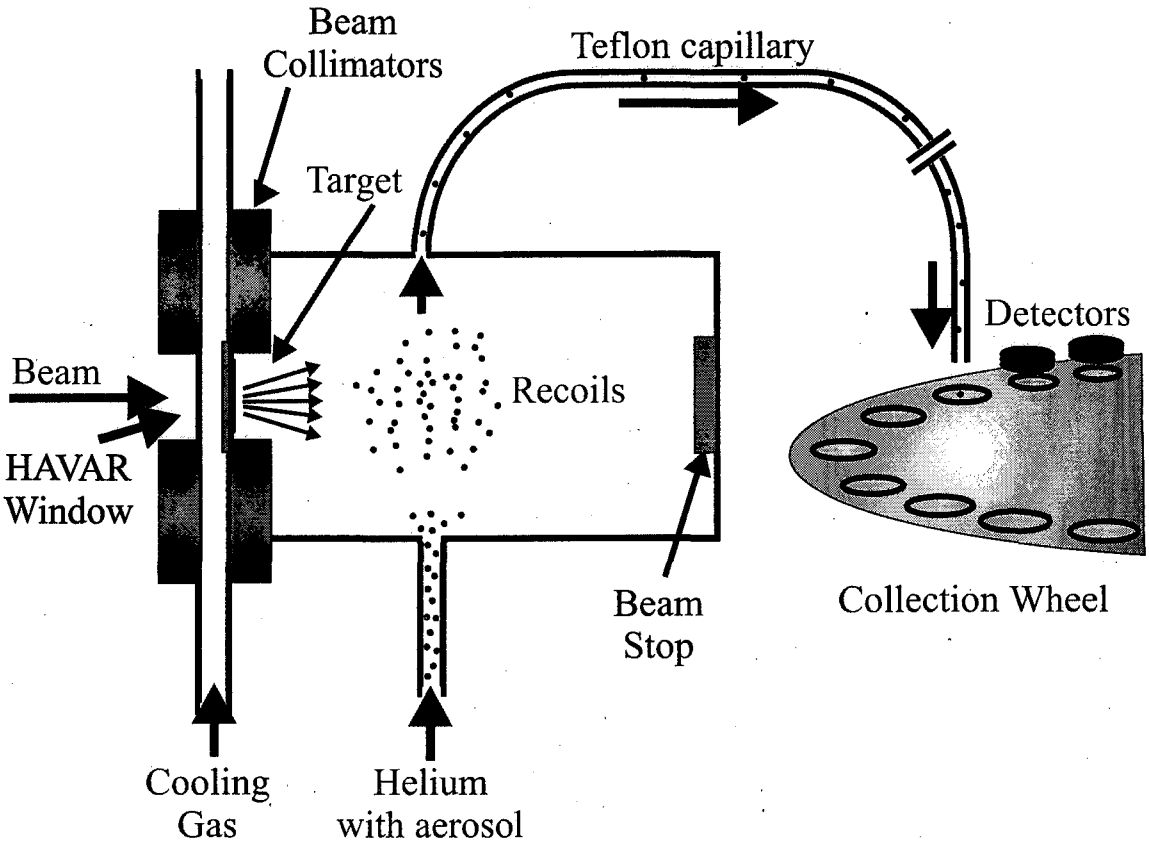

Figure 4.1: Schematic of the target system, reaction recoil chamber, and gas transport system. See text for details.

4.3 Detection system

4.3.1 MG system

For most experiments, we use the MG (Merry-Go-Round) system (Figure 4.2). There are 80 collection sites around the periphery of the 20-inch diameter fiberglass wheel. Each collection site consists of a steel ring with a 0.63-mm diameter hole covered with a 50±10 $\mu g/cm^2$ polypropylene foil. The recoil products are transported and deposited on one of the foils. A stepping motor is used to turn the wheel at pre-determined intervals to position the activity-laden foils between six successive pairs of stationary detectors, positioned above and below the foil (Figure 4.3). This allows us to follow the decay of the products. The wheel regularly was replaced with another wheel with clean foils to minimize the build-up of long-lived activities.

For some of the experiments, a special parent-daughter stepping mode was used to facilitate detection of α-α correlations. In this case, half of the polypropylene foils are removed from the wheels, leaving holes alternating with the foils. The stepping is programmed to proceed in two modes, as shown in Figure 4.4. In the parent search mode, the wheel is double-stepped to position the sources between the first, third, and fifth detector pairs, while detector pairs two, four, and six observe no activity. The wheel will continue to be double-stepped until a potential parent α-particle (one with appropriate energy) is detected in the bottom detector. It is then assumed that the recoil momentum imparted to the daughter is sufficient to eject it from the sample and imbed it in the top detector. The wheel is then single-stepped to enter daughter search mode. The

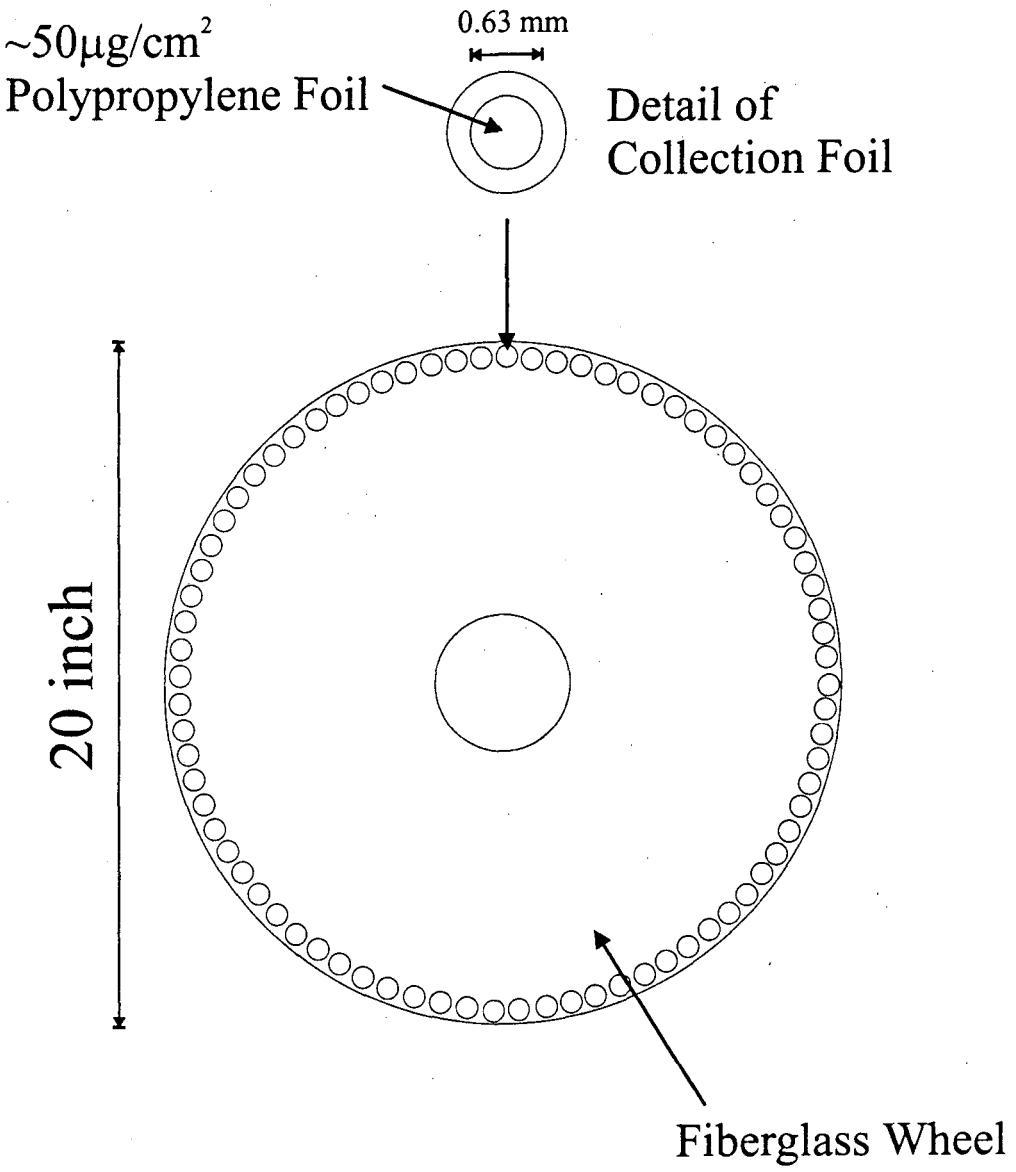

Figure 4.2: The MG rotating wheel used in the experiments.

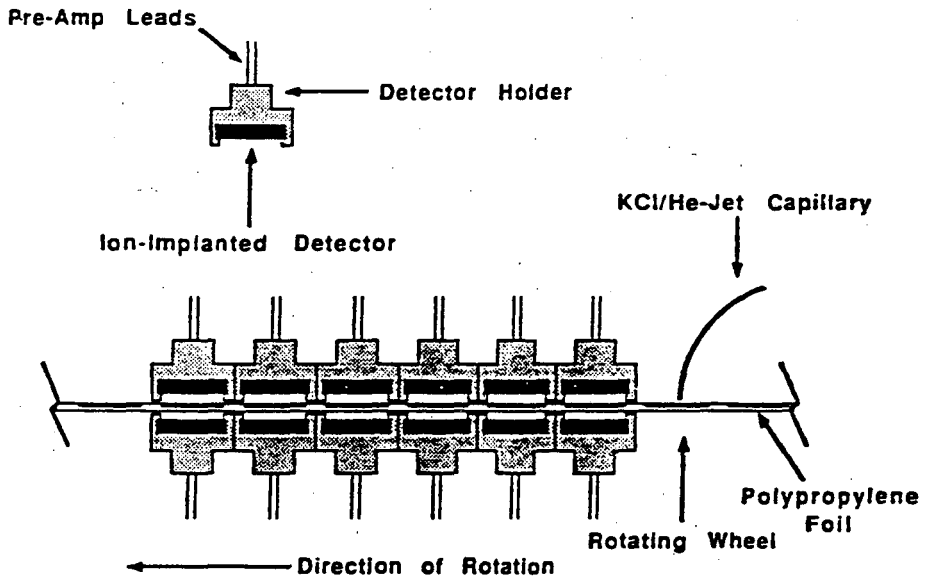

Figure 4.3: Side-view of the PIPS detector system.

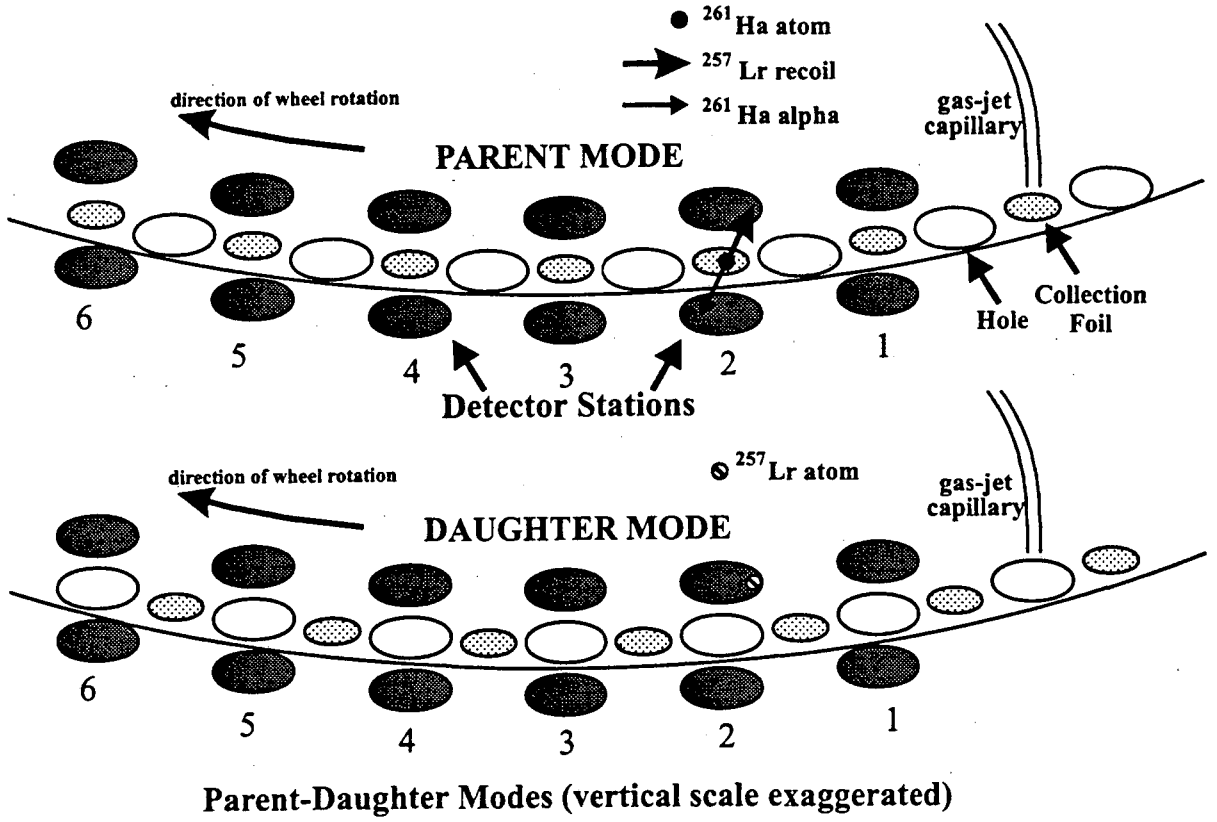

Parent-Daughter Modes (vertical scale exaggerated)

Figure 4.4: Schematic of the parent-daughter wheel-stepping modes used in some of the experiments. The top portion shows the parent search mode and the bottom portion shows the daughter search mode. See text for details.

sources are now between detector pairs two, four, and six, while only holes are between detector pairs one, three, and five. Thus, a search for the correlated α–decay is initiated in a low-background environment nearly eliminating the possibility of random events from the collected sources. The wheel is held in daughter mode for about two or three half-lives of the daughter and is then single-stepped again to realign the sources with detector pairs one, three, and five, re-initiating the parent search mode until the next potential parent is detected.

Details specific to each experiment will be given in Chapter 5.

4.3.2 Detectors

The detectors used are passivated ion-implanted planar silicon (PIPS) detectors (100 mm^2 active area) which measure the kinetic energy of α-particles and SF fragments. The source-to-detector distance is about 2.0 mm, resulting in an efficiency in a given detector of approximately 30% for α-particles and 60% for fission fragments. The α-particle energy resolution (FWHM) is about 40 keV in the top detectors and 60 keV in the bottom detectors; the latter being larger because of energy degradation in the polypropylene foil.

4.4 Data acquisition and analysis

Alpha particles and fission fragments were counted with the "Merry-Go-round Real-time data Acquisition and Graphics System" (MG-RAGS) [Hof80, Ler87]. The MG system is described above. RAGS is then used to record and analyze the data from the individual detectors. Figure 4.5 is a schematic of the MG-RAGS. RAGS is an LSI-11/73 computer-controlled data acquisition system. The amplified output signals of the PIPS detectors from α–decay or SF-decay events are digitized by ORTEC AD811 analog-to-digital converters (ADC). The ADC's are controlled by a Standard Engineering CAMAC crate controller. All events are stored on a hard disk in list mode. Each event is tagged with a time, channel number, and a detector number. Subsequent sorting and grouping of data were performed to extract fission-fragment energy spectra, coincidence data and half-life information.

Off-line energy calibrations were obtained by measuring the spectrum of α-particles from ^{212}Bi (6.051 and 6.090 MeV) and ^{212}Po (8.784 MeV) in equilibrium with a ^{212}Pb source. On-line α-decay energy calibrations were made and are described in Chapter 5 for each experiment. Sources of ^{252}Cf on 50±10 μg/cm^2 polypropylene foils were used for the energy calibration for the SF fragments using the calibration method of Schmitt, Kiker, and Williams (SKW) [Sch65] with constants determined by Weissenberger et al. [Wei86]

Pulses from α-particles between 5 MeV and 10 MeV and fission fragments up to 200 MeV were digitized and stored in list mode, which stores time of event, channel

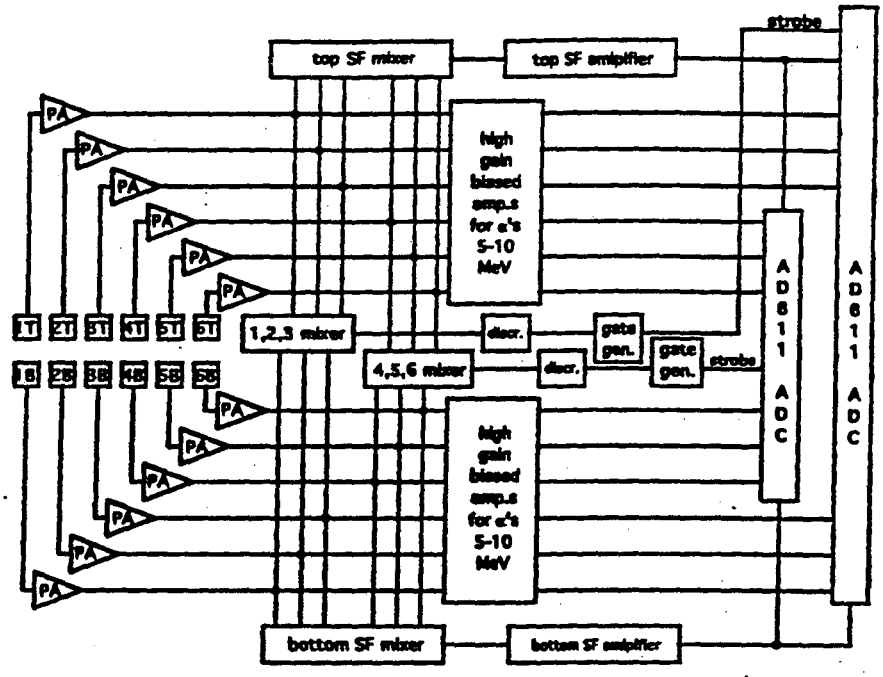

Figure 4.5: RAGS electronic schematic.

number, and detector number. The timing requirement for coincident fission fragments in off-line sorting was about 2 μs. When searching for the α-decay of ^{262}Rf, fission events within 10 ms of an α event with appropriate energy (7.5 MeV to 9 MeV) were considered possible signatures of α-SF coincidences between α-decay of 2.1-s ^{262}Rf and its 1.2-ms ^{258}No daughter which decays by SF.

4.5 Target preparation

Targets are prepared by electrodeposition of the hydrated oxide by the molecular plating method [Bed56,Eva72,Aum74,Mül75] in a 0.6-cm-diam circle on a 2.3 to 2.75-mg/cm^2 beryllium foil. Beryllium was chosen because it was necessary to use target backings that would withstand large beam intensities, minimize beam energy degradation, and would be mechanically strong.

Typically, chemistry is performed to separate the target isotope. It is also desirable to remove as much lead (naturally present) as possible, as lead interacts with the target beam to produce interfering activities. After separation, the target in solution is heated to dryness and then picked up with a small volume of nitric acid and then diluted with isopropanol. A portion of this stock target solution (approximately 0.075 mL) is pipetted into the plating cell. A voltage across the cell of 500 volts at an initial current of approximately 0.5 mA is applied. When the layer of stock target solution is finished plating (noted by a drop in current), the Be foil is baked in an oven at 550 °C. Successive layers are added until a sufficient target thickness is reached.

Details specific to each experiment will be given in Chapter 5.

5 SF properties of Rf

Despite the fact that the existence of SF has been known for over 50 years, it remains a very difficult and confusing subject with regards to calculating properties. As discussed earlier, using the liquid drop model of the nucleus, it was believed that the mass of the two fission fragments should be similar [Hul94], so that a mass yield distribution (%yield vs. fragment mass, normalized to 200% total yield) would have a single-humped Gaussian-like shape. However, until 1971, the only type of SF observed for the heavy actinides (Cf, Es, and the lighter isotopes of Fm) was asymmetric, i.e. the fragment mass yield distributions were double-humped.

Because of this, it was thought that asymmetric fission was the only type in low energy fission. In 1971, it was found that ^{257}Fm exhibited enhanced symmetric yields [Bal71]. Since then, other isotopes have been shown to have even more narrowly symmetric mass yield distributions, such as ^{258,9}Fm, ^{260}Md, and ^{262}No (see Figure 3.5). These nuclei also exhibit very high average total kinetic energies and emit fewer prompt neutrons during fission.

Qualitative theoretical descriptions of SF can be as instructive as quantitative descriptions. For example, symmetric fission can be explained using the shell model where the fissioning nucleus splits into two fragments that have closed shells of protons and neutrons. In the case of ^{264}Fm, one would expect symmetric division into two identical ^{132}Sn fragments, each having closed shells of 50 protons and 82 neutrons. Therefore the nuclei near ^{264}Fm should have a single-humped distribution centered on

mass 132. Even in asymmetric fission, one of the mass peaks is often centered on a mass with a full shell of protons and neutrons. However the shell model alone is not enough to completely describe the precise features of asymmetric fission. The Strutinsky method is a means of combining shell structure as a function of deformation with the basic liquid drop fission barrier to reproduce the double-humped mass distributions (see Section 2.1.3). For heavier nuclei away from shell closures, it reduces to a more liquid drop type distribution (see Section 3.2.1), with a broad symmetric distribution. This is seen experimentally for ^{260}Rf in Figure 3.5.

5.1 ^{259}Rf

Although such qualitative descriptions can explain some fission properties at the regions where there are complete shell closures and where shell effects disappear, it is much more difficult to make predictions for the trans-Fm isotopes, whose properties lie between the extreme cases. It is important to build up the systematics for these nuclei to enhance the understanding of SF-decay. Therefore, we attempted to study the SF-decay of ^{259}Rf to obtain mass-yield and total kinetic energy distributions, and the branching ratio for SF. It is difficult to predict, for example, whether the mass yield distribution will become more symmetric or asymmetric compared to ^{260}Rf. Also it would provide information on odd-mass nuclei, whose SF is hindered by the odd nucleon. All this information will help lead to an increased understanding of the nuclear fission process and its properties.

The branching ratio for SF-decay of ^{259}Rf has been measured previously as listed in Table 5.1. Although the last three studies show a branching ratio of approximately 0.06, there is reason to believe that the branching ratio may be only half this value. Bemis et al. [Bem81] observed a total of 22 fission fragment events. Eight of these were assigned to the long-lived activities of ^{256}Md and ^{256}Fm, leaving 14 SF events. However, ^{256}No is also produced in the same reaction. It has a 3-second SF activity, therefore making it indistinguishable from that of ^{259}Rf. Using the measured ^{256}No activity in the α-decay spectrum and the then-accepted 0.0025 SF branching ratio, they determined that about 5 of the SF events were from the decay of ^{256}No. This left 9.2±5.2 fission fragment pairs assigned to the decay of ^{259}Rf. It is now known that the correct branching ratio for

Experimenter	Reaction	Half-life	SF branch ratio	Reference
Ghiorso et al., 1969	$^{249}Cf(^{13}C,3n)$ & $^{248}Cm(^{16}O,5n)$	~3 sec	"not prominent"	[Ghi69]
Flerov et al., 1971	$^{242}Pu(^{22}Ne,5n)$	4.5±1.5 sec	0.06-0.12	[Fle71]
Druin et al., 1973	$^{246}Cm(^{18}O,5n)$	3.2±0.8 sec	~0.07	[Dru73]
Bemis et al., 1981	$^{249}Cf(^{13}C,3n)$	3.0±1.3 sec	0.063±0.037	[Bem81]

Table 5.1: Results of previous experiments on ^{259}Rf.

^{256}No is 0.005 [Fir96]. So this would mean that about 10 of the 14 events should be assigned to ^{256}No, leaving only 4 events to ^{259}Rf. Consequently, the Bemis ^{259}Rf SF branching ratio will be reduced by roughly a factor of two, i.e., closer to 0.03. One goal of our experiment was to produce enough data to determine a more accurate branching ratio.

An interesting consequence of the ^{259}Rf SF-decay branching ratio is that this may help resolve the dispute over the discovery of element 104. The Soviets made the first claim of discovery, reporting a 0.3-sec SF activity, assigned to ^{260}Rf on the basis of nuclear reaction systematics, from bombardment of ^{242}Pu with ^{22}Ne [Fle64]. Later, they suggested the half-life was 0.1 s, then 80 ms, then 28 ms. Identification of the atomic number of this nuclide by thermochromatography was made in 1966 [Zva66], but if the half-life was indeed 28 ms, it would not have made it through the column, as the transit time was over 1 sec. Later, they claimed they must have been observing 3-sec ^{259}Rf. But this contradicts their original work, which claimed "positively that the half-life could not be 3.7 sec." However, because the Soviets' conclusions are based on a SF activity, if it is shown that the SF branching ratio for ^{259}Rf is much smaller than currently believed, the Soviets' claim can be refuted.

5.1.1 Results

We used the ^{249}Cf(^{13}C,3*n*) reaction to produce the 3.1-s ^{259}Rf. The target was 0.5-mg/cm^2 ^{249}Cf on a 2.75 mg/cm^2 beryllium foil (see Section 7.1 for details on the target preparation). The $^{13}C^{4+}$ beam energy on target was 72 MeV at an intensity of 3 eμA.

Based on the production cross section reported in [Bem81], and taking into account the loss of product from decay, geometry, and detector efficiency, we predicted that we would have observed approximately 1.5 SF events per hour. The MG detection system (see Section 4.3.1) was used with a wheel stepping time of 3 sec. On-line α-energy calibrations were made using $^{211}Po^{g}$ and $^{212}Po^{m}$.

The success of the experiment relied on the suppression of interfering SF activities. Because SF events from various isotopes cannot be distinguished, it must be certain that only the activity of interest is being produced, and not activity from other products. Unfortunately, both ^{256}Fm and ^{256}No were produced in large quantities. Of particular trouble is the high yield of ^{256}No, which is also a spontaneous fission activity with a 3-second half-life. Therefore it is impossible to differentiate the decays from ^{256}No and ^{259}Rf. From the measured α-decay activity of ^{256}No and ^{259}Rf, and knowing the α-decay branches of these activities (99.5% and 93%, respectively [Fir96]), all the SF events must be assigned to ^{256}No.

5.1.2 Discussion

As stated in Section 5.1.1, from the measured amount of ^{256}No and ^{259}Rf α-decay activity produced, and their respective α-decay branching ratios, all the SF-decay activity produced in the ^{249}Cf(^{13}C,3*n*) reaction must be assigned to ^{256}No. Even though some of the events could be from the decay of ^{259}Rf, the SF properties of ^{259}Rf cannot be established. This is because the measured properties would be dominated by those of ^{256}No, the activity which was produced in larger quantities. In other words, ^{259}Rf was not

produced in high-enough abundance to derive any significant results. Clearly, new ways of suppressing the interfering activity content have to be established, as well as new reactions or experimental techniques to increase the ^{259}Rf yield.

5.2 ^{262}Rf

Isotopes around Z = 100 and the deformed neutron shell at N = 152 have been shown to have increased stability toward SF [Hof89]. However, the predicted deformed proton shell at Z = 108 and neutron shell at N = 162 have been the center of some debate. Macroscopic-microscopic calculations using these deformed shells provide two opposing results: one that predicts decreased stability toward SF and one that predicts increased stability. An increase in stability is predicted by Sobiczewski [Sob94] using calculations that include large deformation spaces. A decrease in stability is predicted by Möller et al. [Möl87], caused by the destabilizing effect of a deep new fission valley, which leads to compact fission fragment shapes. A resolution of this difference in predicted half-lives is important because it can influence the future direction of heavy element research. Short SF-decay half-lives prevent effective chemical and nuclear study, as well as positive identification, of the heaviest nuclei ($Z \geq 106$). Previously, no known nuclei were near enough to these shells to assess the influence of these shells on the stability against SF.

The isotopes ^{265}Sg and ^{266}Sg (Z = 106, N = 159,160) were first reported [Lou94,Laz94] to have α-decay half-lives of 2-30 s and 10-30 s, respectively, with SF-decay branches of 50% or less. These half-lives were inferred by using the phenomenological formula of Viola and Seaborg [Vio66] and the measured α-decay energy. The value for ^{266}Sg is closer to the half-life estimated by Smolanczuk et al. [Smo95b] for increased stability (~1 m) than to the half-life estimated by Möller et al. [Möl94] for decreased stability (~100 μs).

In these experiments [Lou94,Laz94], the SF-decay half-life of ^{262}Rf was measured to be $1.2^{+1.0}_{-0.5}$ s, based on the observation of six events in coincidence with the α-decay events from ^{266}Sg. This was the cause of some concern because this is quite different than the previously accepted value of around 50 ms [Tul95]. It was our goal to produce ^{262}Rf via the reaction ^{244}Pu(^{22}Ne,4n) in order to observe the reported 1.2-s activity and verify its half-life and assignment.

In 1981, Hoffman et al. [Hof81] produced a 1.5-s SF activity in the reaction of ^{248}Cm with ^{18}O projectiles. Based on the half-life and the measured SF properties, "the most likely assignment" for this 1.5-s activity was ^{259}Fm. In 1982 and 1985, Somerville et al. [Som85] observed 1.3-s and 47-ms activities using the same reaction. The 47-ms activity was tentatively assigned to the decay of ^{262}Rf and the 1.3-s activity was left unassigned. Although the 1.5-s and 1.3-s activities observed were probably indeed mostly ^{259}Fm (produced by a ^{11}Be transfer reaction), it is likely ^{262}Rf also could have been present from the ^{248}Cm(^{18}O,4*n*) reaction and could not be distinguished because of its similarity in half-life to ^{259}Fm.

A possible explanation for the observation of a 1.2-s SF activity is that there could be two activities for ^{262}Rf, one being the SF-decay from the ground state and the other being the SF-decay from an isomeric state, resulting in two half-lives of 1.5 s and 50 ms. Such SF from K-isomeric states has been predicted by Baran and Lojewski [Bar87] to be possible for heavy nuclei. Therefore, the 1.2-s value by LLNL/Dubna and the 47-ms value by Somerville could both be correct, with the ~1.5-s activities observed by Hoffman et al. and Somerville et al. being a mixture of ^{259}Fm and ^{262}Rf.

To produce ^{262}Rf, we used the ^{244}Pu(^{22}Ne,4n) reaction instead of the ^{248}Cm(^{18}O,4n) reaction because the production cross section for ^{256}Fm and ^{259}Fm from the former reaction should be much smaller [Hof90], thus reducing the amount of interfering background from their SF activity. Our results for fission properties should then be indicative of the properties of ^{262}Rf only.

We also attempted to make a positive assignment of ^{262}Rf by observing alpha correlations with ^{258}No. Using Audi's recent atomic mass compilation [Aud] (which doesn't take into account the effects of the N=162 shell) and the alpha-decay systematics of Hatsukawa et al. [Hat90], ^{262}Rf should decay by alpha-emission with E_α=8.45 MeV. However, when the effects of the N=162 shell [Pat91] are included, E_α=8.26 MeV is predicted. In either case, we could make a positive identification of ^{262}Rf and determine the alpha-branch by observing an alpha particle with energy between approximately 8.1 MeV and 8.6 MeV (^{262}Rf) followed within a few milliseconds by a spontaneous fission event from 1.2-ms ^{258}No, the alpha daughter of ^{262}Rf.

5.2.1 Results

^{262}Rf was produced by the reaction ^{244}Pu(^{22}Ne,4*n*). The target contained 765 μg/cm^2 ^{244}Pu (98% isotopic purity) on a 2.59 mg/cm^2 Be target backing foil. The maximum cross section for the 4*n* reaction was estimated to be 1.5 nb at 112.7 MeV by using the evaporation code JORPLE [Alo73]. A 1.8-mg/cm^2 HAVAR entrance window was used. Total beam energy losses before reaching the center of the target material were 22.6 MeV. The beam energy was chosen to result in a ^{22}Ne^{6+} energy of 114.4 MeV

(laboratory system) at the center of the target material. Beam energies of 109.8 MeV, 119.0 MeV, and 123.6 MeV at the center of the target were also used.

The helium flow rate was 3.0 l/min at 1.0 atm, and the capillaries used were 1.4-mm or 1.6-mm i.d. Teflon. The transport efficiency was approximately 75%.

The standard MG detection system was used with a wheel stepping time of 1.5 or 2.0 sec. The source-to-detector distance was about 2.0 mm, resulting in an efficiency in a given detector of 30% for α-particles and 60% for fission fragments. The wheel was replaced with another wheel with clean foils every thirty minutes to minimize the build-up of long-lived activities. On-line α-energy calibrations were made using the 7.27-MeV and 8.88-MeV α-decay peaks of $^{211}Po^{m}$.

The $^{244}Pu(^{22}Ne,4n)$ reaction was run at 114.4 MeV at an average beam current of 2.0-2.5 eμA for approximately 104 hours, at 109.8 MeV for 3.5 hours, at 119.0 MeV for 12 hours, and at 123.6 MeV for 12.5 hours. The production cross section was measured to be ~0.7 nb at 114.4 MeV. The cross section is calculated by taking into account the mass and thickness of the target, the charge and flux of the beam, the irradiation time, the gas-jet and detector efficiencies, the time between production and detection, the half-life and decay branch of the product, the detection time, the length of the experiment, and the number of events observed.

The production cross-sections at 109.8 MeV, 119.0 MeV, and 123.6 MeV were found to be ~0.6 nb (based on 8 SF events), ~0.5 nb (23 events), and ~0.1 nb (6 events), respectively. The shape and magnitude of the resulting excitation function are consistent

with those expected for the ^{244}Pu(^{22}Ne,4n) reaction, and therefore this activity has been assigned to the decay of ^{262}Rf.

Because of the small number of detected SF events (200) at 114.4 MeV, the half-life for ^{262}Rf was determined by performing a two-component decay curve fit to the SF activity using the maximum likelihood decay by the simplex method (MLDS) code [Gre91]. From the fit, presented in Figure 5.1, the half-life is 2.1±0.2 s. The stated error limits indicate the interval of equal-likelihood chances corresponding to a confidence level of 68%. Long-lived background SF activity was determined to be less than 2% of the total SF activity by counting the wheels with the foils off-line after the experiments.

The kinetic energies of 200 pairs of coincident fission fragments were measured in detector stations 1 through 4 or detector stations 1 through 3 (corresponding to six seconds since the end of collection for stepping times of 1.5 s and 2 s, respectively). The pre-neutron TKE distribution is shown in Figure 5.2. The pre-neutron TKE distribution is not actually measured. Detection occurs well after prompt neutron emission in the fragments. The actual measured post-neutron-emission fragment kinetic energies and derived masses were corrected to pre-neutron-emission values using a saw-toothed $\bar{\nu}(M)$ distribution similar to that measured for ^{252}Cf [Bow63] and ^{256}Fm [Uni74] and used by Balagna et al. [Bal71] for ^{257}Fm. The average number of neutrons emitted per fission, $\bar{\nu}_T$, was normalized to 4.4, a value estimated for ^{262}Rf from a plot of $\bar{\nu}_T$ vs mass number [Hof89]. The best Gaussian fit to the TKE distribution gives a most probable pre-neutron-emission TKE of 215±2 MeV with a full width at half maximum (FWHM) of 50 MeV. The pre-neutron-emission kinetic-energy distributions for the high- and low-

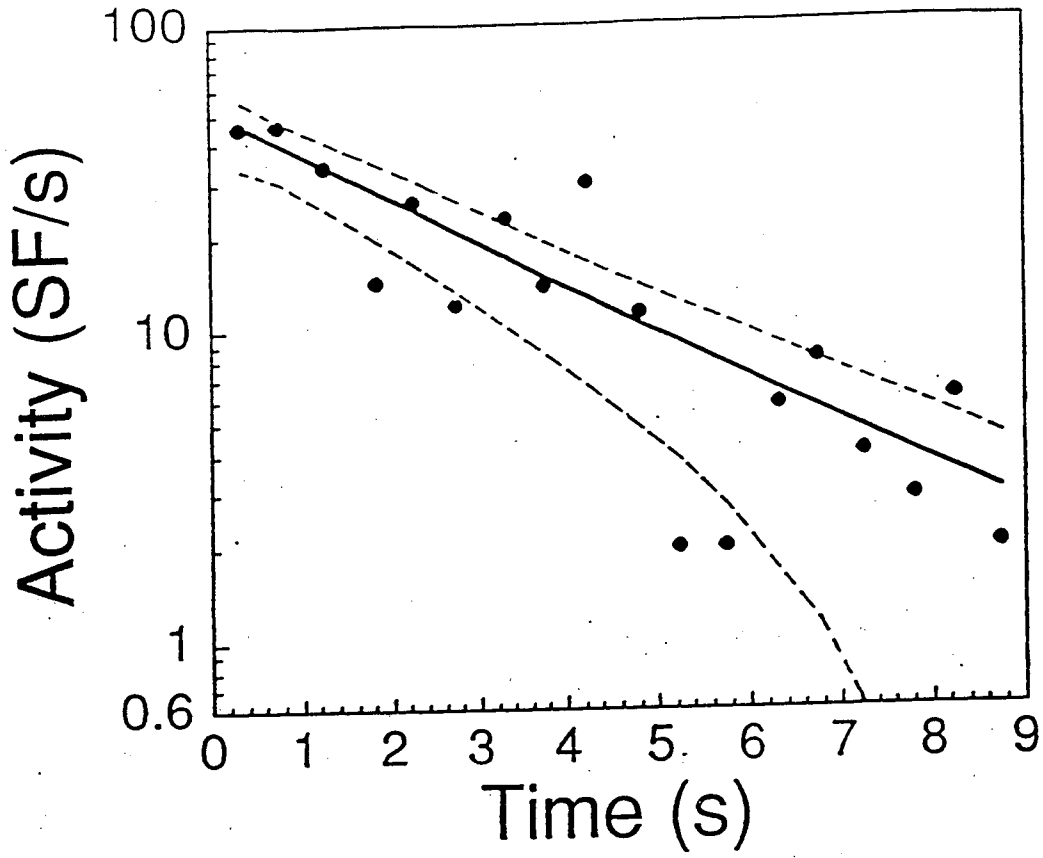

Figure 5.1: Decay curve of the ^{262}Rf SF coincidences. The times indicated are the times since the end of collection of the samples. The average count rates during the time intervals are indicated by the symbols, and the center curve is the most probable fit to the data. The upper and lower curves encompass 68% of the probability in a Poisson distribution centered on the number of counts expected during the interval, obtained from the most probable fit by the simplex method [Gre91].

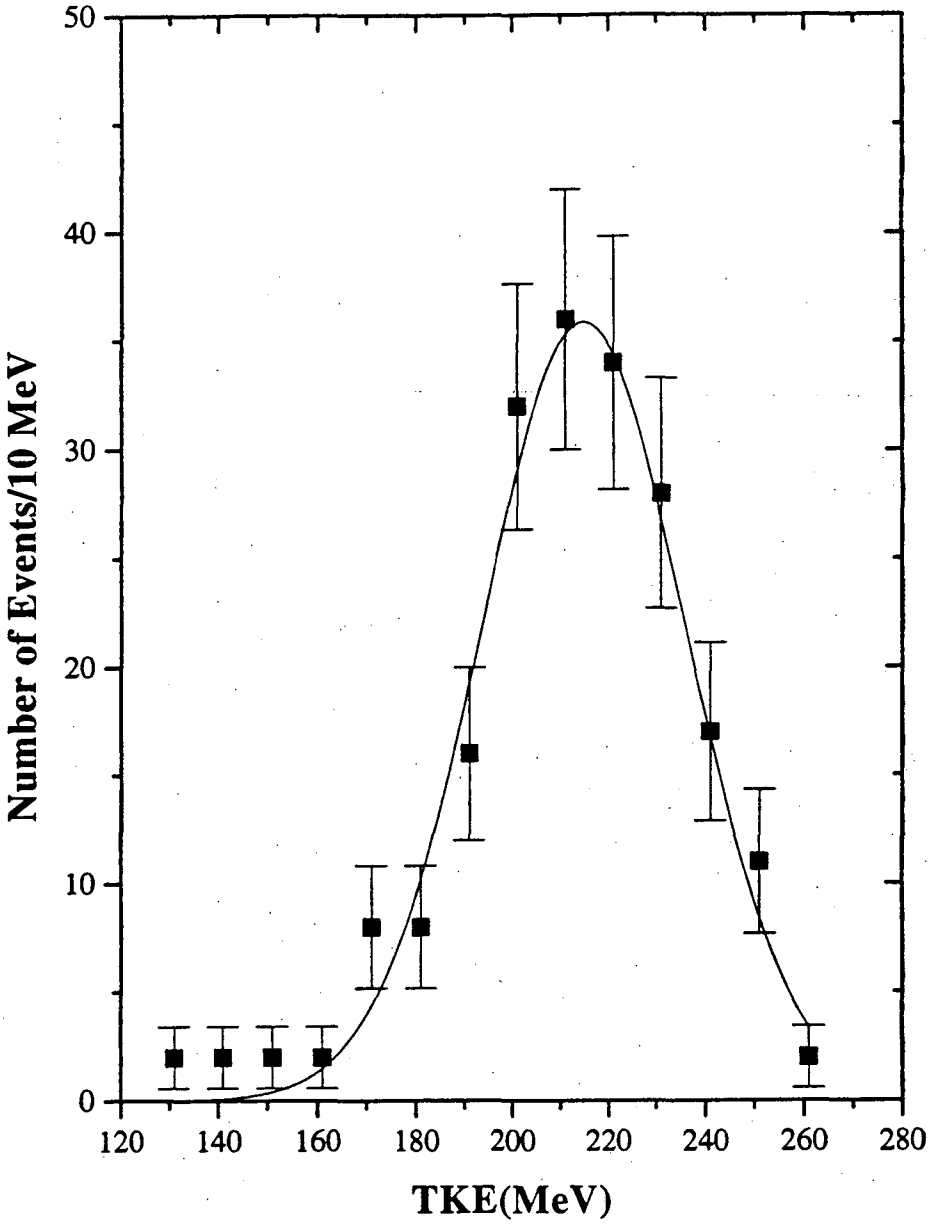

Figure 5.2: Gaussian fit to the pre-neutron-emission TKE distribution from the SF of ^{262}Rf. The data are in groupings of 10 MeV.

energy fragments from SF of ^{262}Rf are shown in Figure 5.3. A summary of the kinetic energy measurements for ^{262}Rf and the ^{252}Cf calibration standard measured in the same system is given in Table 5.2.

The pre-neutron-emission mass-yield distribution is shown in Figure 5.4, along with the provisional distribution (i.e., not corrected for neutron evaporation). The mass-yield data are expressed as yield (%) per mass number with the fragment yield normalized to 200%. The distribution is symmetric and can be fit with a Lorentzian distribution, but not with a single Gaussian. The FWHM is 22 mass numbers.

The contour plot in Figure 5.5 shows the post-neutron-emission TKE and average TKE as a function of mass fraction. The contours are lines representing equal numbers of events based on data groupings of 10 MeV X 0.02 units of mass fraction. Contours labeled 1 through 6 represent 6 equal increments of 4 through 24 events, respectively.

During the ^{262}Rf experiment, we searched for the α-decay of ^{262}Rf to 1.2-ms ^{258}No (which itself decays by SF), but observed no such time-correlated α-SF events. Implications of this are discussed in the next section.

5.2.2 ^{262}Rf

Our value of 2.1±0.2 s for the half-life of ^{262}Rf is within the error limits of the recently reported value of $1.2^{+1.0}_{-0.5}$ s by Lougheed et al. [Lou94,Laz94], but our value is much more accurate because it is based on 200 SF events while their value was based on only six SF events. The values of 1.3±0.1 s and 1.5±0.2 s obtained from ^{248}Cm + ^{18}O by Somerville et al. [Som85] and by Hoffman et al. [Hof81], as stated earlier, are probably

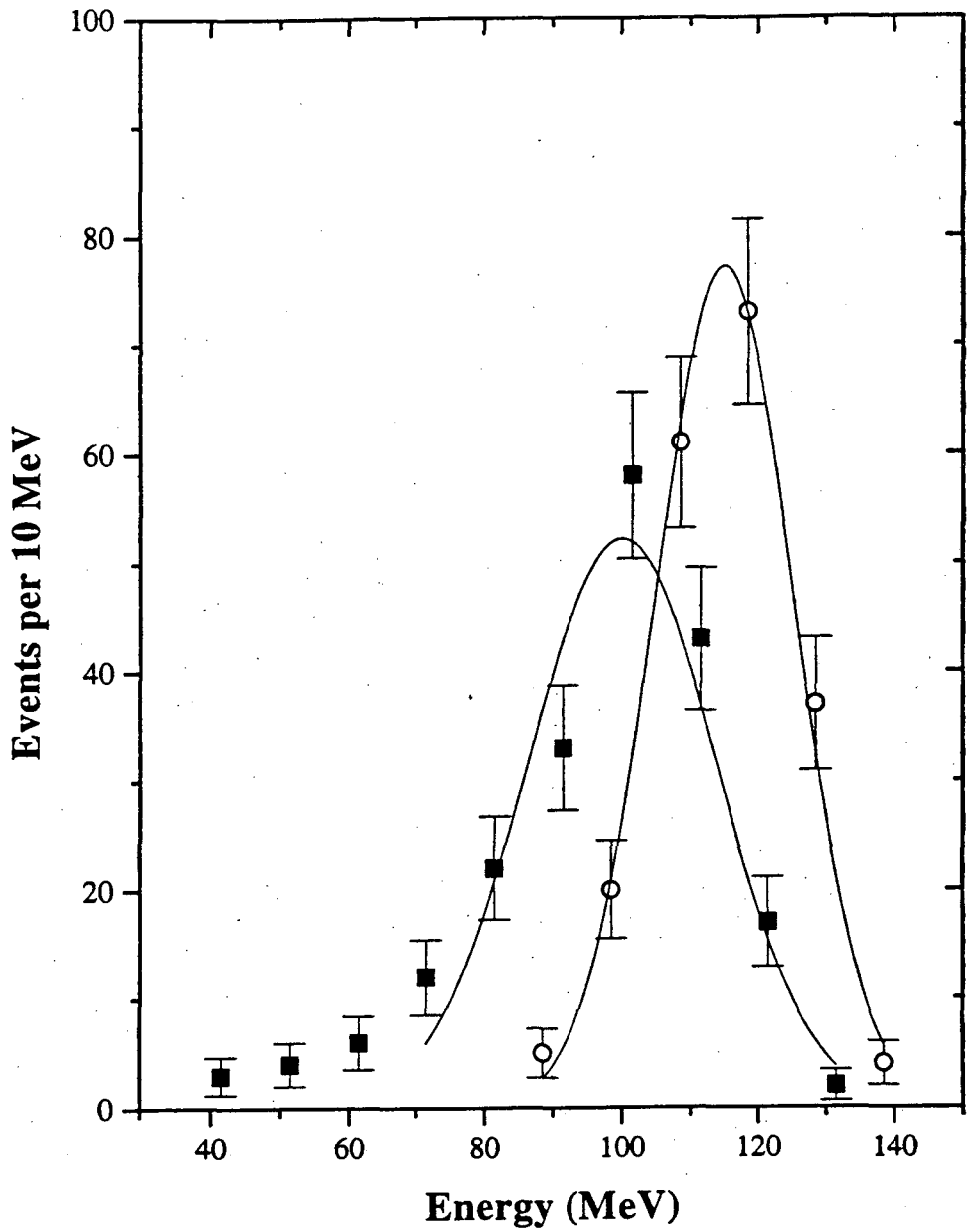

Figure 5.3: Gaussian fit to the pre-neutron-emission TKE distributions for high and low kinetic-energy fragments from the SF of ^{262}Rf.

	^{262}Rf		^{252}Cf	
	Pre-*n*	Post-*n*	Pre-*n*	Post-*n*
Total kinetic energy				
Average	211.9	208.3	179.1	176.4
Most probable[a]	214.7	211.5	180.9	178.1
σ	21.3	20.3	13.3	13.0
FWHM[b]	50.1	47.7	31.3	30.6
Heavy fragment energy				
Average	97.0	95.9	76.8	75.9
Most probable[a]	100.3	98.7	77.1	76.2
σ	14.6	14.9	9.9	9.8
FWHM[b]	34.3	35.0	23.3	23.0
Light fragment energy				
Average	114.9	112.4	102.3	100.5
Most probable[a]	115.6	112.9	103.2	101.4
σ	9.8	9.6	7.4	7.4
FWHM[b]	23.0	22.6	17.4	17.4

[a]Standard deviation of the most probable values from the Gaussian fits is 0.9%.
[b]Full width at half maximum, calculated from 2.35σ for Gaussian fit to the top half of the peak.

Table 5.2: Properties of the measured (post-neutron emission) and calculated initial (pre-neutron emission) fragment kinetic-energy distributions for ^{262}Rf and the ^{252}Cf standard measured in the same system. Energies are given in MeV, based on the SKW calibration method [Sch65] with the Weissenberger constants [Wei86].

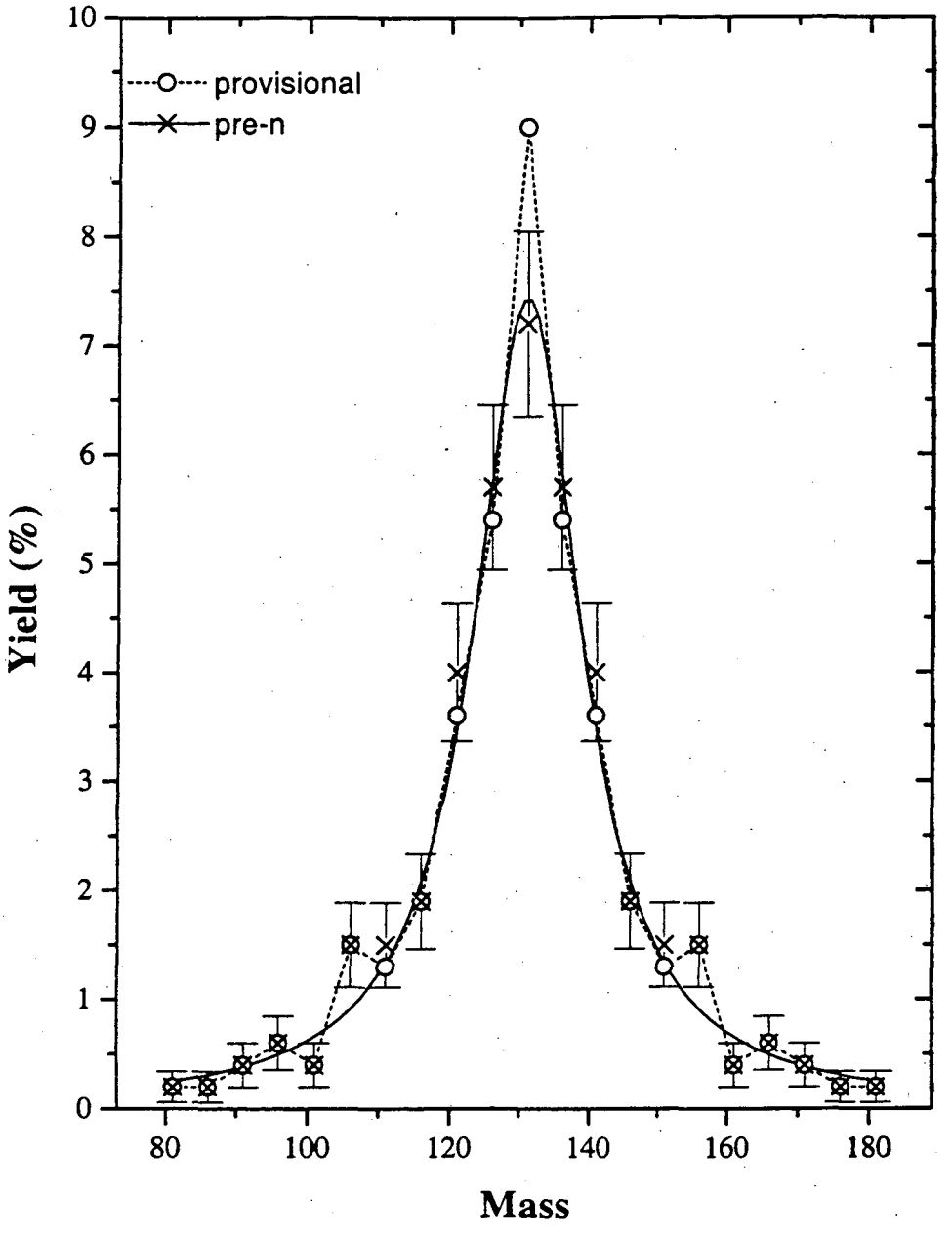

Figure 5.4: Pre-neutron-emission mass-yield distribution for ^{262}Rf (200 events). The pre-neutron-emission TKE was derived from the SF coincidence data using a $\bar{\nu}(M)$ function similar to that used by Balagna et al. [Bal71] for ^{257}Fm, with $\bar{\nu}_T$ = 4.4. The data are in groupings of 5 mass numbers. The curve is a Lorentzian fit. The bars indicate 1σ error limits. Also shown (open circles, dotted line) is the provisional mass-yield curve to which no neutron correction was applied.

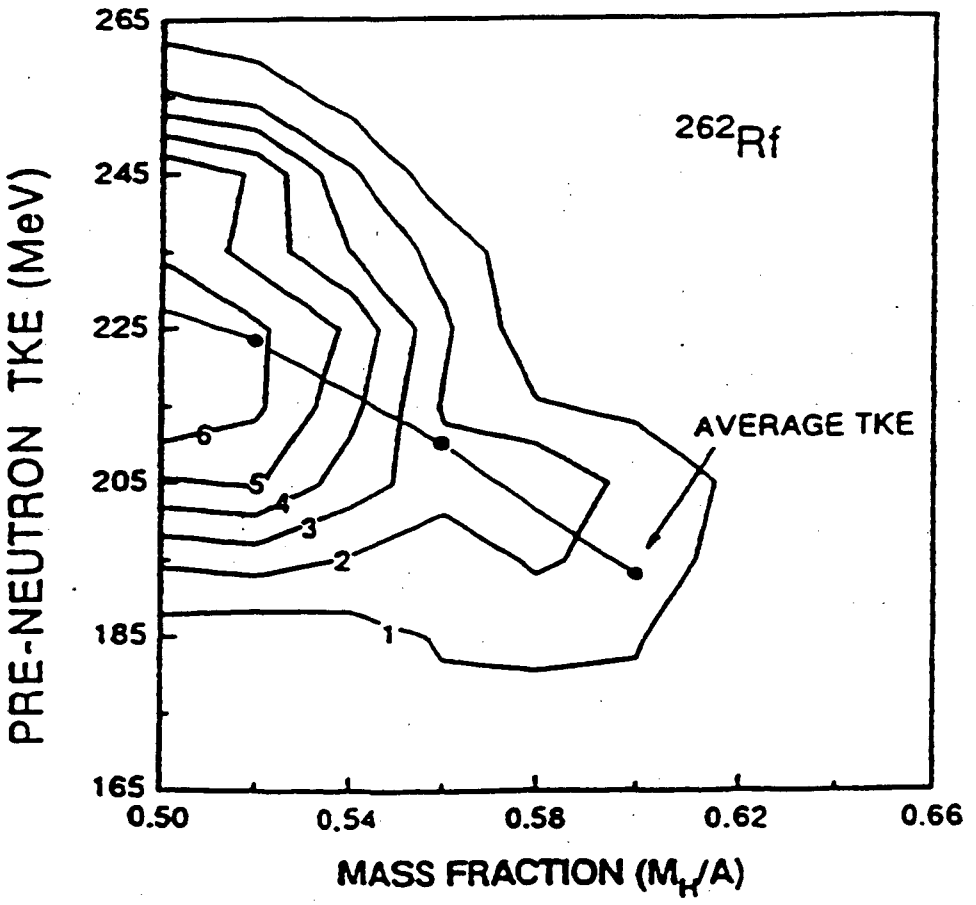

Figure 5.5: Contour plot of pre-neutron-emission TKE vs. mass fraction. The connected points represent average TKE as a function of mass fraction. The contours indicate equal numbers of events based on data groupings of 10 MeV X 0.02 units of mass fraction. Contours labeled 1 through 5 represent 4 through 24 events, respectively.

due mostly to ^{259}Fm ($t_{1/2}$ = 1.5 s) formed via a transfer reaction, with some possible contribution from the 2.1-s ^{262}Rf. Therefore, the 2.1-s and 47-ms activities for ^{262}Rf could both be correct, one for the ground-state decay and one for an isomeric-state decay.

Baran and Lojewski [Bar87] have performed calculations for the SF-decay half-lives of nuclei from K-isomeric states. They find that SF from 2-quasiparticle excited states can occur as well as SF from the ground state. It has been shown [Ghi73] that the even-even nuclei ^{250}Fm and ^{254}No have 2-quasiparticle isomeric states. However, no SF has been observed from the excited states because the half-life for γ-ray emission to the ground state is much shorter than the partial half-life for SF from the isomeric state. Baran and Lojewski state that when the lowest 2-quasiparticle configuration has a particularly high spin projection (such as $K^{\pi} = 9^{+}$), γ-ray emission would be hindered. In such cases, particularly for the heavier nuclei ($Z \geq 104$), SF from the isomeric state can then become observable. Therefore, the 47-ms activity could be fission from the K-isomeric state of ^{262}Rf while the 2.1-s activity is fission from the ground state. This would agree with the similar observation [Hal89] of a shorter isomeric half-life in ^{256}Fm, the only case where SF from a K-isomer in the first well of the potential energy surface has been measured. The partial SF-decay half-life of the $K^{\pi} = 7^{-}$ isomeric level in ^{256}Fm is ~0.8 ms [Hal89], while the partial SF-decay half-life of the ground state is ~2.9 hr [Tul95].

The SF-decay half-life for ^{262}Rf and all the partial SF-decay half-lives for even-even nuclides known as of 1998 are plotted vs. neutron number in Figure 3.1. As can be seen in the figure, the trend extrapolated from lighter even-even Rf (Z = 104) isotopes

would suggest a SF-decay partial half-life of only tens of milliseconds. The observed 2.1-s half-life, then, is evidence for stabilization caused by the $Z = 108$ and $N = 162$ deformed shells, just as the longer half-lives in the region around $Z = 100$ and $N = 152$ (^{250}Cf, ^{252}Fm, and ^{254}No) show the stabilizing effect of the $N = 152$ subshell.

The mass-yield distribution for ^{262}Rf is shown in Figure 3.5 together with those known for other trans-berkelium isotopes. It shows a symmetric mass distribution that could not be fit with a single Gaussian, but is well represented by a Lorentzian. As discussed in Section 3.2.1, only asymmetric mass division had been observed for SF for many years, resulting in a "double-humped" distribution. Then it was discovered [Bal71] that ^{257}Fm had an enhanced yield of symmetric division. Since then, the isotopes ^{258}Fm [Hul89], ^{259}Fm [Hof81,Hul80], and ^{260}Md [Hul89], among others, have been shown to have very symmetric distributions. The explanation for this is that these nuclei are approaching a mass (^{264}Fm) that can fission into two shell-stabilized doubly magic ^{132}Sn fragments, resulting in a greatly enhanced symmetric yield. The mass-yield distribution of ^{256}Rf is somewhat asymmetric. The mass-yield distributions of ^{258}Rf and ^{260}Rf are broadly symmetric, which was attributed to the return of "liquid-drop" type fission and the disappearance of the second barrier in the fission process [Hul94] (see Section 3.2.1). However, if this were the case, the distribution of ^{262}Rf should not be nearly as narrow as the mass distribution we have observed which seems to indicate the influence of shell effects.

The TKE distribution for ^{262}Rf is shown in Figure 3.7 together with those known for other trans-einsteinium isotopes. It appears that ^{262}Rf has only a single component for its distribution, unlike those for ^{258}Fm, ^{259,260}Md, and ^{258,262}No, which have been

decomposed into two Gaussian distributions [Hul89,Lou89], one centered around 200 MeV and the other centered around 235 MeV. This so-called "bimodal" fission [Hul86,Sob94b] results from two fission paths, one leading to symmetric compact spherical shapes which results in a high TKE, and the other leading to symmetric elongated shapes which have a lower TKE (see Section 3.2.1). There is also the possibility of "multimodal" symmetric fission [Bro83,Bro90], when a variety of fission channels or pathways are possible for a fissioning nucleus on the same potential energy surface. The small number of events observed for ^{262}Rf prevents us from conclusively determining if it is monomodal, bimodal, or multimodal fission.

The contour plot for ^{262}Rf (Figure 5.5) together with those for ^{256}No and ^{259}Lr is shown in Figure 3.8, giving a "3-D" picture of the relationship of mass fraction and pre-neutron TKE. It can be seen that the yield is greatest for symmetric division and that, in all cases, the TKE increases as the division becomes more and more symmetric because of the fact that some symmetric fragments with near spherical shapes may be formed, but there is a large variance at symmetry. As can be seen, there is no evidence for the very high-TKE symmetric fission observed for the bimodal isotopes ^{258}Fm, ^{259,260}Md, and ^{258,262}No. However, because of the large variances of the TKE values for symmetric mass division, a variety of different modes resulting in deformed as well as spherical shapes possibly could be involved, indicating "multimodal" fission.

The most probable pre-neutron TKE is plotted in Figure 3.6 as a function of the Coulomb parameter, $Z^2/A^{1/3}$. All nuclei follow a linear trend except the heavy Fm, Md, and No isotopes. These "abnormally" high TKEs can be explained by noting that these isotopes are the ones that have a sharply symmetric mass division into nearly doubly

magic fragments. Therefore, the resulting compact spherical fragments will have higher TKEs than the elongated deformed fragments of other nuclei. The value of 215 MeV plotted for ^{262}Rf is shown to follow the linear fit by Unik [Uni74], but is high relative to the fit by Viola [Vio66b].

During our experiments, we searched for α-decay of ^{262}Rf to 1.2-ms ^{258}No (SF), but observed no such time-correlated α-SF events and have assigned an upper limit of 0.8% (68% confidence level) for an α-decay branch of ^{262}Rf. This corresponds to a partial α-decay half-life of greater than 260 s. Audi's mass compilation [Aud] results in a calculated E_α of 8.45 MeV and a resulting decay branch of 18% [Hat90], much higher than our present limit. However, this mass does not include any effect from the $N = 162$ shell. If a mass is used that takes this shell into account [Pat91], an E_α of 8.26 MeV is obtained, and a partial half-life of 43 s is expected [Hat90], resulting in an α-decay branch of 4.9%. Our result, therefore, is not only a strong indication of the existence of shells at $Z = 108$ and $N = 162$, but also shows that they have an even greater effect than currently suggested. More data on SF and α-decay for nuclides with $Z \geq 104$ will be needed to better quantify the effect of these deformed subshells.

6 Production cross sections for ^{261}Ha

As we attempt to increase the knowledge of chemical properties of elements near the end of the periodic table, chemical procedures have become increasingly more difficult to perform because of the shorter half-lives and smaller cross sections for producing these transactinide isotopes. It is important to investigate the chemistry of the elements where relativistic effects become increasingly more important and new techniques have been developed to facilitate the studies. Both manual and automated rapid chemical procedures [Hof93,Sch89], and even faster gas-phase chromatographic techniques have been used [Gäg91,Kad92]. More recently, a rapid separation and detection system, SISAK-LISSY (Short-lived Isotopes Studied by the AKUFVE technique/Liquid Scintillation System), has been developed to study isotopes with half-lives of the order of seconds [Wie95]. In preparation for experiments to study the chemical properties of hahnium using SISAK-LISSY, it was necessary to determine the best production reaction to use. The reactions studied were ^{250}Cf(^{15}N,4*n*)^{261}Ha and ^{243}Am(^{22}Ne,4*n*)^{261}Ha at 84 MeV and 116 MeV, respectively [Lan98].

In 1971, Ghiorso et al. [Ghi71] produced ^{261}Ha by the reactions ^{250}Cf(^{15}N,4*n*) and ^{249}Bk(^{16}O,4*n*). They were able to assign a half-life of 1.8 ± 0.6 s and an α-decay energy of 8.93 MeV. They observed no SF events, and were only able to set an upper limit of 50% for the SF-decay branch of ^{261}Ha.

CHAPTER SIX: PRODUCTION CROSS SECTIONS FOR ^{261}Ha

The α-decay of 1.8-s ^{261}Ha is shown in Figure 6.1. Because its own α-decay is followed by the α-decay of 0.65-s ^{257}Lr [Bem76], we can make a positive identification of ^{261}Ha by observing α-α correlations. In other words, we search for an α-particle of appropriate energy for the decay of ^{261}Ha (~8.9 MeV) during an appropriate time interval (about four or five times 1.8 s), followed closely (four or five times 0.65 s) by an α-particle of appropriate energy for the decay of ^{257}Lr (~8.8 MeV).

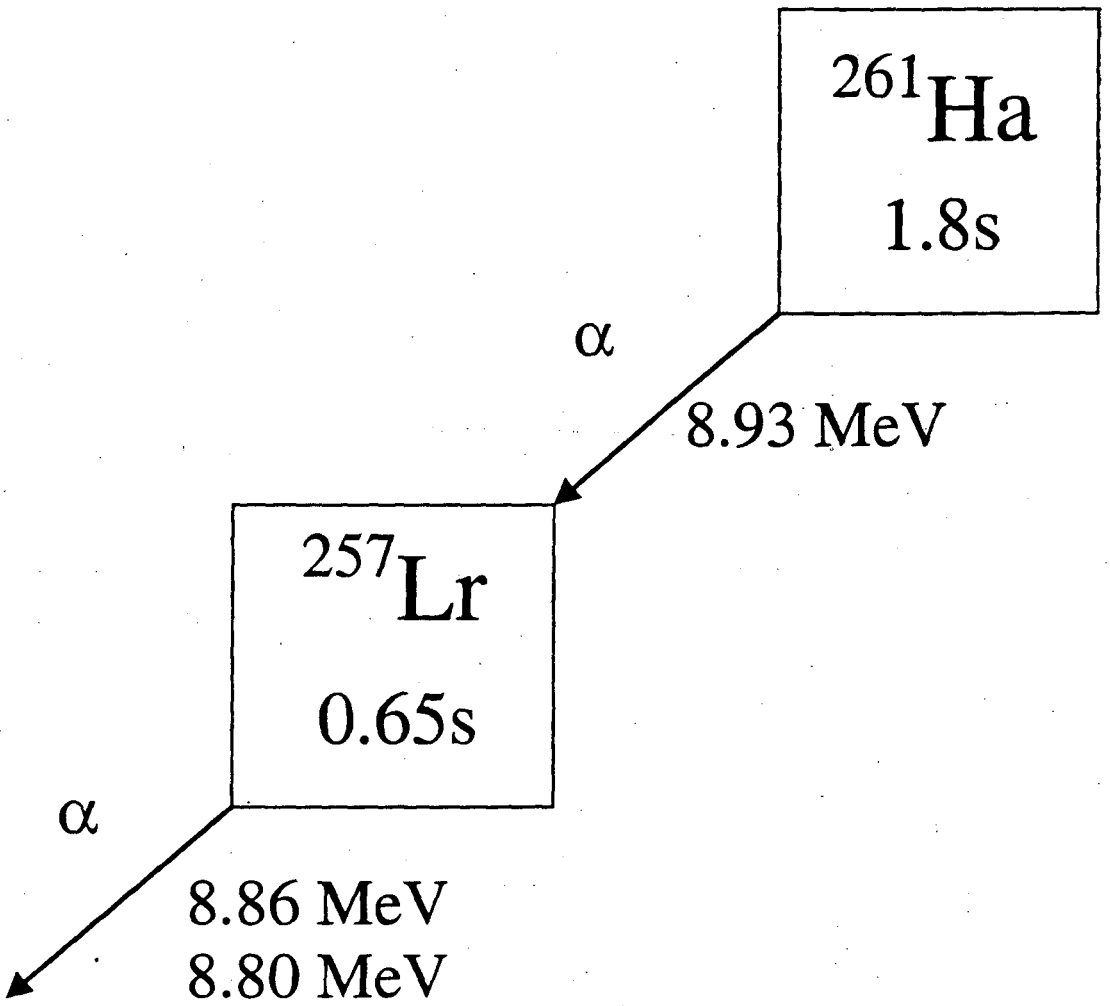

Figure 6.1: The decay of ^{261}Ha.

6.1 $^{250}Cf(^{15}N,4n)^{261}Ha$

6.1.1 Results

The isotope ^{261}Ha was produced via the $^{250}Cf(^{15}N,4n)$. The 0.91 mg/cm^2 ^{250}Cf target (79.5% ^{250}Cf, 10.2% ^{249}Cf, 10.2% ^{251}Cf) contained 0.72 mg/cm^2 ^{250}Cf as the oxide. The target was prepared similar to as described in Section 7.1, using 0.4 F HDEHP in heptane as the organic phase and 0.436 M HCl as the aqueous phase for the extraction. A beam of 95-MeV $^{15}N^{4+}$ ions from the cyclotron passed through a 1.8-mg/cm^2 HAVAR entrance window, the N_2 cooling gas, and the 2.3 mg/cm^2 Be target backing before entering the target material. The total energy loss was ~11 MeV. The beam energy was chosen to result in a $^{15}N^{4+}$ energy of 84 MeV (laboratory system) in the center of the target. The energy loss in the target was about 1.0 MeV.

Reaction products were transported from the recoil chamber via a 1.4 mm i.d. Teflon capillary. The transport time from target to collection foil was measured to be 1.0 ± 0.3 s for our system by measuring the decay of equilibrium sources of 0.84-s ^{8}Li-^{8}Be α-decay activity produced via the irradiation of a stable Be target with 130-MeV ^{19}F ions during a pulsed beam study. The transport and deposition efficiency was determined to be approximately 86 ± 10 % by comparing the ^{254}Fm activity of a post-run off-line measurement of a recently-used wheel to that collected directly on a molybdenum foil located in the recoil chamber 4 mm from the target.

The parent-daughter stepping mode of the MG system was used to facilitate detection of α-α correlations. In parent mode, the stepping time proceeded at 1.5-s

intervals, appropriate for detection of the 1.8-s ^{261}Ha. The wheel is kept in daughter mode for 3 seconds, which spans nearly 5 half-lives of the 0.65-s ^{257}Lr.

The source-to-detector distance was about 1.8 mm and the detector diameter was 11.3 mm, resulting in a geometric efficiency in a given detector of 35% for α-particles and 70% for fission fragments. Once the α-decay daughter recoils into the top detector (refer to Figure 6.2), the efficiency for the detection of the daughter α–particle would be 100% if it decays toward the top detector and 23% if it decays toward the bottom detector (the calculated solid angle assuming a point source), resulting in an overall efficiency of 61% for the detection of the daughter. Therefore, the total probability for observing an α-α correlation is 0.35 times 0.61, or 0.21. The wheel was replaced with another wheel with clean foils every hour to minimize the build-up of long-lived activities. On-line α-decay energy calibrations were made using ^{213}Fr, ^{213}Rn, and ^{212}Po^{m}.

The ^{250}Cf(^{15}N,4*n*) reaction was run at 84 MeV at the center of the target at an average beam current of 2.0 eμA for approximately 16 hours. The total integrated beam was 29131 pμC. The parent mode α-decay spectrum for the second top detector is shown in Figure 6.3. The 6.775-MeV peak is from the decay of ^{213}Fr, the α-decay daughter of ^{217}Ac produced from a small lead impurity in the target. The 8.09-MeV peak is from the decay of ^{213}Rn, the electron-capture (EC) daughter of ^{213}Fr. The 7.68-MeV peak is from the decay of ^{212}At and the 8.88-MeV peak is from the decay of ^{211}Po^{m}, both produced as transfer products from the Pb impurity. The 8.45-MeV peak is from the decay of ^{256}No, probably produced via transfer of ^{6}Be from ^{15}N to the ^{250}Cf. The wide peak at low-energy is from α-particles from the decays of 0.84-s ^{8}Li and 0.77-s ^{8}B produced by

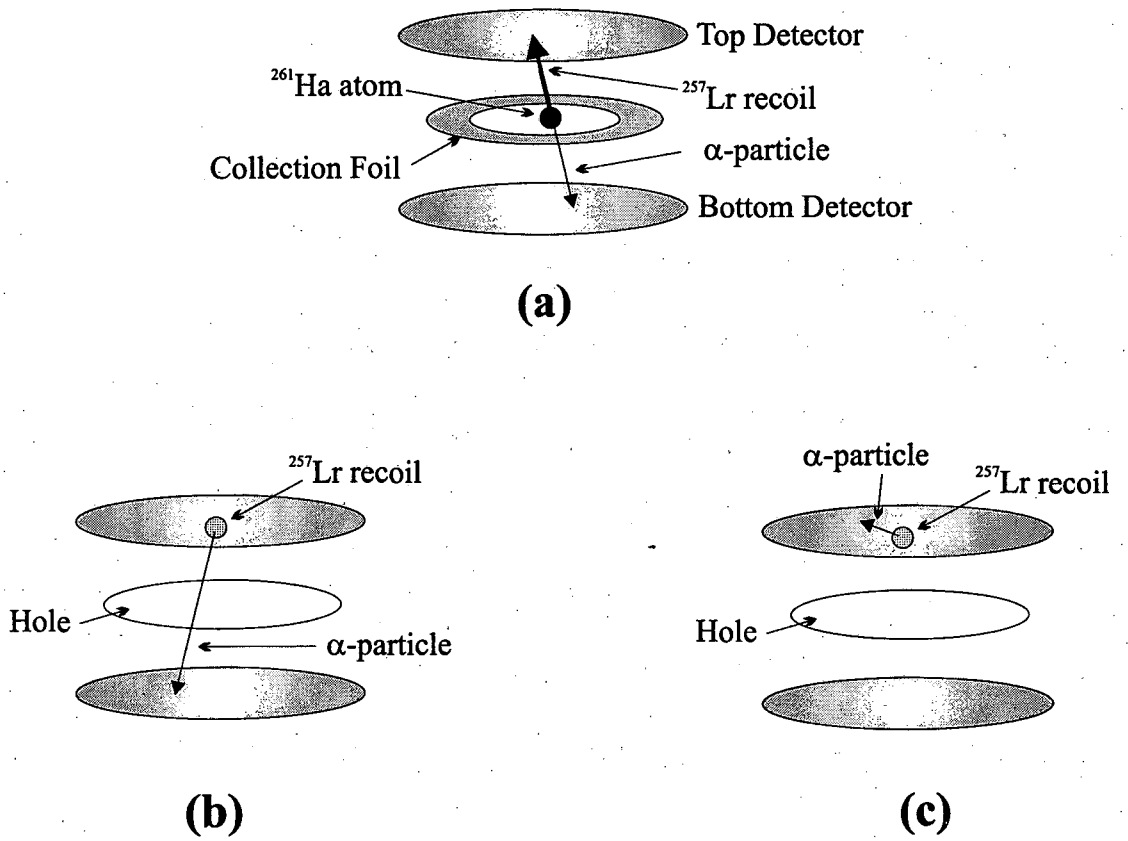

Figure 6.2: (a) There is a 35% probability of detecting an α particle from ^{261}Ha in the bottom detector. By conservation of momentum, the ^{257}Lr recoils into the top detector. (b) The wheel is stepped so that a hole is between the detectors. If the α particle from the decay of ^{257}Lr is emitted downwards, there is a 23% probability of detecting it in the bottom detector. (c) If the α particle is emitted upwards, there is a 100% probability of detecting it in the top detector. Therefore, the total probability of detecting the ^{257}Lr α decay is 61%. The total probability of observing the α-α correlation is 21%.

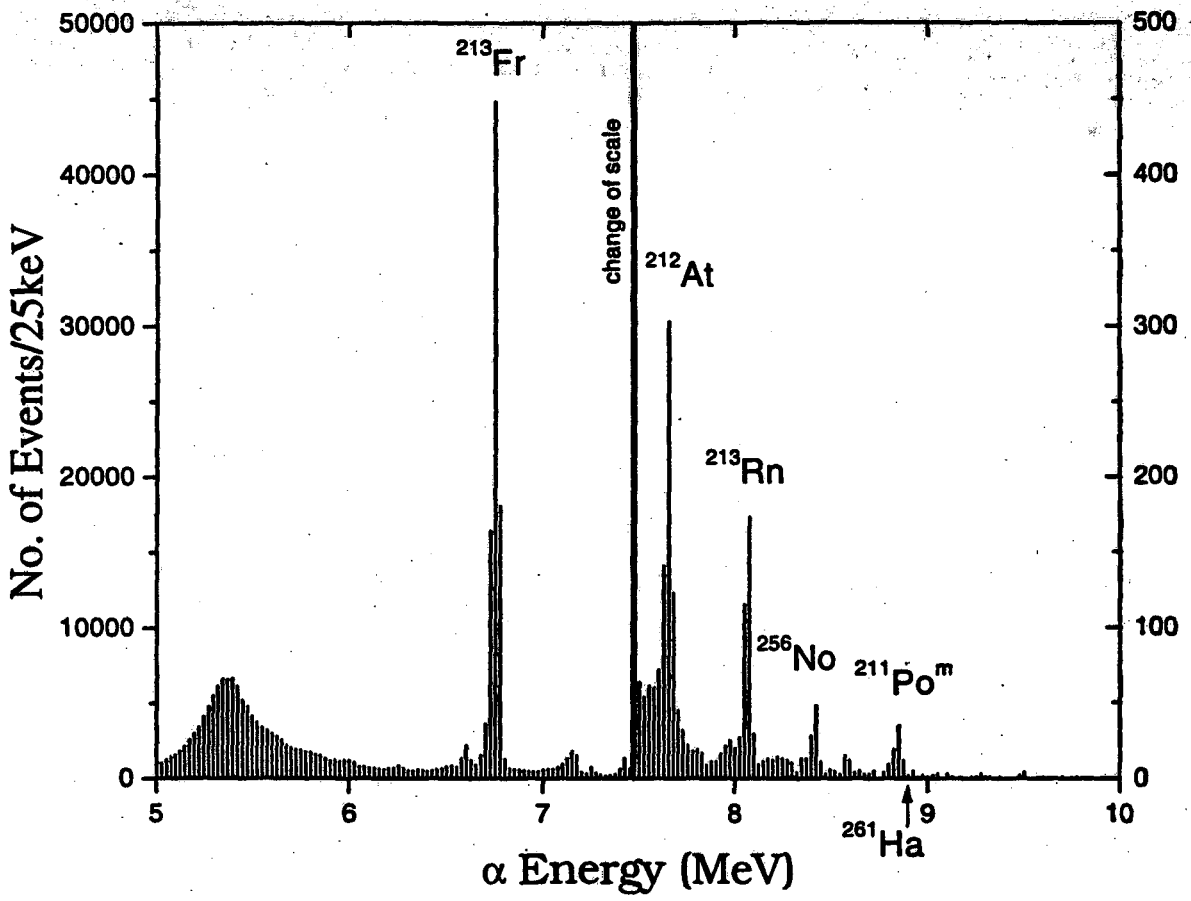

Figure 6.3: The parent mode α spectrum for the reaction $^{250}Cf + ^{15}N$ for top detector 2 for the entire run.

interactions of the beam with the Be target backing foil. The β^-–decay of ^{8}Li and EC-decay of ^{8}B populate excited states in ^{8}Be which then decay into a pair of α-particles emitted at 180° to each other. The summed daughter mode α-decay spectrum for all detectors is shown in Figure 6.4. The 5.5-MeV peak is probably from a small amount of ^{241}Am contamination on the detectors. The 6.775-MeV peak is probably from the decay of ^{213}Fr from the polypropylene collection sites, which although not between a pair of detectors in daughter mode, can still have an extremely small geometric efficiency for decaying into one of the adjacent detector pairs. The 7.45 MeV-peak is from the decay of ^{211}Po^{g}, the α-decay daughter of 2.3-μs ^{215}Rn (E_α = 8.67 MeV), which can also trigger the daughter mode. The ^{215}Rn is from the decay of the granddaughter of ^{223}Th, produced by a (^{15}N,n) reaction with traces of ^{209}Bi in the target.

A total of thirteen α-α correlations were observed. Table 6.1 lists the α-decay energy and lifetime of each parent and daughter event. The energies of each α-α correlation are plotted in Figure 6.5. As a rough guideline only, the literature values for the α-decay energies of ^{261}Ha and ^{257}Lr are shown by the dotted lines.

6.1.2 Discussion

The energies of the thirteen α-α correlation events from Table 6.1 are plotted in Figure 6.5. As can be seen, the energies of most of the events are in accordance with the literature values. The correlations with lower parent α-decay energy are expected and can be explained as follows. The α-decay spectra of the bottom detectors reveal that the

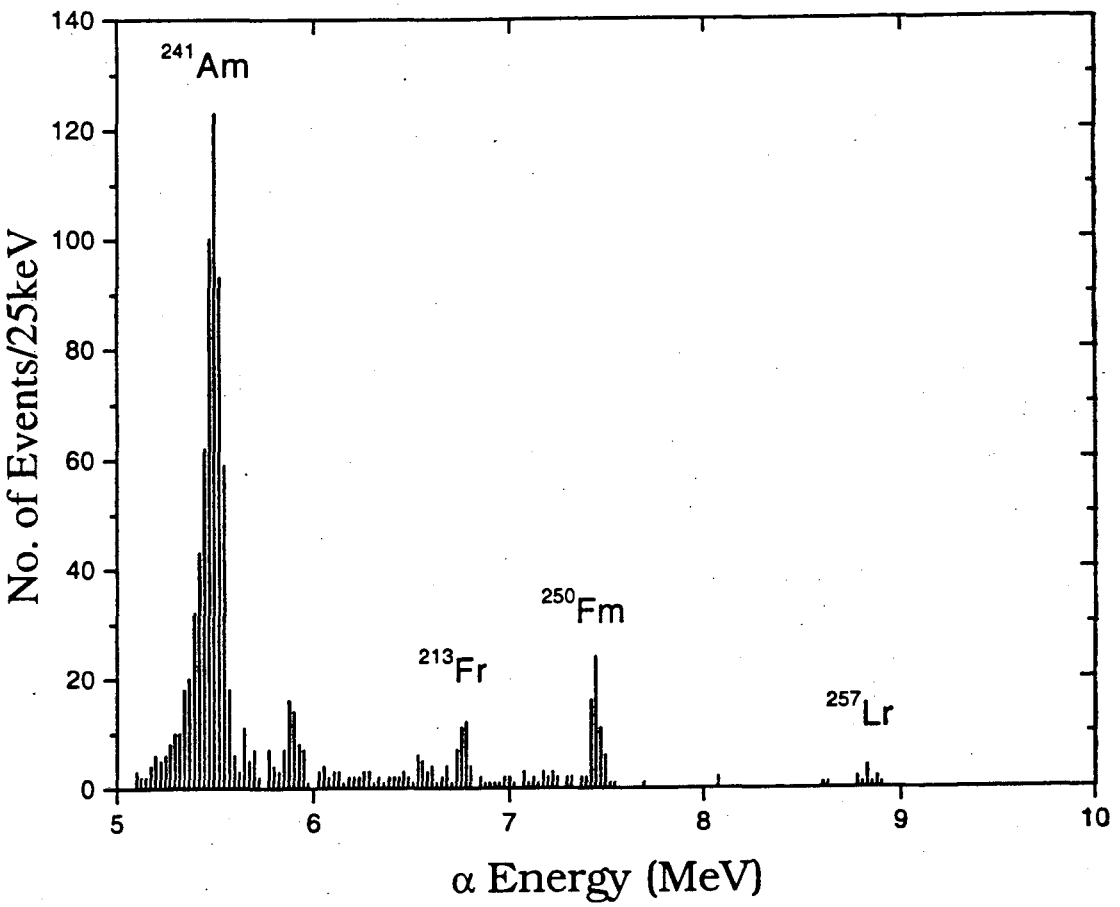

Figure 6.4: The daughter mode α spectrum for the reaction $^{250}Cf + ^{15}N$ for all detector pairs for the entire run.

Parent Energy (MeV)	Parent Lifetime (sec)	Daughter Energy (MeV)	Daughter Lifetime (sec)
8.564	10.925	8.846	1.483
8.820	4.198	8.829	0.670
8.984	2.764	8.904	0.472
8.902	5.148	8.849	0.809
8.662	1.158	8.787	0.688
8.643	0.642	8.800	0.615
8.805	6.362	8.600	1.117
8.931	0.618	8.881	0.950
8.883	5.460	8.849	0.484
8.835	2.651	8.867	1.027
8.646	6.167	8.639	1.272
8.769	0.931	8.887	2.829
8.958	4.978	8.786	0.563

Table 6.1: Lists of the parent and daughter α particle energies and lifetimes for each α-α correlated event for the reaction ^{250}Cf (^{15}N,4*n*).

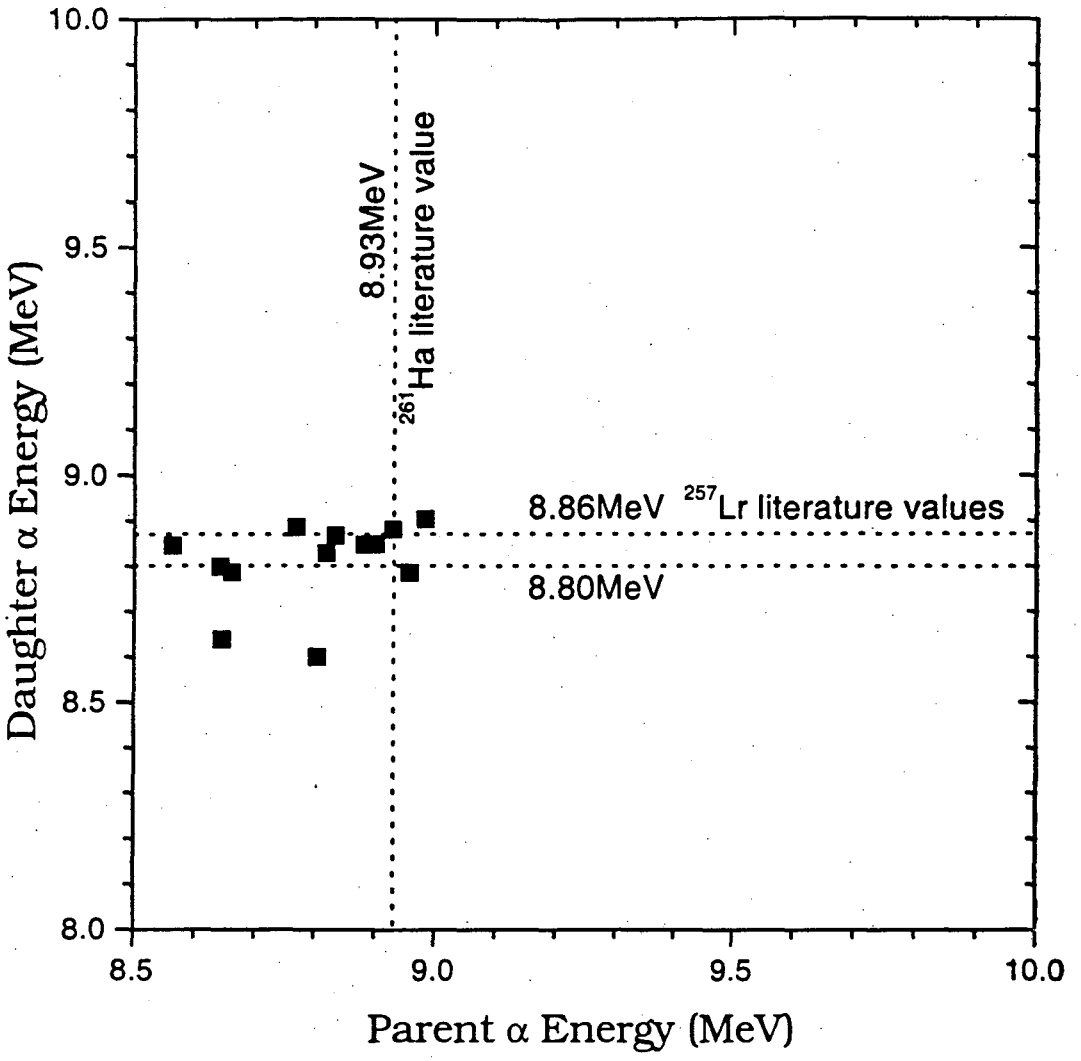

Figure 6.5: Parent-daughter correlations for the reaction $^{250}Cf + ^{15}N$. The α energies of the parent and the daughter for each correlated event are plotted. As a rough guideline, the literature values of the parent and daughter α particle energies are shown by the dotted lines.

α-decay peaks have lower resolution, with a particularly large low-energy tail. This is caused by buildup of the KCl aerosol on the polypropylene foils in addition to energy degradation in the foil. Therefore, a parent α-decay energy may be as much as 200-300 keV lower than the literature value.

Figure 6.6 is used to determine whether the lifetimes of the parent events are consistent with 1.8-s ^{261}Ha. The plotted curve (squares) is the probability of decaying during increasing time intervals for a 1.8-s half-life. The curve for a shorter half-life would show a maximum at shorter times, while the curve for a longer half-life would show a maximum at longer times. Plotted with this curve are the experimental lifetimes of the parent events (circles). As is shown, the lifetimes of these events are consistent with a 1.8-s half-life. However, one should note that this is not a sensitive test for half-lives. No conclusions about the identity of the activity should be drawn from this treatment of the data. For example, the data would be also consistent with a half-life as low as 1 s or as high as 5 s. These curves tell us only that the lifetimes are "reasonable" for such a half-life. Similarly, Figure 6.7 is used to determine whether the experimental lifetimes of the daughter events are consistent with 0.65-s ^{257}Lr. Once again, the lifetimes are consistent with—yet not necessarily indicative of—such a half-life.

The production cross section is calculated using the equation

$$\sigma = \frac{\lambda \cdot (\#\,Events)}{N_t \cdot I \cdot e^{-\lambda t_{start}} \cdot e^{-\lambda t_{trans}} \cdot \left(1 - e^{-\lambda t_{count}}\right) \cdot \left(1 - e^{-\lambda t_{irr}}\right) \cdot eff_{gj} \cdot eff_{det} \cdot (\#\,Expts) \cdot b_\alpha} \qquad (6.1)$$

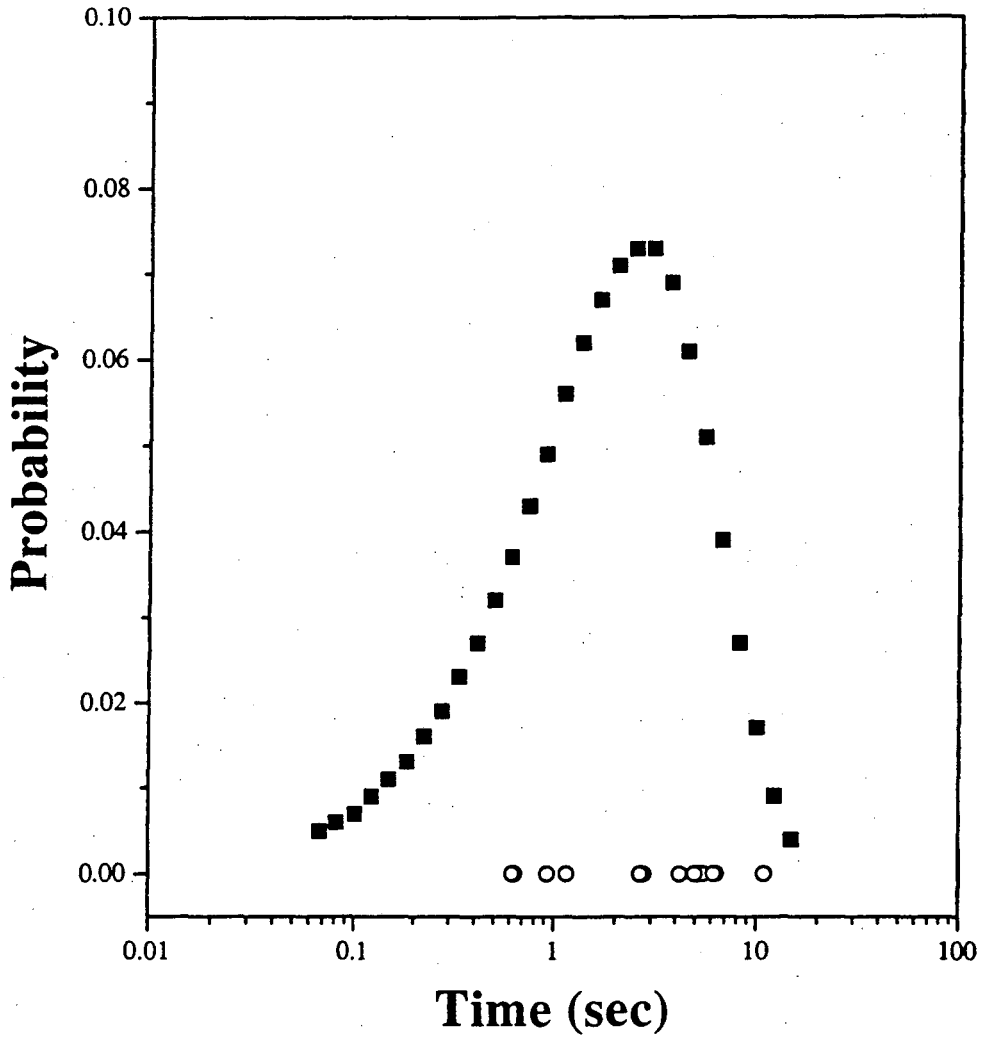

Figure 6.6: Curves plotted (squares) show the probability of decaying during increasing time intervals for a 1.8-sec half-life. The open circles show the experimental lifetimes of the actual events for the reaction $^{250}Cf + {}^{15}N$.

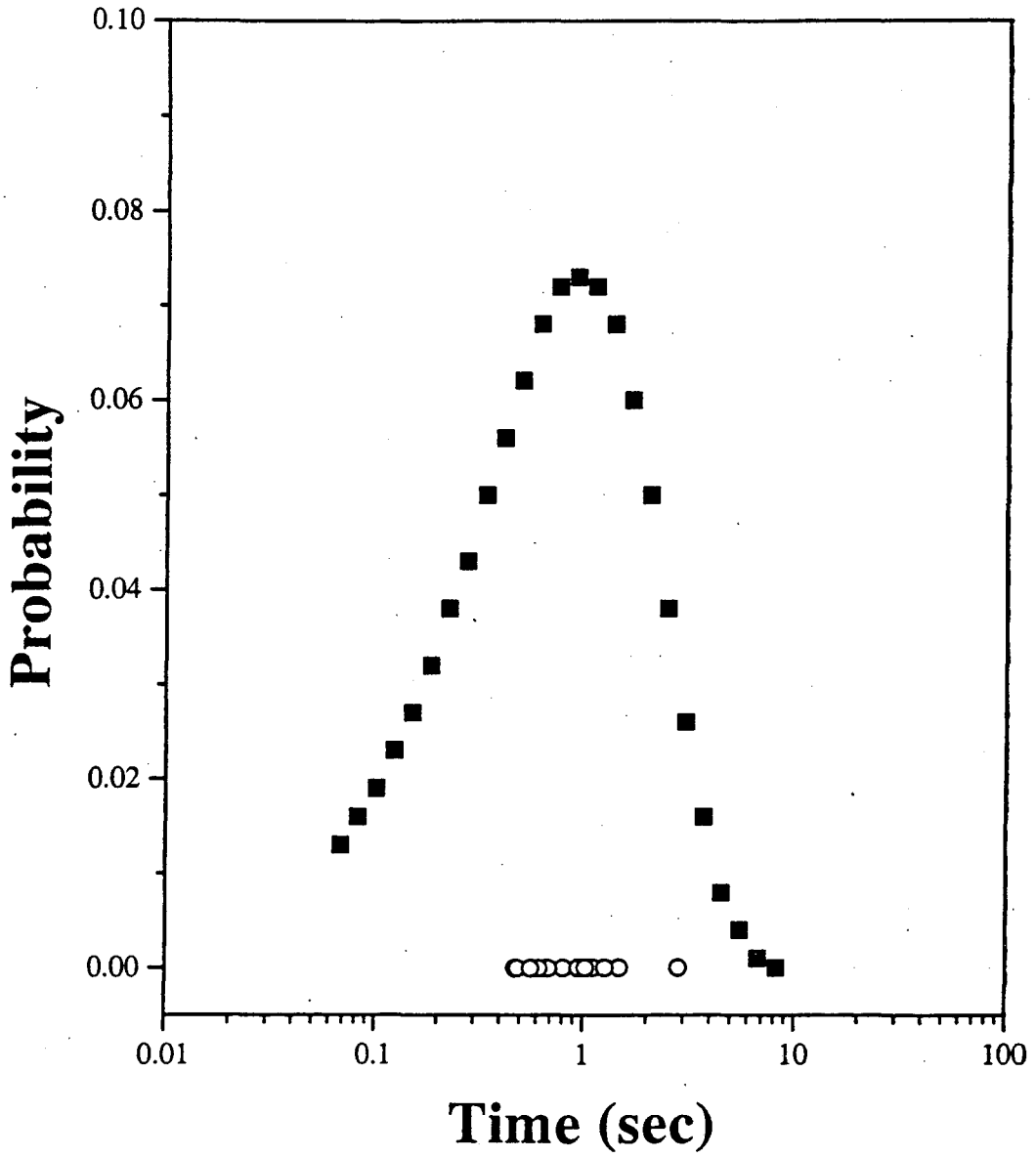

Figure 6.7: Curves plotted (squares) show the probability of decaying during increasing time intervals for a 0.65-sec half-life. The open circles show the experimental lifetimes of the actual events for the reaction $^{250}Cf + {}^{15}N$.

where λ is the decay constant ($ln2/t_{1/2}$), *#Events* is the number of observed α-α correlations (13), N_t is the target thickness (1.73 x 10^{18} cm^{-2}), I is the beam current (2.92 x 10^{12} s^{-1}), t_{start} is the time from end of collection to the beginning of counting (0.1 s), t_{trans} is the transport time from recoil chamber to detection system (1.0 ± 0.3 s), t_{count} is the total counting time of the samples (9 s), t_{irr} is the irradiation time for each sample collected (1.5 s), eff_{gj} is the gas-jet transport yield (86 ± 10 %), eff_{det} is the α-α correlation efficiency (0.21), *#Expts* is the number of samples collected and counted (38005), and b_α is the α branching ratio (assumed to be 100%).

The production cross section of ^{261}Ha from the reaction ^{250}Cf(^{15}N,4*n*) at 84 MeV is 0.51 ± 0.20 nb. This is more than a factor of ten lower than predicted by JORPLE (9.1 nb) and SPIT (6.1 nb) calculations.

6.2 $^{243}Am(^{22}Ne,4n)^{261}Ha$

6.2.1 Results

The isotope ^{261}Ha was produced via the $^{243}Am(^{22}Ne,4n)$ reaction. The 1.78 mg/cm^2 ^{243}Am target (72% ^{243}Am, 28% ^{241}Am) contained 1.28 mg/cm^2 ^{243}Am as the oxide. A beam of 137-MeV $^{22}Ne^{6+}$ passed through a 1.8-mg/cm^2 HAVAR entrance window, the N_2 cooling gas, and 2.3 mg/cm^2 Be target backing before entering the target material. The total energy loss was ~21 MeV. The beam energy was chosen to result in a $^{22}Ne^{6+}$ energy of 116 MeV (laboratory system) in the center of the target. The energy loss in the target was about 2.0 MeV.

The details for gas transport and MG system are the same as in Section 6.1.1 except that the gas jet efficiency was determined to be approximately 74 ± 10 %.

The $^{243}Am(^{22}Ne,4n)$ reaction was run at 116 MeV at the center of the target at an average beam current of 2.0 eμA for approximately 20 hours. The total integrated beam was 25457 pμC. The parent mode α-decay spectrum for the third top detector is shown in Figure 6.8. As before, most of the peaks come from reactions with Pb impurities in the target. The daughter mode α-decay spectrum for all detectors is shown in Figure 6.9. The 6.04-MeV peak is from the decay of ^{209}Rn and ^{210}Rn, the α-decay daughters of ^{213}Ra and ^{214}Ra present in the parent spectrum. Likewise, the 6.14-MeV peak is from the decay of ^{207}Rn and ^{208}Rn, the α-decay daughters of ^{211}Ra and ^{212}Ra present in the parent spectrum. The 7.45-MeV peak is from the decay of $^{211}Po^{g}$, which is produced in a ^{3}He transfer to the ^{208}Pb impurity in the target material.

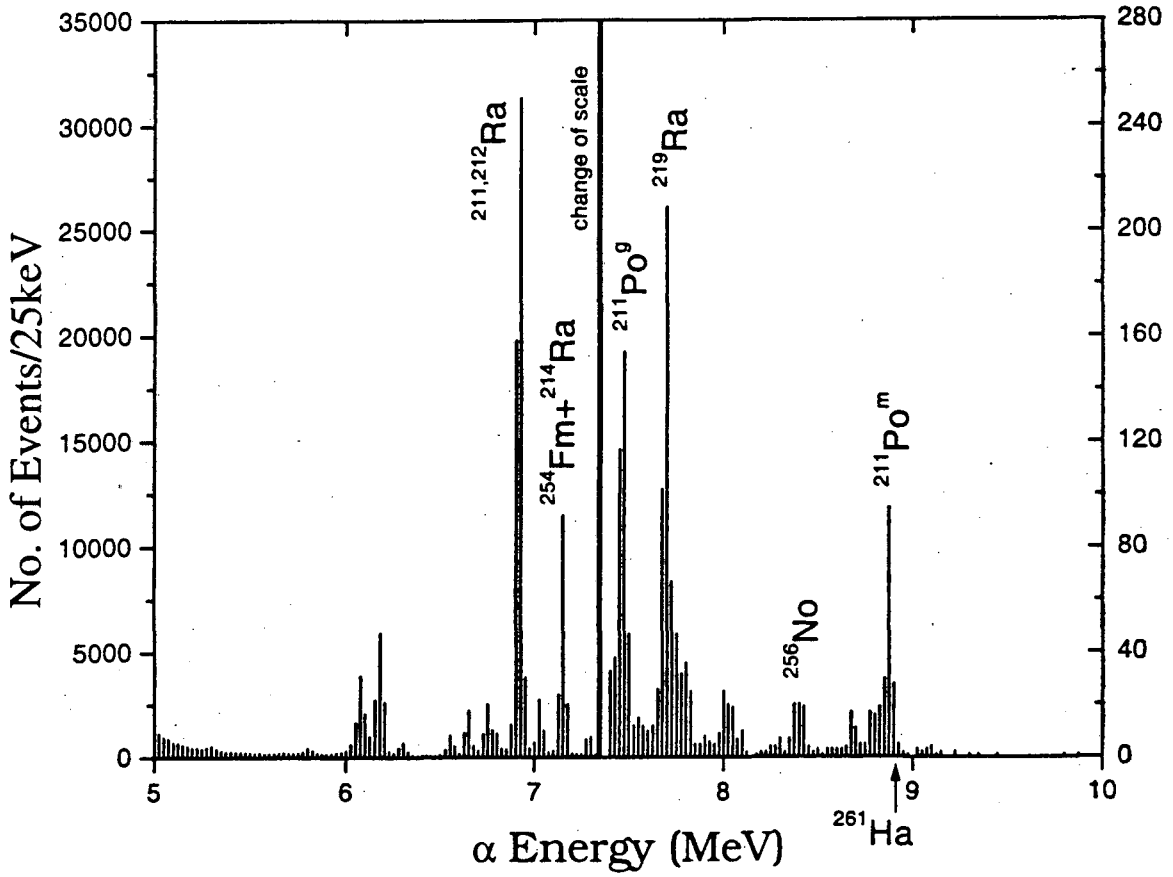

Figure 6.8: The parent mode α spectrum for the reaction $^{243}Am + ^{22}Ne$ for top detector 3 for the entire run.

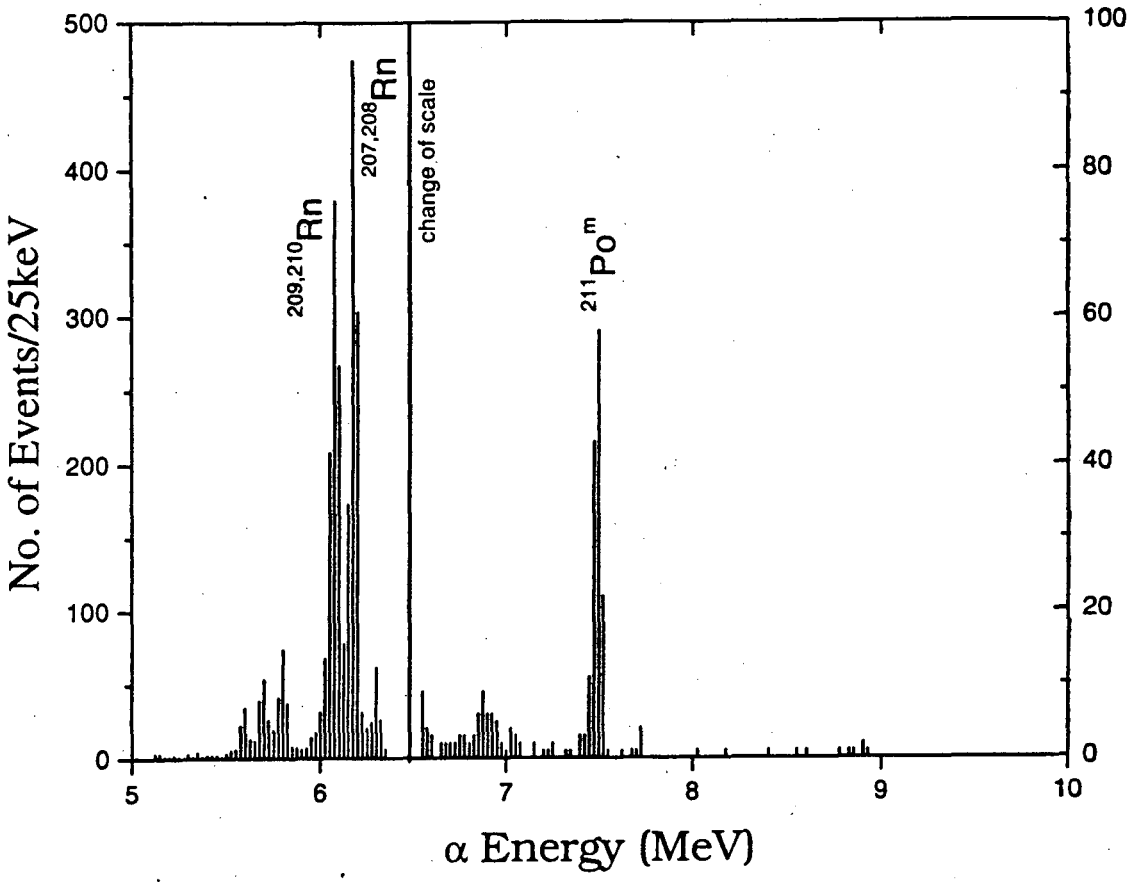

Figure 6.9: The daughter mode α spectrum for the reaction $^{243}Am + ^{22}Ne$ for all detector pairs for the entire run.

A total of nine α-α correlations were observed. Table 6.2 lists the α-decay energy and lifetime of each parent and daughter event. The parent and daughter energies of each α-α correlation are plotted in Figure 6.10. As a rough guideline only, the literature values for the α-decay energies of ^{261}Ha and ^{257}Lr are shown by the dotted lines.

6.2.2 Discussion

The energies of the nine α-α correlation events from Table 6.2 are plotted in Figure 6.10. As can be seen, the energies of most of the events are in accordance with the literature values. The correlations with lower daughter α-decay energy are expected and can be explained as follows. When the parent α-particle is detected in the bottom detector, the daughter nucleus recoils into the top detector. When the daughter nucleus decays, the α-particle can lose energy as it is emitted through the dead layer of the detector at a variety of angles, thereby reducing the measured α-particle energy.

Figure 6.11 is used to determine whether the lifetimes of the parent events are consistent with the 1.8-s ^{261}Ha. As above in Section 6.1.2, the plotted curve (squares) is the probability of decay during increasing time intervals for a 1.8-s half-life. The curve for a shorter half-life would show a maximum at shorter times, while the curve for a longer half-life would show a maximum at longer times. Plotted with this curve are the experimental lifetimes of the parent events (circles). As is shown, the lifetimes of these events are consistent with a 1.8-s half-life. The same warning applies here as in Section 6.1.2. This is not a sensitive test for identification of an activity based on half-life, and

Parent Energy (MeV)	Parent Lifetime (sec)	Daughter Energy (MeV)	Daughter Lifetime (sec)
8.921	4.647	8.856	0.893
8.959	6.885	8.948	1.106
9.069	0.404	8.555	1.392
8.913	0.472	8.405	1.952
8.891	2.044	8.834	0.342
8.910	1.870	8.883	1.350
8.946	5.264	8.799	2.316
8.958	2.453	8.904	0.899
9.038	6.401	8.904	0.454

Table 6.2: Lists of the parent and daughter α particle energies and lifetimes for each α-α correlated event for the reaction $^{243}Am(^{22}Ne,4n)$.

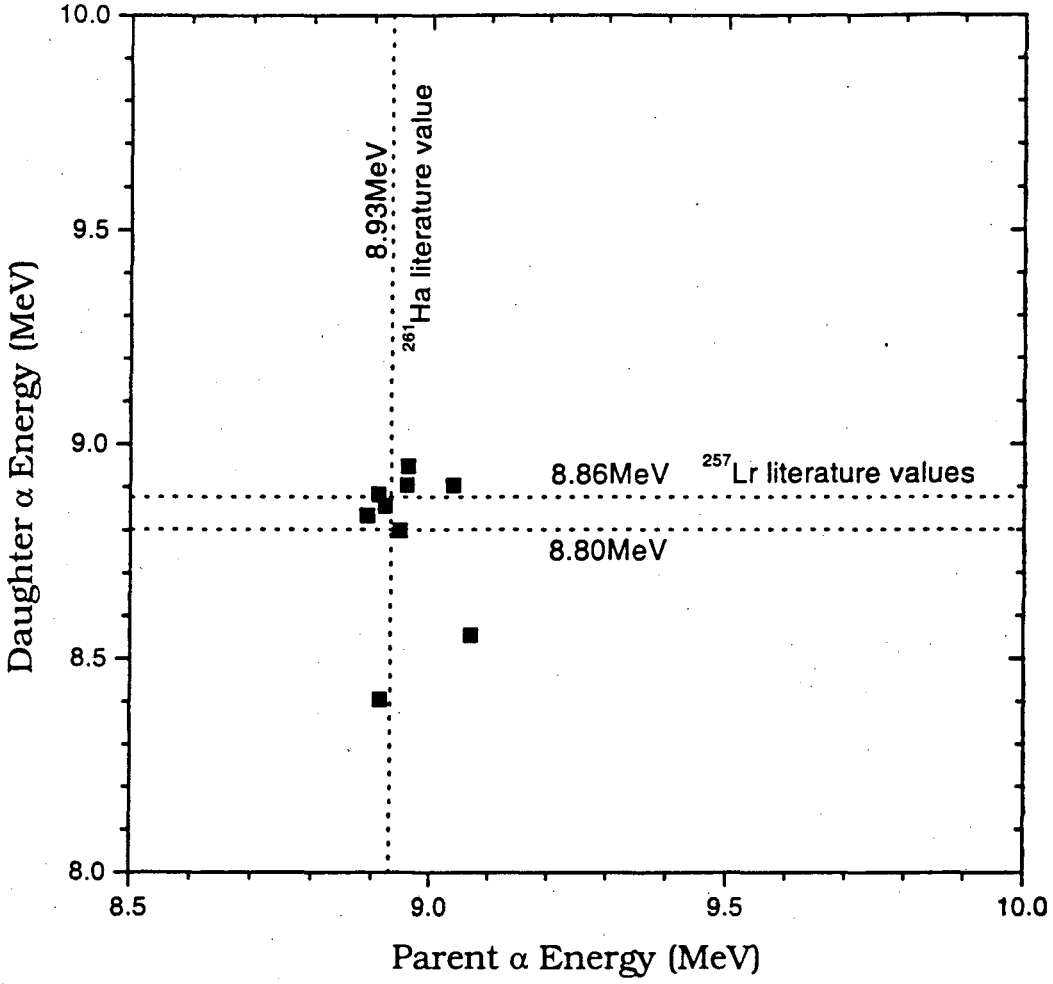

Figure 6.10: Parent-daughter correlations for the reaction $^{243}Am + ^{22}Ne$. The α energies of the parent and the daughter for each correlated event are plotted. As a rough guideline, the literature values of the parent and daughter α particle energies are shown by the dotted lines.

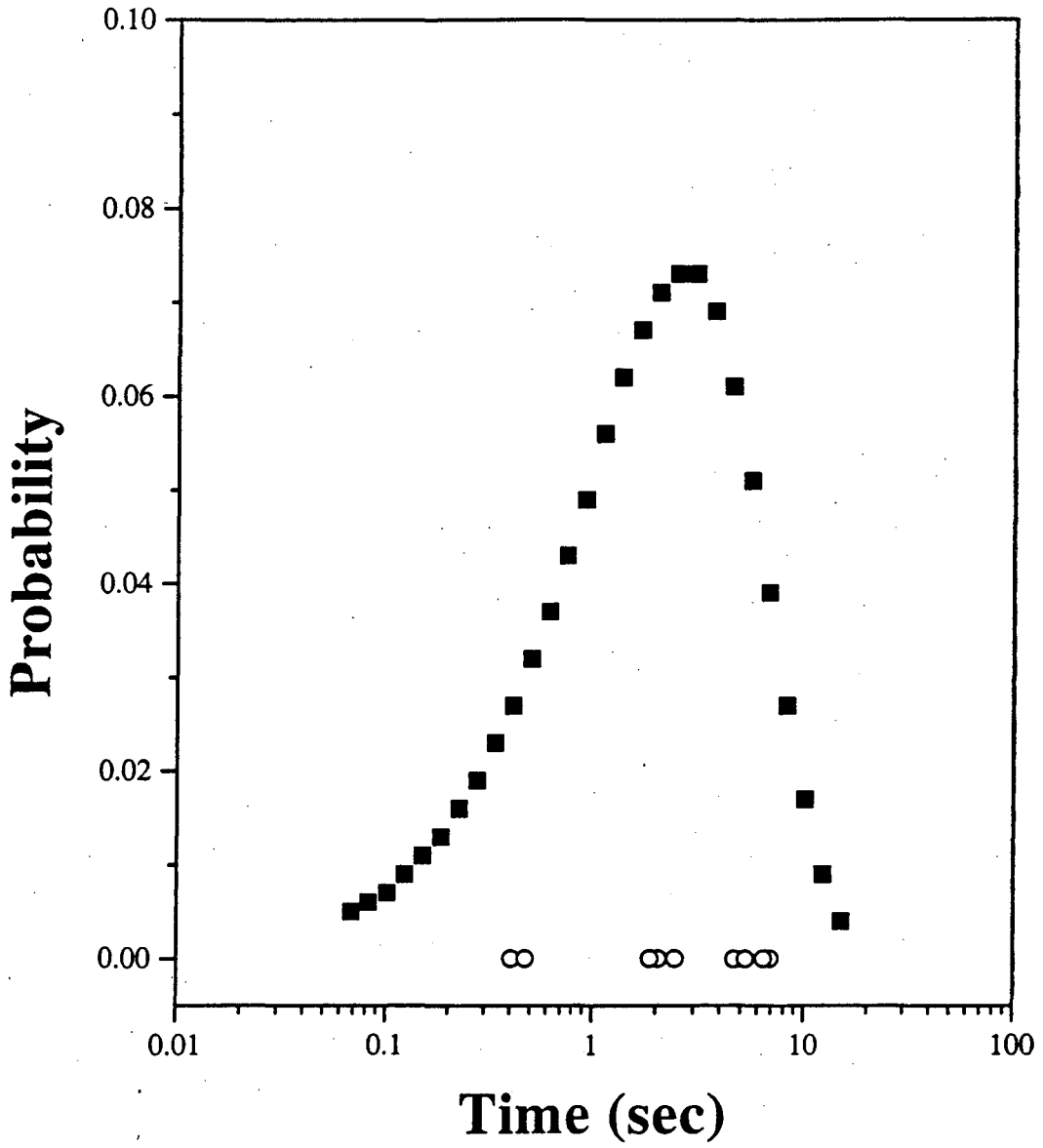

Figure 6.11: Curves plotted (squares) show the probability of decaying during increasing time intervals for a 1.8-sec half-life. The open circles show the experimental lifetimes of the actual events for the reaction $^{243}Am + ^{22}Ne$.

care should be taken in interpreting this data. Similarly, Figure 6.12 is used to determine whether the experimental lifetimes of the daughter events are consistent with 0.65-s ^{257}Lr. Once again, the lifetimes are indeed consistent with—yet not necessarily indicative of—such a half-life.

The production cross section is calculate using Equation 6.1, where λ is the same decay constant ($ln2/t_{1/2}$), *#Events* is the number of observed α-α correlations (9), N_t is the target thickness (3.17 x 10^{18} cm^{-2}), I is the beam current (2.01 x 10^{12} s^{-1}), t_{start} is the time from end of collection to the beginning of counting (0.1 s), t_{trans} is the transport time from recoil chamber to detection system (1.0 ± 0.3 s), t_{count} is the total counting time of the samples (9 s), t_{irr} is the irradiation time for each sample collected (1.5 s), eff_{gj} is the gas-jet transport yield (74 ± 10 %), eff_{det} is the α-α correlation efficiency (0.21), *#Expts* is the number of samples collected and counted (48605), and b_α is the α branching ratio (assumed to be 100%).

The production cross section of ^{261}Ha from the reaction ^{243}Am(^{22}Ne,4*n*) at 116 MeV is 0.25 ± 0.11 nb. Once again, this is lower than expected from the theoretical predictions of JORPLE (0.87 nb) and SPIT (0.83 nb).

The total number of coincident fission events in this reaction was nine for the entire experimental time of twenty hours. By performing a fit of the events using the maximum likelihood decay by the simplex method [Gre91], we have been able to set an upper limit of 18% (68% confidence level) for the SF-decay branch of ^{261}Ha, considerably lower than that of 50% set by Ghiorso et al. [Ghi71]. Our value corresponds to a partial SF-decay half-life of > 10 s (based on a total half-life of 1.8 s) and an HF of

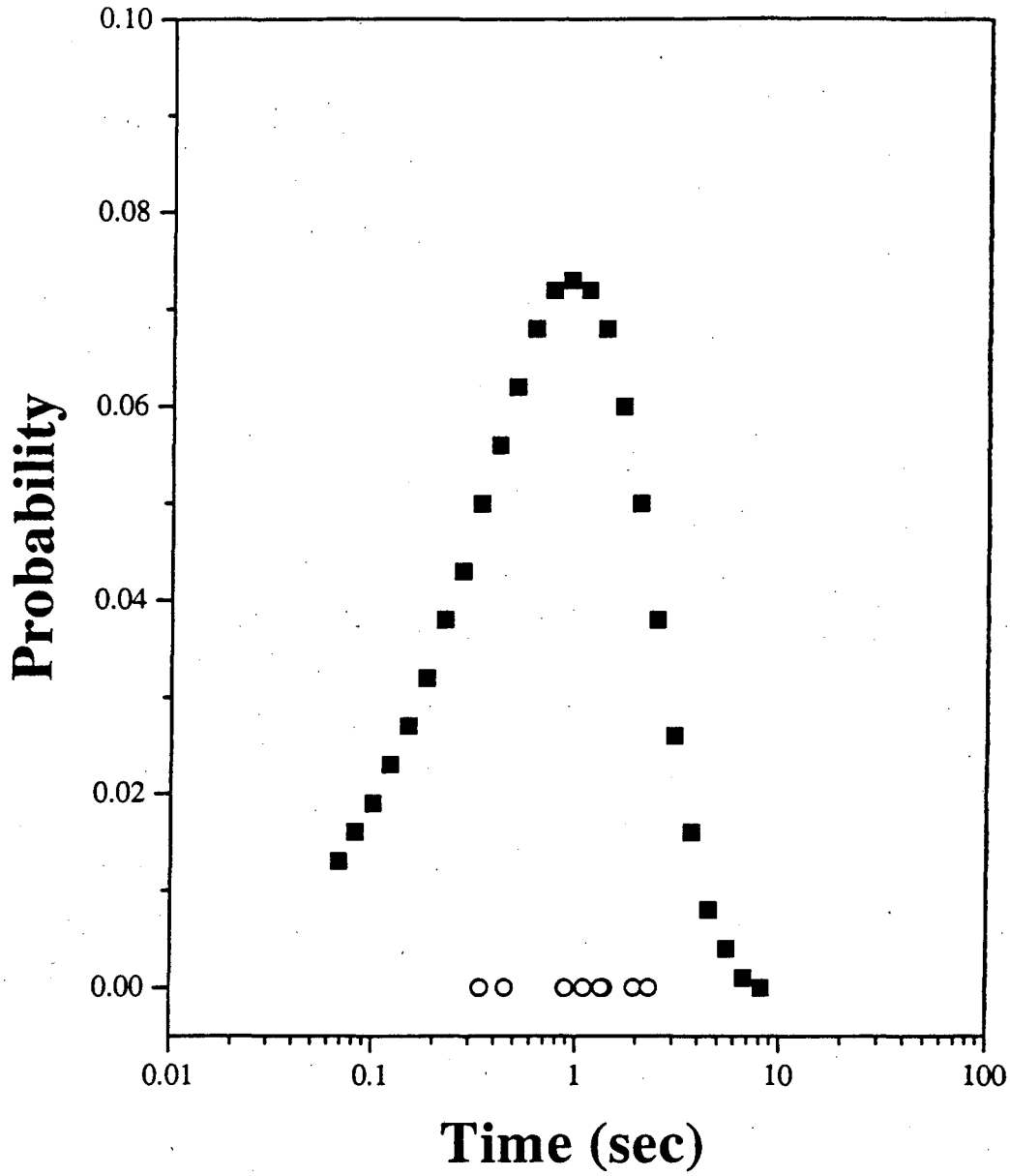

Figure 6.12: Curves plotted (squares) show the probability of decaying during increasing time intervals for a 0.65-sec half-life. The open circles show the experimental lifetimes of the actual events for the reaction $^{243}Am + ^{22}Ne$.

> 500 (log HF > 2.7) relative to 20-ms ^{260}Rf. This value of log HF is consistent with others observed for Z = 105. For example, the other isotopes with an even neutron number, ^{257}Ha and ^{263}Ha, have log HFs of 3.4 and 1.4, respectively (see Figure 3.4).

7 Confirmation of element 106

In 1974, two experiments were performed concurrently to produce and identify element 106. The first was by A. Ghiorso et al. [Ghi74]. Using an ^{18}O ion beam to bombard a ^{249}Cf target, they claimed to have produced the isotope $^{263}106$. To identify it, they observed the time-correlated α-decay events as shown in the decay scheme in Figure 7.1. This proven method has been used earlier to discover rutherfordium (element 104) [Ghi69] and hahnium (element 105) [Ghi70]. They observed 73 total events in the regions around 9.06 MeV and 9.25 MeV, and observed 14 events in those regions that were closely followed by events at 8.77 MeV and 8.86 MeV, which correspond to the α-decay of $^{259}104$, the daughter of $^{263}106$. Furthermore, they were able to observe the α-decay of ^{255}No, the granddaughter of $^{263}106$. Using these events, they established that the prominent α-group of Element 106 is at 9.06±0.04 MeV, and that the half-life is 0.9±0.2 sec.

The second experiment of that year was by Yu. Ts. Oganessian et al. [Oga74]. In order to overcome the extremely small cross sections involved in making heavy elements such as 106, it was decided to use a heavy ion beam on lead instead of a lighter ion beam on californium. In this way, the compound nucleus will have less excitation energy (so-called "cold fusion") and the number of emitted neutrons will decrease, thereby increasing the production of nuclei in the ground state. To produce element 106, a target

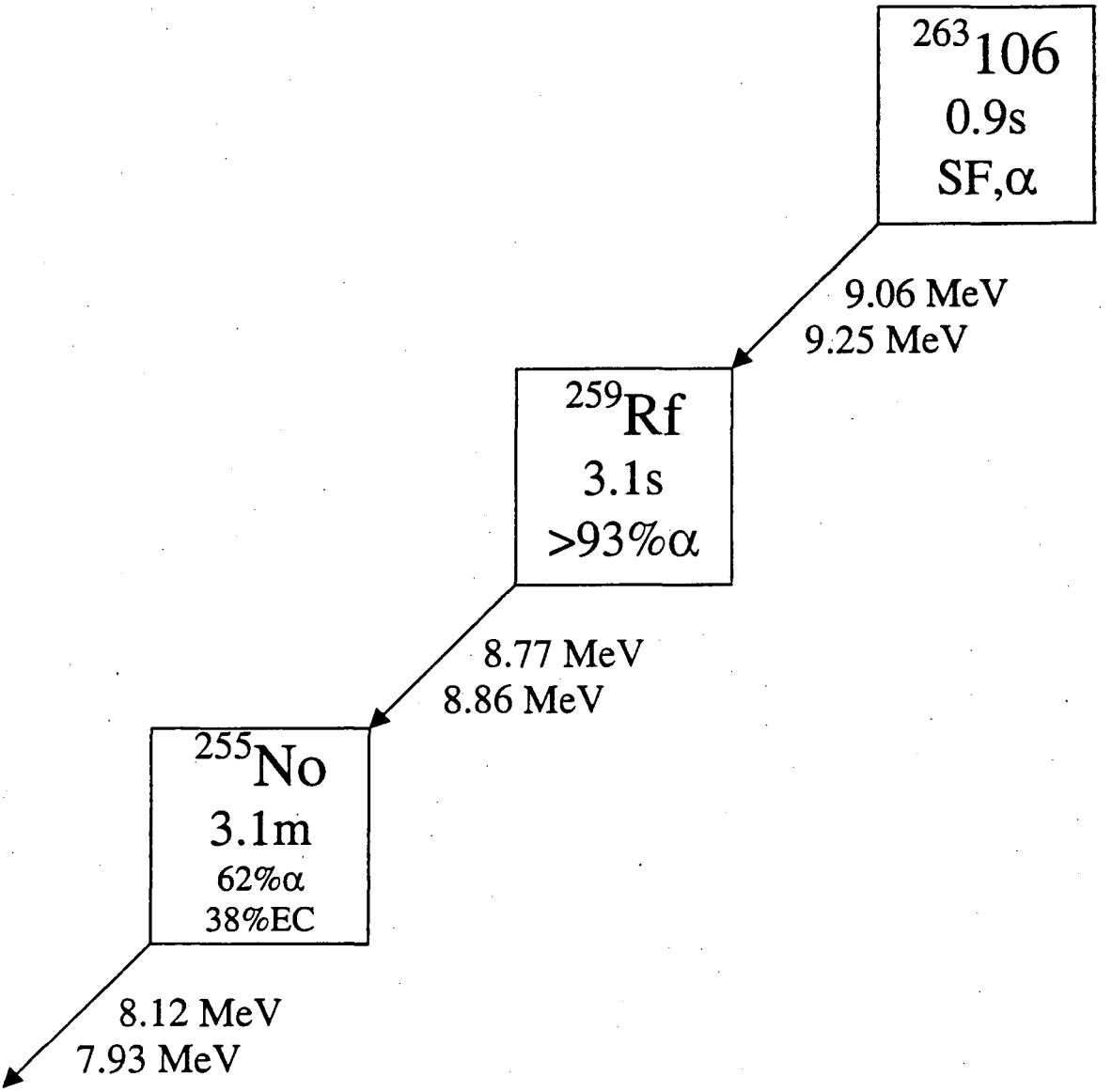

Figure 7.1: Decay of ^{263}106 and its daughter activities.

of ^{206,207,208}Pb was bombarded by a ^{54}Cr ion beam. They observed a total of 50 SF events with a half-life of 4-10 ms. Based on the yield with the different lead isotopes and on SF systematics, the activity was assigned to ^{259}106. However, later experiments in Dubna [Dem84] and Darmstadt [Mun85] were unable to observe this SF activity and, therefore, could not confirm the Oganessian results. It is believed that the SF activity they were primarily observing was from the α-decay daughters of element 106, ^{255,256}Rf. It was the goal of our experiment to confirm the results of A. Ghiorso et al. so that they could propose a name for element 106.

7.1 Results

The isotope $^{263}106$ was produced via the reaction $^{249}Cf(^{18}O,4n)^{263}106$. The 0.80-mg/cm^2 californium oxide target was actually a ^{249}Bk target that was prepared 16 months earlier. ^{249}Bk has a half-life of 320 days and produces ^{249}Cf via β^-–decay. ^{249}Cf has a half-life of 351 years and so builds up with time. At the time of the experiment, the target consisted of approximately 0.52-mg/cm^2 ^{249}Cf and 0.28-mg/cm^2 ^{249}Bk.

The original berkelium target was prepared as follows. The berkelium with the californium daughter was dissolved in 10 M HNO_3 and was oxidized by $KBrO_3$ to the (IV) oxidation state. The 4+ species will extract into 0.5 M di-2-ethylhexylorthophosphoric acid (HDEHP) in heptane, while the 3+ species will not. The organic phase was washed with 10 M HNO_3 containing $KBrO_3$ to improve the separation between the 4+ species and any remaining 3+ species in solution. The Bk^{4+} was then shaken with 0.2 M nitric acid containing a small amount of H_2O_2 to reduce the Bk^{4+} to Bk^{3+}, which will still remain in the organic phase while Pb^{2+} will extract into the aqueous phase. The Bk^{3+} is then finally back extracted into 10 M HNO_3 containing H_2O_2 and washed twice with heptane to remove traces of HDEHP.

The 114 MeV beam of $^{18}O^{5+}$ ions passed through a 2.4 mg/cm^2 HAVAR vacuum window, the N_2 cooling gas, and the 2.5 mg/cm^2 beryllium target backing before passing into the californium target. The projectile energy was chosen as to result in an energy at the center of the target of 94.5-96.0 MeV. The average beam intensity was approximately 350 pnA over approximately sixty hours of experiment time.

Reaction products were transported from the recoil chamber through a 2.1-mm i.d. capillary with a helium flow rate of 4.0 l/min at 1.0 atm. The transport time of the products from the recoil chamber to the detection site located 7.6 m away was approximately 0.4 s.

The parent-daughter stepping mode of the MG system (see Section 4.3.1) was used to facilitate detection of α-α correlations. In parent mode, the stepping time proceeded at 0.7-s intervals, and α-particle energies between 8.9 and 9.2 MeV would trigger daughter mode. The wheel is kept in daughter mode for 7 seconds. On-line energy calibrations were obtained using the α-decay peaks of ^{211}Po (7.45 MeV), ^{215}Rn (8.67 MeV), and ^{212}Po^{m3} (11.65 MeV).

Many events with energies near that expected for ^{263}106 (between 8.9 and 9.2 MeV) were detected, causing initiation of the daughter search mode. Most were caused by pileup of lower-energy α-particles, as discussed in Section 6.1.1. To reduce the time spent in daughter mode (i.e. the mode in which we are not searching for ^{263}106), we limited the beam current to 350 pnA. The time spent in daughter mode was cut to 15% of the total experiment time. The acquisition dead time was reduced to <1% and the volume of data was kept lower by recording events greater than 7 MeV only. Because wheel movement can be the source of noise, data acquisition was disabled for the first 100 ms after the wheel steps.

The resulting α-energy spectrum obtained from summing the data from all the measurements in the daughter mode is shown in Figure 7.2. The ^{252}Fm is present as the daughter of ^{256}No. The long-lived activities on the top detectors were characterized in a

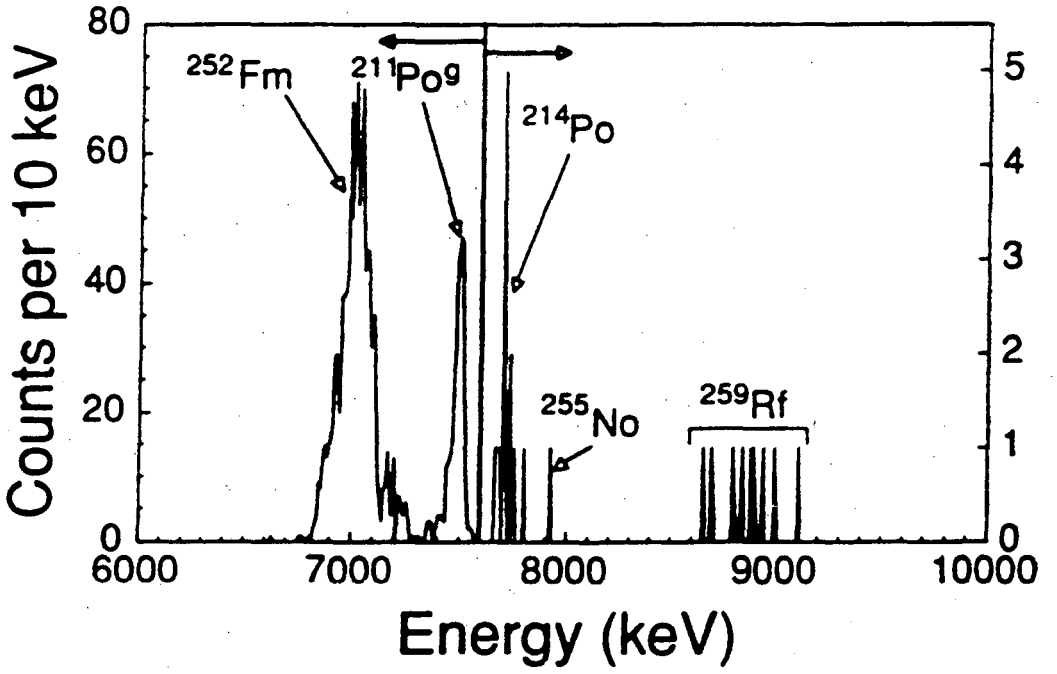

Figure 7.2: The spectrum of all α-particle energies recorded in the odd-numbered detector pairs during the daughter search mode for the reaction $^{249}Cf(^{18}O,4n)$. Note the change in vertical scale at 7.6 MeV.

30-h post-experiment background measurement. In this measurement, the 7.0-MeV α-group was found to decay with the ^{252}Fm half-life of 25.4 h. There was also a small component from the 6.9-MeV α-group of ^{253}Fm, present as the daughter of ^{257}No. ^{211}Po^{g} is present on the top detectors from the α-decay of ^{223}Th and its daughter activities. ^{223}Th is produced by the ^{208}Pb(^{18}O,3*n*) reaction on a small Pb impurity in the ^{249}Cf target. The 7.45-MeV α-group of ^{211}Po^{g} decayed with the known 0.52-s half-life for this isotope during the daughter mode intervals. ^{214}Po is present from the natural content of ^{222}Rn in the air, which comes from the decay of ^{nat}U. In the daughter mode spectrum, the region above the ^{214}Po energy is free of activities other than those from the decay of ^{259}Rf and ^{255}No, the daughter and granddaughter of ^{263}106.

A total of nine daughter events were observed, along with one granddaughter α-decay event (i.e., from the decay of ^{255}No, the daughter of ^{259}Rf). The resulting correlations are shown in Table 7.1.

	Parent			Daughter		
Event#	Detector	Lifetime (s)	Energy (MeV)	Detector	Lifetime (s)	Energy (MeV)
1				3 bottom	0.717	8.70
2	1 bottom	0.283	8.99	1 bottom	0.717	8.66
3	1 bottom	0.283	9.09	1 top	2.850	8.99
4	3 bottom	1.117	9.00	3 top	1.933	8.93
5	3 bottom	1.183	9.05	3 top	0.267	8.80
6	3 bottom	0.783	9.08	3 top	5.467	8.87
7	1 bottom	0.200	8.95	1 top	10.883	8.90
8	5 bottom	1.733	8.90	5 top	0.517	8.83
9				5 top	4.633	9.10

Table 7.1: Daughter mode ^{259}Rf events and ^{263}106 events which initiated the daughter mode.

7.2 Discussion

Table 7.1 lists the detectors, lifetimes and energies of the nine ^{259}Rf events in the odd detector pairs in the daughter mode. Also listed are the detectors, lifetimes and energies of the ^{263}106 events that initiated the daughter search mode intervals for each daughter event. Correlations 3 to 6 and 8 are the type that is expected to predominate. An α-particle of the required energy (between 8.9 and 9.2 MeV) from the decay of ^{263}106 is detected in a bottom detector. The recoil energy of the daughter nucleus ^{259}Rf ($t_{1/2}$ = 3.1 s, E_α = 8.77, 8.87 MeV) is sufficient to eject it from the polypropylene foil and implant it in the top detector. The detected α-particle of the parent causes the wheel to single-step to initiate the search for the daughter. During the daughter mode, the ^{259}Rf decays and the emitted α-particle is detected by the top detector.

In the first and last events, the daughter search mode was initiated by an unrelated event in a different detector pair. Thus, the ^{263}106 parents of these ^{259}Rf events were not detected. Each of these two events can be explained in one of three ways:

(1) The ^{263}106 parent α-particle was emitted in a direction such that it missed the bottom detector and caused the ^{259}Rf to recoil onto the top detector or the top detector holder. The daughter search mode was then initiated by an unrelated event. During this daughter search mode, the ^{259}Rf emitted an α-particle which was detected.

(2) The ^{263}106 decayed in the 100-ms interval around the wheel step during which the data acquisition was disabled, causing the ^{259}Rf

daughter to recoil onto the top detector surface or top detector holder. The daughter search mode was initiated by an unrelated event, allowing the decay of the ^{259}Rf daughter to be detected in either the top or bottom detector.

(3) The daughter mode event is from a long-lived background activity and is unrelated to the decay of any ^{263}106 atom.

A statistical analysis based on the number of α–α correlations observed, detection and recoil efficiencies, half-lives, stepping times, and the numbers of parent and daughter mode intervals resulted in the expectation of 0.24 events of type (1) and 0.25 events of type (2). The observation of one long-lived 8.8-MeV event in the post-run background measurement and assuming this background rate applies to the whole experiment would result in 0.40 events of type (3). The total of expected events of type (1), (2), and (3) is therefore 0.89. The observation of two such events in our experiments is not inconsistent with this value.

The daughter α-decay for the seventh event in Table 7.1 has a lifetime which is longer than the 7-s daughter interval. This can easily be explained by assuming the ^{259}Rf survived the daughter interval initiated by its ^{263}106 parent. The decay of the ^{259}Rf was then detected during a daughter interval initiated by an unrelated event. A statistical analysis indicates 0.89 of these events is expected, which is consistent with the one event observed.

In the remaining six events in Table 7.1, both the ^{263}106 parent and the ^{259}Rf daughter with normal lifetimes were observed. The lifetimes of the seven parent events

were used to determine the $^{263}106$ half-life by a maximum likelihood technique [Gre91], resulting in a half-life of $1.1^{+2.8}_{-0.6}$ s. The error limits indicate the half-life limits for which the likelihood drops to one half its initial value while holding the initial activity at the value from the best fit. This half-life is consistent with the 0.9 s reported by Ghiorso et al [Ghi74]. The distribution of parent energies is fit well with a single α–group at 9.01 ± 0.06 MeV after our 100-keV resolution in the bottom detectors during the parent search mode is considered. This is consistent with that of 9.06 ± 0.04 MeV observed by Ghiorso et al. [Ghi74] for the main α-group from the decay of $^{263}106$. As further argument against a random correlation explanation of these data, it should be noted that the energy distribution of these seven parent events differs from that in the overall parent-mode spectra, where the numbers of events decrease sharply with increasing energy.

Similarly, the lifetimes of the 8 daughter events were used to determine the half-life of the ^{259}Rf. The 10.883-s lifetime of the seventh event in Table 7.1 could not be used since it was outside the daughter mode interval of 7 s, making it difficult to determine a weighting factor for this event. The maximum likelihood fit [Gre91] resulted in a half-life of $1.7^{+0.8}_{-0.5}$ s. This value is consistent with the 3.1 s previously reported [Tul90]. Alpha-groups at 8.866 MeV (40%) and 8.770 MeV (60%) have been reported for the decay of ^{259}Rf [Tul90]. The distribution of ^{259}Rf energies in the present work appears to be broader than this, considering the 40-keV resolution in the daughter search mode. There are two reasons for this difference. Since the ^{259}Rf atoms have recoiled into the face of the top detectors, is possible to detect ^{259}Rf α-particles which are emitted in a direction nearly parallel to the detector surface. The detected energy in these events will

be lower because of the energy loss in the front window of the detector. Also, any conversion electrons which accompany the α-particles have a 50% probability of depositing some energy in the detector. This conversion electron energy will sum with the α–particle energy, producing a prominent high-energy tail on the α-peaks. This effect is more prominent than in [Tul90] because in our experiment the Rf atoms are on the detector surface, resulting in a 50% efficiency for conversion electron summing, and since the depletion depth in our detectors is 300 μm (we assume the detectors in [Tul90] had 100-μm depletion depth), conversion electrons can deposit more energy in our detectors.

The 7.92-MeV event observed in the daughter spectrum can be interpreted as the decay of ^{255}No present on the detector surface from the decay of ^{259}Rf that had recoiled into the detector from the α-decay of ^{263}106. A statistical analysis of the number of such events expected based on the number of ^{259}Rf decays observed in the daughter mode, the fraction of time spent in daughter mode, and the 61.4% α-decay branch in ^{255}No results in the expectation of 1.05 daughter-mode ^{255}No events.

The gas-jet yield was determined by measuring the ^{252}Fm produced in this experiment and comparing with production rates calculated from cross sections for transfer reactions measured previously [Lee83]. ^{252}Fm production in this experiment was determined by measuring the long-lived α-activities in some of the polypropylene foils after removing the wheel from the detector chamber. The gas-jet yield was determined in this way to be near 30% throughout the experiment. Using this gas-jet yield and the other

experimental parameters, we calculate the same $^{263}106$ production cross section of 0.3 nb reported by Ghiorso et al. [Ghi74].

We have produced 0.9-s $^{263}106$ by the $^{249}Cf(^{18}O,4n)$ reaction and identified it by correlating the 9.06-MeV α-decay of $^{263}106$ with the α-decay of the 3.1-s ^{259}Rf daughter. The activities were detected on a rotating wheel system that was run in a parent-daughter mode which minimized the effect of random parent-daughter correlations. The measured decay energies and half-lives of $^{263}106$ and ^{259}Rf are consistent with those previously published, as is the $^{263}106$ production cross section. In our experiment, detection of the 9.06-MeV α-particle from the decay of $^{263}106$ initiated the low-background daughter search mode, providing a direct correlation between parent and daughter α-decays. In the Ghiorso experiment [Ghi74], detectors were put into the low-background positions at preset intervals and an indirect correlation between these low-background daughter events and the $^{263}106$ parent was made based on a half-life argument.

In 1985, the IUPAP and IUPAC formed a Transfermium Working Group (TWG) to consider questions of priority in the discovery of the transfermium elements. The TWG report [Bar92], published in 1992, assigned credit for the discovery of element 106 to Ghiorso et al. based on the experiment described in [Ghi74]. However, in the 1976 article, *Criteria for the Discovery of Chemical Elements* [Har76], the authors state that, "the name for a new element should not be proposed by the discoverers until the initial discovery is confirmed." Our experiment [Gre94b] provided this confirmation of the discovery of element 106. The name seaborgium (Sg) was subsequently proposed by the

discoverers (1994 Meeting of the American Chemical Society) and approved by IUPAC on August 30, 1997.

8 Conclusions and future

Because of the stabilizing effect of the $Z = 108$ and $N = 162$ deformed shells, the SF-decay and α-decay half-lives of the even-even isotopes with $Z \geq 104$ are not decreasing as rapidly as previously anticipated (see Figures 3.1 and 3.2). The recent discoveries of longer than expected half-lives for the e-e isotopes ^{262}Rf (2.1 s SF), ^{265}Sg (~7 s), and ^{266}Sg (~21 s) and isotopes of elements 107 through 111 [Hof95c] (see Figure 8.1) which decay predominantly by α-emission support the results of the calculations of Sobiczewski, Smolanczuk, et al. [Smo95b]. It appears that SF should compete with α-decay in the e-e isotopes of $Z = 108$ with N around 166 to 168, of $Z = 110$ and 112 with $N \geq 170$ with half-lives in the range of tenths of seconds to tens of seconds. For $Z = 114$, α-decay appears to dominate for isotopes in this half-life range. The odd-odd isotopes would be expected to have still longer SF-decay half-lives because of the odd particle hindrances (Figure 3.4) discussed earlier; therefore, α-decay should predominate in these isotopes as well so the SF-decay branches may be too small for study. One question to be answered will obviously be whether these odd-particle hindrances will be as large as previously observed for the lighter isotopes. Another question to be investigated is the possible existence of SF isomers and how to verify this experimentally.

Because the calculation of SF-decay half-lives is extremely sensitive to the path of fission and the fission barriers, work has been done to improve the theoretical understanding of the details of the fission process. As a result, much progress has now

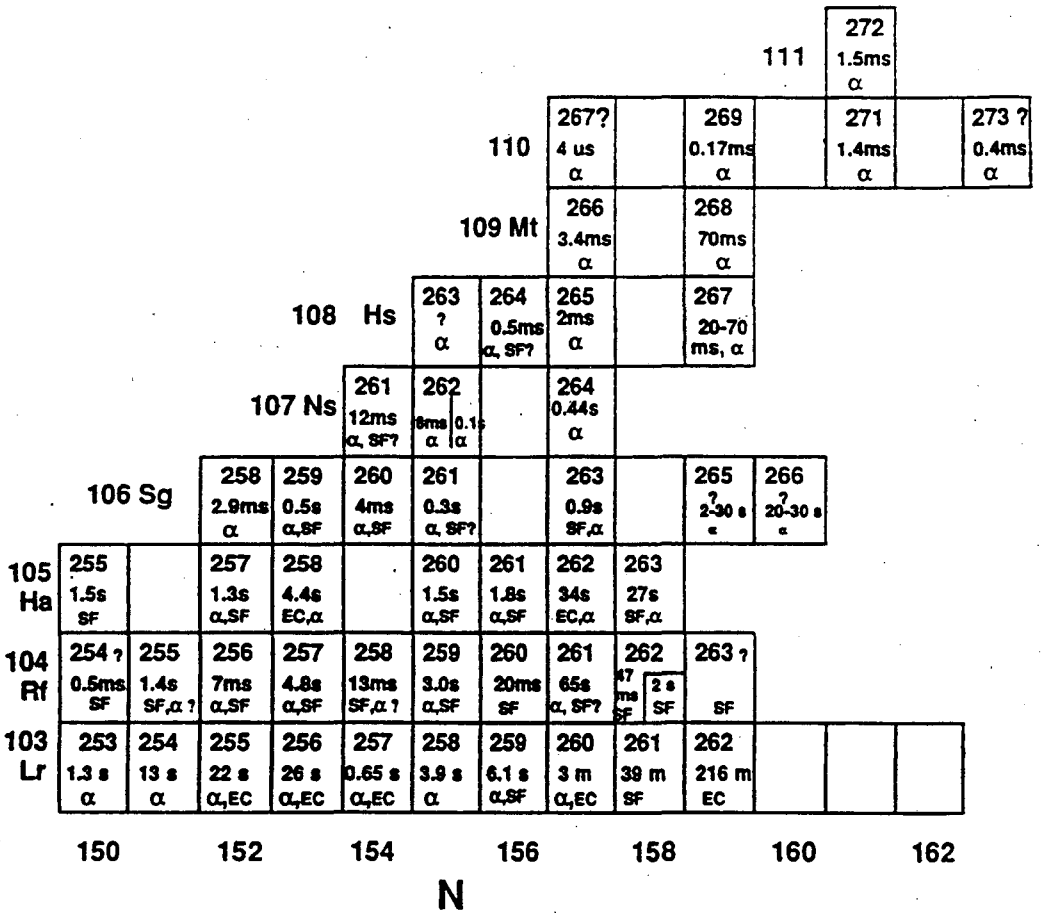

Figure 8.1: Chart of the trans-nobelium isotopes.

been made in developing models with capabilities for predicting half-lives and scission configurations as well as properties of the fission fragments. Now, many challenges remain for the experimentalists seeking to obtain more information about SF in these new, still higher Z isotopes. The first will be to produce a sufficient number of atoms for study, which involves more investigations of possible production reactions. Multiple-target systems utilizing the most neutron-rich actinides that can be made available, such as ^{244}Pu, ^{250}Cm, ^{249}Bk and ^{254}Es, together with appropriate high-intensity, neutron-rich heavy ion beams should greatly help in gaining access to isotopes with half-lives of seconds or longer. Another challenge will be to devise efficient, high-resolution techniques for positively assigning the atomic number and mass of nuclides which cannot be linked by α-decay genetics to known daughter or even granddaughter isotopes. In some cases, such as for Sg (106), Bh (107), Hs (108), and Mt (109), chemical separations may be feasible [Wie95] and experiments to perform chemical separations of Sg are being conducted by an international collaboration. For isotopes with half-lives much less than a second and production cross sections of picobarns or less, on-line or near on-line instrumentation techniques which can provide Z and A resolution sufficient for positive identification, as well as information about mass division, kinetic-energy distributions and neutron and photon emission from the fragments need to be developed. For these reasons, the Berkeley Gas-filled Separator (BGS) [Nin97] has been designed and built and uses a magnetic deflection system filled with gas at low pressure. The recoils undergo atomic collisions in the gas and become ionized. The resulting well-defined average charge state allows high efficiency. Furthermore, these techniques need to be

efficient enough to obtain statistically significant results in a finite length of time. However, the exciting possibility of extending our knowledge of the fission process, the influence of nuclear shells, and the limits to nuclear stability at the heaviest end of the chart of the nuclides appears especially promising.

Appendix A

RECOMMENDED VALUES OF HALF-LIVES AND PARTIAL SF HALF-LIVES OR BRANCHES FOR SF ACTIVITIES[a]

Nuclide	$T_{1/2}$	$T^{SF}_{1/2}$ or % SF	Ref.
^{8}Be	$(6.7^{+2.2}_{-1.3})\times10^{-17}$ sec	$(6.7^{+2.2}_{-1.3})10^{-17}$ sec	
^{230}Th	$(7.54+0.03)\times10^{4}$ years	$>2\times10^{18}$ years	[Hol90]; SF [Hol]
^{232}Th	$(1.40+0.01)\times10^{10}$ years	$>(1.0+0.3)\times10^{21}$ years	[Hol90]; SF [Hol]
^{231}Pa	$(3.25+0.01)\times10^{4}$ years	$>2\times10^{17}$ years	[Hol90]; SF [Hol]
^{234}Pa, g	6.75±0.03 hr	$\leq3\times10^{-10}$% SF	
m	1.17±0.03 min	$\leq10^{-10}$% SF	[Tul95]
^{238}Pa	2.3±0.1 min	$<2.6\times10^{-6}$% SF	
^{230}U	20.8 days	$>4.\times10^{10}$ years	[Tul95]; SF [Hol]
^{232}U	70+1 years	$(8+6)\times10^{13}$ years[b]	[Hol89]
^{233}U	$(1.5911\pm0.0015)\times10^{5}$ years	$>2.7\times10^{17}$ years	
^{234}U	$(2.455+0.006)\times10^{5}$ years	$(1.5+0.2)\times10^{16}$ years	[Hol89]
^{235}U	$(7.04+0.01)\times10^{8}$ years	$(1.0+0.3)\times10^{19}$ years	[Hol89]
^{236}U	$(2.342+0.004)\times10^{7}$ years	$(2.5+0.1)\times10^{16}$ years	[Hol89]
^{238}U	$(4.47+0.02)\times10^{9}$ years	$(8.2+0.1)\times10^{15}$ years	[Hol89]
		$(9.86+0.29)\times10^{15}$ years[c]	[Liu91]
^{237}Np, g	$(2.14\pm0.01)\times10^{6}$ years	$>1\times10^{18}$ years	
^{228}Pu	If $T_{1/2}\cong2$ min, then	$T^{SF}_{1/2}>22$ min	
^{236}Pu	2.87+0.01 years	$(2.1+0.1)\times10^{9}$ years	[Hol89]
^{238}Pu	87.7±0.01 years	$(4.75\pm0.09)\times10^{10}$ years	[Hol89]

Nuclide	$T_{1/2}$	$T_{1/2}^{SF}$ or % SF	Ref.
^{239}Pu	$(2.410\pm0.003)\times10^{4}$ years	$(8\pm2)\times10^{15}$ years	[Hol89]
^{240}Pu	$(6.56\pm0.01)\times10^{3}$ years	$(1.14\pm0.01)\times10^{11}$ years	[Hol89]; SF [Dyt89]
^{241}Pu	14.4 ± 0.1 years	$< 6\times10^{16}$ years	[Hol89]
^{242}Pu	$(3.75\pm0.02)\times10^{5}$ years	$(6.77\pm0.07)\times10^{10}$ years	[Hol89]
^{244}Pu	$(8.00\pm0.09)\times10^{7}$ years	$(6.6\pm0.2)\times10^{10}$ years	[Hol89]
^{241}Am	432.7 ± 0.6 years	$(1.0\pm0.4)\times10^{14}$ years	[Hol89]
^{242}Am, m	141 ± 2 years	$>3\times10^{12}$ years	[Hol89]
^{243}Am	$(7.37\pm0.02)\times10^{3}$ years	$(2.0\pm0.5)\times10^{14}$ years	[Hol89]
^{232}Cm	If $T_{1/2}\cong1$ min, then	$T_{1/2}^{SF}>3.3$ min	
^{240}Cm	26.8 days	$(1.9\pm0.4)\times10^{6}$ years	
^{242}Cm	162.8 ± 0.2 days	$(7.0\pm0.2)\times10^{6}$ years	[Hol89]
^{243}Cm	29.1 ± 0.1 years	$(5.5\pm0.9)\times10^{11}$ years	[Hol89]
^{244}Cm, g	18.1 ± 0.1 years	$(1.32\pm0.02)\times10^{7}$ years	[Hol89]
m	34 ± 2 msec	$\geq1.4\times10^{2}$ years	[Laz89]
^{245}Cm	$(8.48\pm0.06)\times10^{3}$ years	$(1.4\pm0.2)\times10^{12}$ years	[Hol89]
^{246}Cm	$(4.76\pm0.04)\times10^{3}$ years	$(1.81\pm0.02)\times10^{7}$ years	[Hol89]
^{248}Cm	$(3.48\pm0.06)\times10^{5}$ years	$(4.15\pm0.03)\times10^{6}$ years	[Hol89]
^{250}Cm	$\sim9.7\times10^{3}$ years	$(1.13\pm0.05)\times10^{4}$ years	[Hol89]
^{249}Bk	325 ± 7 days	$(1.87\pm0.09)\times10^{9}$ years	
^{237}Cf	2.1 ± 0.3 sec	~10%	[Laz95b]
^{238}Cf	If $T_{1/2}\cong1$ sec, then	$T_{1/2}^{SF}>4$ sec	
	21 msec	~100%	[Laz95b]
^{240}Cf	0.9 ± 0.2 min	~2%	[Laz95b]

Nuclide	$T_{1/2}$	$T^{SF}_{1/2}$ or % SF	Ref.
^{242}Cf	3.4±0.2 min	≤0.014%	[Laz95b]
^{246}Cf	35.7±0.5 hr	$(1.8\pm0.6)\times10^{3}$ years	[Tul95]; SF [Hol]
^{248}Cf	333.5±2.8 days	$(3.2\pm0.3)\times10^{4}$ years	
^{249}Cf	351±2 years	$(8\pm1)\times10^{10}$ years	[Tul95]; SF [Hol]
^{250}Cf	13.08±0.09 years	$(1.7\pm0.1)\times10^{4}$ years	[Tul95]; SF [Hol]
^{252}Cf	2.645±0.008 years	85±1 years	[Tul95]; SF [Hol]
^{254}Cf	60.5±2 days	60.9±0.9 days	[Tul95]; SF [Hol]
^{256}Cf	12.3±1.2 min	12±1 min	[Tul95]; SF [Hol]
^{253}Es	20.47±0.03 days	$(6.3\pm0.2)\times10^{5}$ years	[Tul95]; SF [Hol]
^{254}Es, g	275.7±0.5 days	$>2.5\times10^{7}$ years	
m	39.3±0.2 hr	>10 years	[Tul95]
^{255}Es	39.8±1.2 days	$(2.44\pm0.14)\times10^{3}$ years	[Tul95]; SF [Hol]
^{257}Es	1-3 sec ??	1-3 sec ??	
^{242}Fm	0.8±0.2 msec	0.8±0.2 msec	
^{243}Fm	$0.18^{+0.08}_{-0.04}$ sec	≥50 sec	
^{244}Fm	3.3±0.5 msec	3.3±0.5 msec	
^{245}Fm	4.2±1.3 sec	>4000 sec	
^{246}Fm	1.1±0.2 sec	15±5 sec	[Tul95]; SF [Hol]
^{248}Fm	36±3 sec	10±5 hr	[Tul95]; SF [Hol]
^{250}Fm, g	30±3 min	0.83±0.15 years	[Laz89]
m	1.8±0.1 sec	≥0.07 years	[Laz89]
^{252}Fm	25.39±0.05 hr	125±8 years	[Tul95]; SF [Hol]
^{254}Fm	3.240±0.002 hr	228±1 days	[Tul95]; SF [Hol]

Nuclide	$T_{1/2}$	$T_{1/2}^{SF}$ or % SF	Ref.
^{255}Fm	20.07±0.07 hr	$(1.0\pm0.6)\times10^{4}$ years	[Tul95]; SF [Hol]
^{256}Fm	157.6±1.3 min	2.9±0.1 hr	[Tul95]; SF [Hol]
^{257}Fm	100.5±0.2 days	131±3 years	
^{258}Fm	0.37±0.04 msec	0.37±0.04 msec	[Hof89b]; SF [Hol]
^{259}Fm	1.5±0.2 sec	1.5±0.2 sec	[Hol]; SF [Hol]
^{260}Fm	~4 msec	~4 msec	[Lou92]
^{248}Md	7±3 sec	≤0.05% SF	
^{255}Md	27±2 min	≥12.5 days	
^{256}Md	78.1±1.8 min	<2.8% (>1.9 days)	[Moo92]; SF [Hol]
^{257}Md	5.52±0.05 hr	≤1% (≥23 days)	[Moo92]
^{258}Md, g	51.5±0.3 days	$\leq3\times10^{-3}$% ($\geq5\times10^{3}$ years)	[Moo92]
m	57.0±0.9 min	≤30%	[Moo93]
^{259}Md	1.60±0.06 hr	≈100%	[Moo92]
^{260}Md	27.8±0.8 days	>73%	[Lou92]
		(27.8 days<$T_{1/2}^{SF}$<38.1 days)	
^{250}No	0.25±0.05 msec ??	0.25±0.05 msec ??	
^{251}No	$0.60^{+0.25}_{-0.15}$ sec	>7.5 sec	[Hes85]
^{252}No	$2.25^{+0.18}_{-0.16}$ sec	26.9% (8.36 sec)	[Laz89]; SF [Tul95]
	2.44±0.12 sec		[Wil94]
		(21.6±4.2)%	[And93]
^{254}No, g	55±5 sec	$(3.2\pm0.9)\times10^{4}$ sec	[Tul95]; SF [Laz89]
		$(2.2^{+2.0}_{-1.0})\times10^{4}$ sec	[Tür88]
	53±20 sec	(0.17±0.02)%	[Wil94]

Nuclide	$T_{1/2}$	$T_{1/2}^{SF}$ or % SF	Ref.
^{254}No, m	0.28±0.04 sec	≥1.4x10^{2} sec	[Laz89]
^{256}No	2.91±0.05 sec	550^{+40}_{-70} sec	[Hof90b]
^{258}No	1.2±0.2 msec	1.2±0.2 msec	[Hul89]
^{259}No	58±5 min	>9.7 hr	
^{260}No	106±8 msec ??	106±8 msec ??	
^{262}No	~5 msec	~5 msec	[Lou87], [Lou89]
^{252}Lr	If $T_{1/2}$ >1 sec, then	$T_{1/2}^{SF}$≥100 sec	
^{253}Lr	$1.3^{+0.6}_{-0.3}$ sec	≥2.2 min	
^{254}Lr	$13\pm^{3}_{2}$ sec	≥10^{4} sec	
^{255}Lr	22±5 sec	≥6 hr	
^{256}Lr	25.9±1.7 sec	≥10^{5} sec	
^{257}Lr	0.646±0.025 sec	≥10^{5} sec	
^{258}Lr	$3.92^{+0.35}_{-0.31}$ sec	<5.0% (>78 sec)	[Gre92]
^{259}Lr	6.14 ±0.36 sec	(20±2%)[d] 31±4 sec	[Ham92]
^{261}Lr	39±12 min	100%?	[Lou87]
^{262}Lr	216±15 min	<10.0% (>2160 min)	[Lou87]
^{253}Rf	1.8 sec ??	3.6 sec ??	
^{254}Rf	0.5±0.2 msec?	0.5±0.2 msec?	
^{255}Rf	1.4±0.2 sec	2.7±0.5 sec	
^{256}Rf	6.7±0.2 msec[d]	$6.9^{+0.6}_{-0.2}$ msec	
	6.6±1.1 msec		[Wil94]
^{257}Rf	4.76±0.53 sec	200±25 sec ??	
^{258}Rf	13±2 msec	13±2 msec ≤$T_{1/2}^{SF}$≤15±2 msec	

Nuclide	$T_{1/2}$	$T_{1/2}^{SF}$ or % SF	Ref.
	14±2 msec		[Wil94]
^{259}Rf	3.1±0.7 sec	0.7±0.4 min	[Tul95]; SF [Hol]
^{260}Rf	20.1±0.7 msec	20±1 msec	[Tul95]; SF [Hol]
^{261}Rf	65±10 sec	≥650 sec	
^{262}Rf	47±5 msec	47±5 msec	
	2.1±0.2 sec	2.1±0.2 sec	[Lan96]
^{255}Ha	$1.6^{+0.6}_{-0.4}$ sec	>3 sec	
^{256}Ha	2.6 sec??	≤40%??	[Oga83]
^{257}Ha	$1.3^{+0.5}_{-0.3}$ sec	(17±11%)[d] 8±6 sec	[Tul95]; SF [Hol]
^{258}Ha	$4.4^{+0.9}_{-0.6}$ sec	$\geq 13^{+4}_{-3}$ sec	
^{260}Ha	1.52±0.13 sec	15.8±1.7 sec ?	
^{261}Ha	1.8±0.6 sec	"several times" 2 sec	
		≥3.6 sec	
^{262}Ha	34±4 sec	≈33%[d] (≈102 sec)	[Tul95]; SF [Kra92]
^{263}Ha	27^{+10}_{-7} sec	57^{+13}_{-15}%[d] (47 sec)	[Kra92]
^{259}Sg	$0.48^{+0.28}_{-0.13}$ sec	>2.4 sec	
^{260}Sg	$3.6^{+0.9}_{-0.6}$ msec	$7.2^{+4.8}_{-2.7}$ msec	
^{261}Sg	$0.26^{+0.11}_{-0.06}$ sec	>2.6 sec	
^{263}Sg	0.9±0.2 sec	1.3 sec ??	
	$1.1^{+2.8}_{-0.6}$ sec		[Gre94b]
^{265}Sg	$7.4^{+3.3}_{-2.7}$ sec	≤35%	[Tür98]
^{266}Sg	21^{+20}_{-12} dec	≤82%	[Tür98]
^{261}Bh	$11.8^{+5.3}_{-2.8}$ msec	<10% (>0.12 sec)	[Mün89]; SF [Tul95]

Nuclide	$T_{1/2}$	$T_{1/2}^{SF}$ or % SF	Ref.
^{262}Bh, g	102±26 msec	≤20% (≥510 msec)	[Mün89]; SF [Tul95]
m	8.0±2.1 msec	<30% (>27 msec)	[Mün89]; SF [Tul95]
^{264}Bh	440^{+600}_{-160} msec	ND[e]	[Hof95e]
^{263}Hs	<1 sec	"mainly α decay"	
^{264}Hs	76^{+364}_{-36} μsec	>5 msec	
^{265}Hs	$1.8^{+2.2}_{-0.7}$ msec	≥20 msec	
^{267}Hs	19^{+29}_{-10} msec	≤20%	[Laz95]
^{266}Mt	$3.4^{+6.1}_{-1.3}$ msec	≥62 msec	[Mün89]; SF [Hof89b]
^{268}Mt	70^{+100}_{-30} msec	ND[e]	[Hof95e]
^{269}110	270^{+1300}_{-120} μsec	ND[e]	[Hof95d]
^{272}110	$8.6^{+4.0}_{-2.4}$ msec ??	$8.6^{+4.0}_{-2.4}$ msec ??	
^{272}111	$1.5^{+2.0}_{-0.5}$ msec	ND[e]	[Hof95e]
^{277}112	240^{+430}_{-90} μsec	ND[e]	[Hof96]

a This table is a revised and updated version of Table 1 from [Hof89b]. References are given here for all new or revised values. Half-lives of fission isomers are given in [Poe95].

b This activity, originally attributed to SF, is now believed to be from ^{24}Ne emission [Bar85,Bon90].

c This value has been recommended for use in fission track age calculations.

d These fission branches assume the primary modes of decay are SF and α-particle decay.

e No SF events were observed.

Appendix B

PROPERTIES OF MASS AND TKE DISTRIBUTIONS FOR SF

Nuclide	Peak-to-Valley Ratio[a]	$\overline{TKE}$[b,c] (MeV)	FWHM of TKE[d] (MeV)	Ref.
^{238}U	>500 (RC)	163±3		[Hof74,Ter59]
^{236}Pu	≥700 (SS)[e]	176.3±0.5	24	[Wag89]
^{238}Pu	≥700 (SS)[e]	177.0±0.5	25	[Wag89]
		177.0±0.3		[Sch92]
^{240}Pu	>270 (RC), ≥4000 (SS)[e]	179.4±0.5	28	[Wag89]
		179.4±0.1		[Sch92]
^{242}Pu	≈500 (SS)[e]	180.7±0.5	27	[Wag89]
		180.7±0.1		[Sch92]
^{244}Pu		184±1	28	[All82]
	≥2000 (SS)[f]	181±2	27	f
^{242}Cm	>700 (RC)	180±10		[Hof74,Ter59]
^{244}Cm	>5700 (RC)	183.7[g]		[Hof74]
	86 (SS)	183.6±1		[Cay83]
		188.6		[Hof74]
^{246}Cm	142 (SS)	184.2±0.3	27	[Ple73]
		183.9±0.5	25	[Uni74]
^{248}Cm	asym (SS)	182.2±0.9	25	[Uni74]
		182.0		[Ben93]
^{250}Cm	>10 (SS)	179.8±2.7	29	[Hof73]

Nuclide	Peak-to-Valley Ratio[a]	$\overline{TKE}$[b,c] (MeV)	FWHM of TKE[d] (MeV)	Ref.
^{248}Cf		189.9±1.3[h]		[Vio66b]
^{250}Cf	≥300 (RC)	187.0±0.5	27	[Hof89b,Uni74]
		184.3±2.8	30	[Hof73]
^{252}Cf	≥750 (RC)	186.5 (183.9)	27	[Sch65,Sch66,Wei86]
^{254}Cf	≥145 (RC)	186.9±0.5	28	[Uni74]
^{256}Cf	asym (SS)	189.8±0.9	34	[Hof80c]
^{253}Es	326 (RC)	188±3[i]	31	[Fly76,Bra63]
^{244}Fm	asym (IC)	196±4	--	[Bog82]
^{246}Fm	asym (SS)	199±4	35	[Hof80]
^{248}Fm	asym (SS)	198±4	34	[Hof80]
^{254}Fm	60 (RC)	195.1±1	27	[Gin77]
^{256}Fm	12 (SS)	197.9±0.5	34	[Uni74]
^{257}Fm	≈1.5 (SS)	197.6±3 (194, 227)	36	[Bal71]
^{258}Fm	sym (SS), 8	238±3*	34	[Hof80c]
		230.6[#] (205, 50%; 230, 50%)[j]		[Hul89]
^{259}Fm	sym (SS), 11	242±6[#]	49	[Hul80]
	sym (SS), 12	234±2*	48	[Hof81]
^{259}Md	sym (SS), 27	200.6[#] (202, 88%; 234, 12%)[j]	≈60	[Hul89]
^{260}Md	sym (SS), 7.9	232.5[#] (200, 42%; 234, 58%)[j]	≈35	[Hul89]
^{252}No	asym (SS)	202.4	36	[Bem77]
	~1.6 (SS)	194.3[#]	--	[Hul89b]
		194.3*		[Wil94]

Nuclide	Peak-to-Valley Ratio[a]	$\overline{TKE}$[b,c] (MeV)	FWHM of TKE[d] (MeV)	Ref.
^{254}No		189.2*		[Wil94]
^{256}No	1-1.5 (SS), ~50	196±3#	42	[Hof90b]
^{258}No	sym (SS)	203.2# (204, 95%; 232, 5%)[j]	≈50	[Hul89]
^{262}No	sym (SS), 12	(237, 65%; 200, 35%)[j]		[Lou87,Lou89]
^{259}Lr	≈sym (SS), 20	214±3	40	[Ham92]
^{256}Rf		207±13		[Hes85b]
		197.6±1.1*		[Wil94]
^{258}Rf		220±15		[Hes85b,Hes84]
		198.9±4.4*		[Wil94]
^{260}Rf	sym (SS), 36	200	44	[Hul89]
^{262}Rf		215±2#		[Lan96]
^{262}Ha	asym (SS) or if sym, >47			[Bem77b]
^{263}Ha	sym (SS)	≈210[k]		[Kra92]
^{263}Sg		<30%		[Laz95]

a Ratios derived from radiochemical (RC) data, or from ionization chamber (IC) or solid-state (SS) detector measurements of the kinetic energies of the fission fragments. For symmetric fission, values of the full-width-at-half maximum (FWHM) are given after the method.

b These are average values of the pre-neutron emission TKE's except for those denoted by (#) which are most probable values of the pre-neutron emission TKE's or by (*) which are most probable TKE's from a provisional mass analysis without corrections for neutron emission as a function of fragment mass.

c Solid-state measurements of TKE prior to about 1982 were usually normalized to a post-neutron emission average TKE ($\overline{TKE}$) value of 183.1 MeV (corresponding to a pre-neutron emission value of 186.5±1.2 MeV) for ^{252}Cf according to the method of Schmitt *et al.* [Sch65,Sch66]. Measurements of TKE denoted by (#) have been normalized to a post-neutron emission value for ^{252}Cf of 181.0 MeV (corresponding to a pre-neutron value of about 183.9 MeV), recently redetermined by Weissenberger *et al.* [Wei86] and are derived from a provisional mass analysis without corrections for neutron emission. Henschel *et al.* [Hen81] have also redetermined the TKE of ^{252}Cf as 181.25±1.3 MeV and 184.07±1.3 MeV for the post- and pre-neutron emission values, respectively.

d Full width at half maximum of TKE distribution as measured, or calculated from 2.35 times σ for the TKE distribution.

e Value derived from data in [Wag89] based on the absence of events in a valley region of 5 mass units (C. Wagemans, private communication, 1992).

f Values based on measurements in progress; peak-to-valley ratio based on a valley width of 5 mass units (C. Wagemans, private communication, 1992).

g Time-of-flight measurement.

h Corrected to pre-neutron emission $\overline{TKE}$ for ^{252}Cf = 185.7 MeV, in [Vio66b].

i Relative to pre-neutron emission $\overline{TKE}$ for ^{252}Cf = 183.0 MeV.

j Values in parentheses are those of the two Gaussian functions by which the TKE distributions could be represented [Hul89,Lou87,Lou89].

k A pre-neutron emission value was estimated from the post-neutron emission value of 207±7 MeV given in [Kra92].

Appendix C

EXPERIMENTAL VALUES OF $\bar{\nu}_T$ AND σ_ν^2 FOR SPONTANEOUS FISSION

Nuclide	$\bar{\nu}_T$ [a]	σ_ν^2 [b]	Standard [c]	Ref.
^{238}U	1.98±0.03	0.80±0.15	^{252}Cf = 3.735	[Laz77]
	1.99±0.03[d]		^{252}Cf = 3.757	[Hol83]
^{236}Pu	2.23±0.19		^{240}Pu = 2.19	[Ort71]
	2.12±0.13	1.26±0.20	^{252}Cf = 3.735	[Laz77]
^{238}Pu	2.26±0.08		^{240}Pu = 2.19	[Ort71]
	2.21±0.07	1.29±0.05	^{252}Cf = 3.735	[Laz77]
^{240}Pu	2.19±0.03		^{252}Cf = 3.77	[Ort71]
	2.14±0.01	1.32±0.01	^{252}Cf = 3.735	[Laz77]
	2.141±0.016	1.3099	^{252}Cf = 3.743	[Hua84]
^{242}Pu	2.15±0.05		^{244}Cm = 2.73	[Ort71]
	2.12±0.01	1.31±0.01	^{252}Cf = 3.735	[Laz77]
^{244}Pu	2.30±0.19		^{252}Cf = 3.77	[Ort71]
^{242}Cm	2.57±0.09		^{240}Pu = 2.19	[Ort71]
	2.51±0.06	1.21±0.03	^{252}Cf = 3.735	[Laz77]
	2.562±0.020	1.3312	^{252}Cf = 3.743	[Hua84]
	2.54±0.020[d]	1.22	^{252}Cf = 3.757	[Hol86]
^{244}Cm	2.73±0.04		^{240}Pu = 2.19	[Ort71]
	2.76±0.09		^{240}Pu = 2.19	[Ort71]

Nuclide	$\bar{\nu}_T$ [a]	σ_ν^2 [b]	Standard [c]	Ref.
	2.69±0.01	1.23±0.05	^{252}Cf = 3.735	[Laz77]
	2.721±0.021	1.3246	^{252}Cf = 3.743	[Hua84]
	2.72±0.02[d]	1.26	^{252}Cf = 3.757	[Hol86]
^{246}Cm	3.19±0.22		^{252}Cf = 3.77	[Ort71]
	2.94±0.03	1.31±0.02	^{252}Cf = 3.735	[Laz77]
	2.93±0.03[d]	1.28	^{252}Cf = 3.757	[Hol86]
^{248}Cm	3.11±0.09		^{252}Cf = 3.77	[Ort71]
	3.10±0.01	1.37±0.01	^{252}Cf = 3.735	[Laz77]
	3.13±0.03[d]	1.29	^{252}Cf = 3.757	[Hol86]
^{250}Cm	3.31±0.08		^{252}Cf = 3.77	[Ort71]
	3.30±0.08[d]		^{252}Cf = 3.757	[Hol86]
^{249}Bk	3.40±0.05[d]		^{252}Cf = 3.757	[Hol86]
^{246}Cf	2.83±0.19		^{240}Pu = 2.19	[Ort71]
	3.14±0.09	1.66±0.31	^{252}Cf = 3.735	[Laz77]
	3.1±0.1[d]	1.68	^{252}Cf = 3.757	[Hol86]
^{250}Cf	3.53±0.09		^{252}Cf = 3.77	[Ort71]
	3.49±0.04	1.49±0.03	^{252}Cf = 3.735	[Hof80d]
	3.53±0.02	1.52±0.02	^{252}Cf = 3.735	[Laz77]
	3.51±0.04[d]	1.53	^{252}Cf = 3.757	[Hol86]
^{252}Cf	3.771±0.031		Abs. m., 1963	[Hop63]
	3.738±0.015	1.566±0.003	Abs. m., 1974	[Bol74]
	3.7509±0.0107		Abs. m., 1985	[Axt85]

Nuclide	$\bar{\nu}_T$ [a]	σ_ν^2 [b]	Standard [c]	Ref.
	3.773±0.007	1.5824	Abs. m., 1981	[Spe82]
	3.757±0.010[d]	1.59	^{252}Cf = 3.757	[Hol86]
^{254}Cf	3.93±0.05		^{252}Cf = 3.77	[Ort71]
	3.77±0.05	1.56±0.01	^{252}Cf = 3.735	[Hof80d]
	3.85±0.06[d]	1.53	^{252}Cf = 3.757	[Hol86]
^{253}Es	4.7[e]			[Uni74]
^{254}Fm	3.96±0.14	1.50±0.20	^{252}Cf = 3.735	[Laz77]
	4.00±0.19		^{252}Cf = 3.77	[Ort71]
	4.0±0.3[d]		^{252}Cf = 3.757	[Hol86]
^{256}Fm	3.91±0.03	2.02±0.13	^{252}Cf = 3.755	[Sok89]
	3.73±0.18	2.30±0.65	^{252}Cf = 3.735	[Laz77]
		1.82±0.08	^{252}Cf = 3.735	[Hof80d]
	3.59±0.06	2.16±0.05	^{252}Cf = 3.735	[Ter81]
	3.63±0.06[d]		^{252}Cf = 3.757	[Hol86]
^{257}Fm	3.77±0.02	2.49±0.06	^{252}Cf = 3.735	[Bal73]
	3.85±0.05	2.51±0.02	^{252}Cf = 3.735	[Hof80d]
	3.77±0.02	2.49±0.06	^{252}Cf = 3.735	[Laz77]
	3.87±0.05[d]		^{252}Cf = 3.757	[Hol86]
^{259}Md	4.2			[Ter87]
^{260}Md	2.58±0.11	2.57±0.13	^{252}Cf = 3.773	[Wil90]
^{252}No	4.15±0.30	4.0±1.3	^{252}Cf = 3.735	[Laz77]
	4.20±0.30	4.2	^{252}Cf = 3.757	[Hol86]

a $\bar{\nu}_T$ is the average number of neutrons emitted per fission event.

b σ_ν^2 is the variance for the neutron multiplicity distribution.

c Abs. m. means "Absolute measurement".

d Evaluated value from Holden and Zucker, [Hol83] and [Hol86].

e Estimated by comparison of pre- and post-neutron-emission mass-yield curves from SS and RC measurements.

Bibliography

General References

Friedlander, G., Kennedy, J.W., Macias, E.S., Miller, J.M., Nuclear and Radiochemistry, 3rd Edition, John Wiley & Sons, New York (1981).

Hoffman, D.C., Hamilton, T.M., Lane, M.R., Nuclear Decay Modes, Inst. of Phys. Publ., Bristol, England, ed. D.N. Poenaru (1995).

Krane, K.S., Introductory Nuclear Physics, John Wiley & Sons, New York (1988).

Seaborg, G.T. and Loveland, W.D., The Elements Beyond Uranium, John Wiley & Sons, Inc., New York (1990).

Smolanczuk, R., Skalski, J., Sobiczewski, A., Phys. Rev. C **52**, 1871 (1995).

Sobiczewski, A., Phys. Part. Nucl. **25**, 119 (1994).

Vandenbosch, R. and Huizenga, J.R., Nuclear Fission, Academic Press, Inc., New York (1973)

Specific References

[Adl93] Adloff, J.P. and Guillaumont, R., Fundamentals of Radiochemistry, pp. 327-341, CRC Press, Inc., Boca Raton, FL, USA (1993).

[Alk88] Alkhazov, I.D., Gerasimenko. B.F., Kuznetsov, A.V., Petrov, B.F., Rubchenya, V.A., Shpakov, V.I., Sov. J. Nucl. Phys. **48**, 978 (1988).

[Alk88b] Alkhazov, I.D., Dmitriev, V.D., Kovalenko, S.S., Kuznetsov, A.V., Malkin, L.Z., Petrzhak, K.A., Petrov, B.F., Shpakov, V.I., Sov. J. Nucl. Phys. **47**, 773 (1988).

[All82] Allaert, E., Wagemans, C., Wegener-Penning, G., Deruytter, A. J., Barthélémy, R., Nucl. Phys. A **380**, 61 (1982).

[Alo73] Alonso, J., Gmelin Handbuch der Anorganischen Chemie, Verlag Chemie, GmbH Weinheim/Bergstrasse, Band 7b Part A1 (1973).

[And93] Andreyev, A.N., Bogdanov, D.D., Chepigin, V.I., Kabachenko, A.P., Malyshev, O.N., Sagaidak, R.N., Salamatin, L.I., Ter-Akop'yan, G.M., Yeremin, A.V., Z. Phys. A **345**, 389 (1993).

[Aud] G. Audi, Private Communication (1993).

[Aum74] Aumann, D. and Mullen, G., Nucl. Instrum. Methods **115**, 75 (1974).

[Axt85] Axton, E J. and Bardell, A.G., Metrologia **21**, 59 (1985).

[Bal71] Balagna, J.P., Ford, G.P., Hoffman, D.C., Knight, J.D., Phys. Rev. Lett. **26**, 145 (1971).

[Bal73] Balagna, J.P., Farrell, J.A., Ford. G.P., Hemmendinger, A., Hoffman, D.C., Veeser, L.R., Wilhelmy, J.B., in Proc. IAEA Symp. Phys. Chem. of Fission, 3rd, Vol. II, Rochester, New York, August 13-17, 1973, ed. Mautner Markhof, F., Int. Atomic Energy Agency, Vienna, Austria, p. 191 (1974).

[Bar57] Bardeen, J., Cooper, L.N., Shrieffer, J.R., Phys. Rev. **108**, 1175 (1957).

[Bar81] Baran, A., Pomorski, K., Lukasiak, A., Sobiczewski, A., Nucl. Phys. A **361**, 83 (1981).

[Bar85] Barwick, S.W., Price, P.B., Stevenson, J.D., Phys. Rev.C **31**, 1984 (1985).

[Bar87] Baran, A. and Lojewski, Z., Nucl. Phys. A **475**, 327 (1987).

[Bar92] Barber, R.C., Greenwood, N.N., Hrynkiewicz, A.Z., Jeannin, Y.P., Lefort, M., Sakai, M., Ulehla, I., Wapstra, A.H., Wilkinson, D.H., Prog. Part. Nucl. Phys. **29**, 453 (1992).

[Bat88] Batenkov, O.I., Blinov, A.B., Blinov, M.V., Smirnov, S.N., Atomnaya Energiya **64**, 6, 429 (1988).

[Bec96] Becquerel, H., Compt. Rend. **122**, 501, 559, 689, 762, 1086 (1896).

[Bed56] Bedov, V.B. and Kosyakov, V.N., Proc. Intl. Conf. on Peaceful Uses of Atomic Energy, **7**, 369 (1956).

[Bem73] Bemis, Jr., C.E., McGowan, F.K., Ford, Jr., J.L.C., Milner, W.T., Stelson, P.H., Robinson, R.L., Phys. Rev. C **8**, 1466 (1973).

[Bem76] Bemis Jr., C.E., Hensley, D.C., Dittner, P.F., Hahn, R.L., Silva, R.J., Tarrant, J.R., Hunt, L.D., ORNL Report 5137, 73 (1976).

[Bem77] Bemis, C.E. Jr., Ferguson, R.L., Plasil, F., Silva. R.J., Pleasonton, F., Hahn, R. L., Phys. Rev. C **15**, 705 (1977).

[Bem77b] Bemis, C.E. Jr., Ferguson, R.L., Plasil, F., Silva, R.J., Hulet, E.K., Lougheed, R.W., Phys. Rev. Lett. **39**, 1246 (1977).

[Bem81] Bemis, Jr., C.E., Dittner, P.F., Ferguson, R.L., Hensley, D.C., Plasil, F., Pleasonton, F., Phys. Rev. C **23**, 555 (1981).

[Ben93] Benoufella, A., Barreau, G., Asghar, M., Audouard, P., Brisard, F., Doan, T.P., Hussonnois, M., Leroux, B., Trochon, J., Moore, M.S., Nucl. Phys. A **565**, 563 (1993).

[Ber96] Berger, J.F., Bitaud, L., Decharge, J., Girod, M, Peru-Desenfants, S., in Proc. Intl. Workshop XXIV on Gross Properties of Nuclei and Nuclear excitations "Extremes of Nuclear Structure", Hirschegg (Austria), eds. H. Feldmeier, J. Knoll, W. Nörenberg (GSI, Darmstadt) p. 43 (1996).

[Bog82] Bogdanov, D.D., Ivanov, M.P., Popeko, G.S., Rodin, A.M., Ter-Akopyan, G.M., Vakatov, V.I., Voronin, A.S., Phys. Lett. B **113B**, 213 (1982).

[Boh39] Bohr, N., and Wheeler, J.A., Phys. Rev. **56**, 426 (1939).

[Boi84] Boissevain, J.G., Fowler, M.M., Gavron, A.I., Hoffman, D.C., Lysaght, P., Wilhelmy, J.B., Isotope and Nuclear Chemistry Division Annual Report FY 1984, Los Alamos National Laboratory Progress Report LA-10366-PR, p. 147 (1984).

[Bol74] Boldeman, J.W., Nucl. Sci. and Eng. **55**, 188 (1974).

[Bon90] Bonetti, R., Fioretto, E., Migliorino, C., Pasinetti, A., Barranco, F., Vigezzi, E., Broglia, R.A., Phys. Lett. B **241**, 179 (1990).

[Bow63] Bowman, H.R., Milton, J.C.D., Thompson, S.G., Swiatecki, W.J., Phys. Rev. **129**, 2133 (1963).

[Bra63] Brandt, R., Thompson, S.G., Gatti, R.C., Phillips, L., Phys. Rev. **131**, 2617 (1963).

[Bri82] Britt, H.C., Actinides in Perspective, p. 245, ed. N.M. Edelstein, Pergamon, Oxford (1982).

[Bro83] Brosa, U. and Grossmann, S., Z. Phys. A **310**, 177 (1983).

BIBLIOGRAPHY

[Bro90] Brosa, U., Grossmann, S., Müller, A., Phys. Reports C **197**, 167 (1990).

[Bud88] Budtz-Jørgensen, C. and Knitter, H-H., Nuc. Phys. A **490**, 307 (1988).

[Cay83] Caytucoli, F., Asghar, M., Leroux, B., Barreau, G., Hamadache, K., Sicre, A., Doan, T.P., Allab, M, Nucl. Phys. A **394**, 360 (1983).

[Cha32] Chadwick, R., Proc. Roy. Soc. **A136**, 692 (1932).

[Cur98] Curie, P., and Sklodowska Curie, M., Compt. Rend. **127**, 175 (1898).

[Cwi87] Cwiok, S., Dudek, J., Nazarewicz, W., Skalski, J., Werner, T., Comput. Phys. Commun. **46**, 379 (1987).

[Cwi89] Cwiok, S., Rozmej, P., Sobiczewski, A., Patyk, Z., Nucl. Phys. A **491**, 281 (1989).

[Cwi92] Cwiok, S., Sobiczewski, A., Z. Phys. A **342**, 203 (1992).

[Cwi96] Cwiok, S., Dobaczewski, J., Heenen, P.-H., Magierski, P., Nazarewicz, W., Nucl. Phys. A **611**, 211 (1996).

[Dem84] Demin, A.G., Tretyakova, S.P., Utyonkov, V.K., Shirokovsky, I.V., Z. Phys. A **315**, 197 (1984).

[Dem95] Dematté, L., Wagemans, C., D'hondt, P., Deruytter, A., in *Seminar on Fission "Pont d'Oye III"*, May 1995.

[Dou84] Dougan, R.J., Lougheed, R.W., Hulet, E.K., Bethune, G.R., Nucl. Chem. Div. FY-84 Annual Report, Lawrence Livermore National Laboratory Report UCAR 10062-84/1, 2-15 (1984).

[Dru73] Druin, V.A., Lobanov, Yu.V., Nadkarni, D.M., Kharitonov, Yu.P., Korotkin, Yu.S., Tretyakova, S.P., Krashonkin, V.I., At. Energ. **35**, 279 (1973) [Sov. J. At. En. **35**, 946 (1974)].

[Dyt89] Dytlewski, N., Hines, M.G., Boldeman, J.W., Nucl. Sci. and Eng. **102**, 423 (1989).

[Eva72] Evans, J.E., Lougheed, R.W., Coops, M.S., Hoff, R.W., Hulet, E.K., Nucl. Instr. Meth. **102**, 389 (1972).

[Fer34] Fermi, E., Z. Phys. **88**, 161 (1934).

[Fer34b] Fermi, E., Nature **133**, 898 (1934).

[Fir96] Firestone, R.B., Shirley, V.S., Baglin, C.M., Chu, S.Y.F., Zipkin, J., Table of Isotopes, 8th Edition, John Wiley & Sons, New York (1996).

[Fle64] Flerov, G.N., Oganessian, Y.T., Lobanov, Y.V., Kuznetsov, V.I., Druin, V.A., Perelygin, V.P., Gavrilov, K.A., Tret'yakova, S.P., Plotko, V.M., Phys. Lett. **13**, 73 (1964).

[Fle71] Flerov, G.N., Lazarev, Yu.A., Lobanov, Yu.V., Oganesyan, Yu.Ts., Tretyakova, S.P., in *Proc. Intl. Conf. on Heavy Ion Physics, Dubna, 1971*, JINR-D7-5769, p. 125 (ORNL-tr-2711).

[Fly76] Flynn, K.F., Gindler, J.E., Glendenin, L.E., Sjoblom, R.K., J. Inorg. Nucl. Chem. **38**, 661 (1976).

[Gäg91] Gäggeler, H.W., Jost, D.T., Baltensperger, U., Weber, A., Kovacs, A., Vermeulen, D., Türler, A., Nucl. Instr. and Meth. A **309**, 201 (1991).

[Ghe96] Gherghescu, R.A., Patyk, Z., Skalski, J., Sobiczewski, A., Proc. Intern. Workshop: Research with Fission Fragments, Benediktbeuern (Germany) 1996, eds. T. von Egidy, D. Habs, F.J. Hartmann, K.E.G. Löbner, J. Nifenecker (World Scientific, Singapore 1997) p. 116.

[Ghi69] Ghiorso, A., Nurmia, M., Harris, J., Eskola, K., Eskola, P., Phys. Rev. Lett. **22**, 1317 (1969).

[Ghi70] Ghiorso, A., Nurmia, M., Eskola, K., Harris, J., Eskola, P., Phys. Rev. Lett. **24**, 1498 (1970).

[Ghi71] Ghiorso, A., Nurmia, M., Eskola, K., Eskola, P., Phys. Rev. C **4**, 1850 (1971).

[Ghi73] Ghiorso, A., Eskola, K., Eskola, P., Nurmia, M., Phys. Rev. C **7**, 2032 (1973).

[Ghi74] Ghiorso, A., Nitschke, J.M., Alonso, J.R., Alonso, C.T., Nurmia, M., Seaborg, G.T., Hulet, E.K., Lougheed, R.W., Phys. Rev. Lett. **33**, 1490 (1974).

[Ghi95] Ghiorso, A., Lee, D., Somerville, L.P., Loveland, W., Nitschke, J.M., Ghiorso, W., Seaborg, G.T., Wilmarth, P., Leres, R., Wydler, A., Nurmia, M., Gregorich, K.E., Czerwinski, K., Gaylord, R., Hamilton, T., Hannink, N.J., Hoffman, D.C., Jarzynski, C., Kacher, C., Kadkhodayan, B., Kreek, S., Lane, M.R., Lyon, A., McMahan, M.A., Neu, M., Sikkeland, T., Swiatecki, W.J., Türler, A., Walton, J.T., Yashita, S., Phys. Rev. C **51**, R2293 (1995).

[Gin77] Gindler, J.E., Flynn, K.F., Glendenin, L.E., Sjoblom, R.K., Phys. Rev. C **16**, 1483 (1977).

[Glä89] Gläßel, P., Schmid-Fabian, R., Schwalm, D., Habs, D., v.Helmolt, H.U., Nucl. Phys. A **502**, 315c (1989).

[Gre91] Gregorich, K.E., Nucl. Instrum. Methods Phys. Res., Sect. A **302**, 135 (1991).

[Gre92] Gregorich, K.E., Hall, H.L., Henderson, R.A., Leyba, J.D., Czerwinski, K.R., Kreek, S.A., Kadkhodayan, B., Nurmia, M.J., Lee, D.M., Hoffman, D.C., Phys. Rev. C **45**, 1058 (1992).

[Gre94] Gregorich, K. E., Hoffman, D. C., Lee, D. M., Mohar, M. F., Lane, M. R., Hannink, N. J., Kacher, C. D., M. P. Neu, Sylwester, E. R., Hsu, M., Yang, J. C. Nucl. Sci. Div. 1993 Annual Report, Lawrence Berkeley Laboratory Report LBL-35768, 75 (1994).

[Gre94b] Gregorich, K.E., Lane, M.R., Mohar, M.F., Lee, D.M., Kacher, C.D., Sylwester, E.R., Hoffman, D.C., Phys. Rev. Lett. 72, 1423 (1994).

[Hah39] Hahn, O. and Strassman, F., Naturwissenschaften **27**, 11 (1939).

[Hal89] Hall, H.L, Gregorich, K.E., Henderson, R.A., Lee, D.M., Hoffman, D.C., Bunker, M.E., Fowler, M.M., Lysaght, P., Starner, J.W., Wilhelmy, J.B., Phys. Rev. C **39**, 1866 (1989).

[Ham92] Hamilton, T.M., Gregorich, K.E., Lee, D.M., Czerwinski, K.R., Hannink, N.J., Kacher, C.D., Kadkhodayan, B., Kreek, S.A., Nurmia, M.J., Lane, M.R., Neu, M.P., Türler, A., Hoffman, D.C., Phys. Rev. C **46**,1873 (1992).

[Har76] Harvey, B.G., Herrmann, G., Hoff, R.W., Hoffman, D.C., Hyde, E.K., Katz, J.J., Keller, Jr., O.L., Lefort, M., Seaborg, G.T., Science **193**, 1271 (1976).

[Hat90] Hatsukawa, Y., Nakahara, H., Hoffman, D.C., Phys. Rev. C **42**, 674 (1990).

[Hen81] Henschel, H., Kohnle, A., Hipp, H., Gönnenwein, G., Nucl. Instr. and Meth. **190**, 125 (1981).

[Hes84] Hessberger, F.P., Münzenberg, G., Hofmann, S., Agarwal, Y.K., Armbruster, P., Poppensieker, K., Reisdorf, W., Schmidt, K.-H., Sahm, C.-C., Schneider, J.R.H., Schneider, W.F.W., Thuma, B., Vermeulen, D., GSI Ann. Report, Gesellschaft für Schwerionenforschung, Darmstadt, 1984.

[Hes85] Hessberger, F.P., GSI-85-11, GSI, Darmstadt, West Germany (1985).

[Hes85b] Hessberger, F.P., Münzenberg, G., Hofmann, S., Reisdorf, W., Schmidt, K.H., Schoett, H.J., Armbruster, P., Hingmann, R., Thuma, B., Vermeulen, D., Z. Phys. A **321**, 2, 317 (1985).

[Hof73] Hoffman, D.C., Ford, G.P., Balagna, J.P., Phys. Rev. C **7**, 276 (1973).

[Hof74] Hoffman, D.C. and Hoffman, M.M., Annu. Rev. Nucl. Sci. **24**, 151 (1974).

[Hof80] Hoffman, D.C., Lee, D., Ghiorso, A., Nurmia, M., Aleklett, K., Phys. Rev. C **22**, 1581 (1980).

[Hof80b] Hoffman, D.C., Paper IAEA/Sm-241/F14, in Proc. Int. Symp. Physics and Chem. of Fission 1979, Vol. II., Jülich, ed. J.W. Weil, International Atomic Energy Agency, Vienna, 275 (1980).

[Hof80c] Hoffman, D.C., Wilhelmy, J.B., Weber, J., Daniels, W.R., Hulet, E.K., Lougheed, R.W., Landrum, J.H., Wild, J.F., Dupzyk, R. J., Phys. Rev. C **21**, 972 (1980).

[Hof80d] Hoffman, D.C., Ford, G.P., Balagna, J.P., Veeser, L.R., Phys. Rev. C **21**, 637 (1980).

[Hof81] Hoffman, D.C., Lee, D., Ghiorso, A., Nurmia, M.J., Aleklett, K., Leino, M., Phys. Rev. C **24**, 495 (1981).

[Hof89] Hoffman, D.C., in Proceedings of the Conference on 50 Years with Nuclear Fission, National Institute of Standards and Technology, Gaithersburg, 1989 (American Chemical Society, LaGrange Park, 1989), Vol. I, p. 83; Lawrence Berkeley Laboratory Report No. LBL-27093 (1989).

[Hof89b] Hoffman, D.C. and Somerville, L.P., Charged Particle Emission from Nuclei, Vol. III, CRC Press, Inc., Boca Raton, Florida, eds. D.N. Poenaru and M.S. Ivascu, Chapter One (1989).

[Hof89c] Hoffman, D.C., Nucl Phys. A **502**, 21c (1989).

[Hof90] Hoffman, D.C. and Hoffman, M.M., Lawrence Berkeley Laboratory Report No. LBL-29502, 1990.

[Hof90b] Hoffman, D.C., Lee, D.M., Gregorich, K.E., Nurmia, M.J., Chadwick, R.B., Chen, K.B., Czerwinski, K.R., Gannett, C.M., Hall, H.L., Henderson, R.A., Kadkhodayan, B., Kreek, S. A., Leyba, J.D., Phys. Rev. C **41**, 631 (1990).

[Hof93] Hoffman, D.C., Radiochim. Acta **61**, 123 (1993).

[Hof95] Hoffman, D.C., Hamilton, T.M., Lane, M.R., Nuclear Decay Modes, Inst. of Phys. Publ., Bristol, England, ed. D.N. Poenaru (1995).

[Hof95b] Hoffman, D.C. and Lane, M.R., Radiochim. Acta **70/71**, 135 (1995).

[Hof95c] Hofmann, S., GSI Report GSI-95-25 (1995).

[Hof95d] Hofmann, S., Ninov, V., Hessberger, P., Folger, H., Münzenberg, G., Schött, H.J., Popeko, A.G., Yeremin, A.V., Andreyev, A.N., Saro, S., Janik, R., Leino, M., Z. Phys. A **350**, 277 (1995).

[Hof95e] Hofmann, S., Ninov, V., Hessberger, P., Folger, H., Münzenberg, G., Schött, H.J., Popeko, A.G., Yeremin, A.V., Andreyev, A.N., Saro, S., Janik, R., Leino, M., Z. Phys. A **350**, 281 (1995).

[Hof96] Hofmann, S., Ninov, V., Heßberger, F.P., Armbruster, P., Folger, H., Münzenberg, G., Schött, H.J., Popeko, A.G., Yeremin, A.V., Saro, S., Janik, R., Leino, M., Z. Phys. A **354**, 229 (1996).

[Hol] Holden, N.E. and Hoffman, D.C., Report BNL-46463, revision in preparation.

[Hol83] Holden, N.E., and Zucker, M.S., in *Proc. ANS/INMM Topical Meeting on Safeguards and Technology, Hilton Head, South Carolina, 1983,* Trans. Amer. Nucl. Soc. **45**, Suppl. 1, 23 (1983).

[Hol86] Holden, N.E. and Zucker, M.S., Radiation Effects **96**, 1-4, 289 (1986).

[Hol89] Holden, N.E., Pure & Appl. Chem. **61**, 8, 1483 (1989).

[Hol90] Holden, N.E., Pure & Appl. Chem. **62**, 5, 941 (1990).

[Hop63] Hopkins, J.C. and Diven, B.C., Nucl. Phys. **48**, 433 (1963).

[Hua84] Huanqiao, Z., Zuhua, L., Shengyue, D., Shaoming, L., Nucl. Sci. and Eng. **86**, 315 (1984).

[Hul80] Hulet, E.K., Lougheed, R.W., Landrum, J.H., Wild, J.F., Hoffman, D.C., Weber, J., Wilhelmy, J.B., Phys. Rev. C **21**, 966 (1980).

[Hul86] Hulet, E.K., Wild, J.F., Dougan, R.J., Lougheed, R.W., Landrum, J.H., Dougan, A.D., Schädel, M., Hahn, R.L., Baisden, P.A., Henderson, C.M., Dupzyk, R.J., Sümmerer, K., Bethune, G.R., Phys. Rev. Lett. **56**, 313 (1986).

[Hul89] Hulet, E.K., Wild, J.F., Dougan, R.J., Lougheed, R.W., Landrum, J.H., Dougan, A.D., Baisden, P.A., Henderson, C.M., Dupzyk, R.J., Hahn, R.L., Schädel, M., Sümmerer, K., Bethune, G.R., Phys. Rev C **40**, 770 (1989).

[Hul89b] Hulet, E.K., Wild, J.F., Lougheed, R.W., Dougan, R.J., Moody, K.J., Report LLNL UCAR 10062-89, Lawrence Livermore National Laboratory, 1989, p. 86.

[Hul90] Hulet, E.K., J. Radioanal. Nucl. Chem. Articles **142**, 79 (1990).

[Hul94] Hulet, E.K., Phys. Atomic Nuclei **57**, 1099 (1994).

[Hyd87] Hyde, E.K., Hoffman, D.C., Keller, Jr., O.L., Radiochim. Acta **42**, 57 (1987).

[Kad92] Kadkhodayan, B., Türler, A., Gregorich, K.E., Nurmia, M.J., Lee, D.M., Hoffman, D.C., Nucl. Instr. and Meth. A **317**, 254 (1992).

[Kas89] Kasagi, J., Hama, H., Yoshida, K., Sakurai, M., Ishii, K., in Proceedings of the Fifth Conference on Clustering Aspects in Nuclear and Subnuclear Systems, Kyoto, 1989, J. Phys. Soc. Japan **58**, 620 (1989).

[Kra79] Krappe, H.J., Nix, J.R., Sierk, A.J., Phys. Rev. C **20**, 992 (1979).

[Kra88] Krane, K.S., Introductory Nuclear Physics, John Wiley & Sons, New York (1988).

[Kra92] Kratz, J.V., Gober, M.K., Zimmermann, H.P., Schädel, M., Brüchle, W., Schimpf, E., Gregorich, K.E., Türler, A., Hannink, N.J., Czerwinski, K.R., Kadkhodayan, B., Lee, D.M., Nurmia, M.J., Hoffman, D.C., Gäggeler, H., Jost, D., Kovacs, J., Scherer, U.W., Weber, A., Phys. Rev. C **45**, 1064 (1992).

[Lal96] Lalazissis, G.A., Sharma, M.M., Ring, P., Gambhir, Y.K., Nucl. Phys. A **608**, 202 (1996).

[Lan96] Lane, M.R., Gregorich, K.E., Lee, D.M., Mohar, M.F., Hsu, M., Kacher, C.D., Kadkhodayan, B., Neu, M.P., Stoyer, N.J., Sylwester, E.R., Yang, J.C., Hoffman, D.C., Phys. Rev. C **53**, 2893 (1996).

[Lan98] Lane, M.R., Gregorich, K.E., Lee, D.M., Wierczinski, B., McGrath, C.A., Hendricks, M.B., Shaughnessy, D.A., Strellis, D.A., Sylwester, E.R., Wilk, P.A., Hoffman, D.C., Phys. Rev. C **58**, 3413 (1998).

[Laz77] Lazarev, Yu.A., Atomic Energy Rev. **15**, 1, 75 (1977).

[Laz89] Lazarev, Yu.A., Lobanov, Yu.V., Sagaidak, R.N., Utyonkov, V.K., Hussonnois, M., Kharitonov, Yu.P., Shirokovsky, I.V., Tretyakova, S.P., Oganessian, Yu.Ts., Physica Scripta **39**, 422 (1989)

[Laz94] Lazarev, Yu.A., Lobanov, Yu.V., Oganessian, Yu.Ts., Utyonkov, V.K., Abdullin, F.Sh., Buklanov, G.V., Gikal, B.N., Iliev, S., Mezentsev, A.N., Polyakov, A.N., Sedykh, I.M., Shirokovsky, I.V., Subbotin, V.G., Sukhov, A.M., Tsyganov, Yu.S., Zhuchko, V.E., Lougheed, R.W., Moody, K.J., Wild, J.F., Hulet, E.K., McQuaid, J.H., Phys. Rev. Lett. **73**, 624 (1994).

[Laz95] Lazarev, Yu.A., Lobanov, Yu.V., Oganessian, Yu.Ts., Tsyganov, Yu.S., Utyonkov, V.K., Abdullin, F.Sh., Iliev, S., Polyakov, A.N., Rigol, J., Shirokovsky, I.V., Subbotin, V.G., Sukhov, A.M., Buklanov, G.V., Gikal, B.N., Kutner, V.B., Mezentsev, A.N., Sedykh, I.M., Vakatov, D.V., Lougheed, R.W., Wild, J.F., Moody, K.J., Hulet, E.K., JINR Report E7-95-100, March, 1995.

[Laz95b] Lazarev, Yu.A., Shirokovsky, I.V., Utyonkov, V.K., Tretyakova, S.P., Kutner, V.B., Nucl. Phys. A **588**, 501 (1995).

[Laz96] Lazarev, Yu.A., Lobanov, Yu.V., Oganessian, Yu.Ts., Utyonkov, V.K., Abdullin, F.Sh., Polyakov, A.N., Rigol, J., Shirokovsky, I.V., Tsyganov, Yu.S., Iliev, S., Subbotin, V.G., Sukhov, A.M., Buklanov, G.V., Gikal, B.N., Kutner, V.B., Mezentsev, A.N., Subotic, K., Wild, J.F., Lougheed, R.W., Moody, K.J., Phys. Rev.C **54**, 620 (1996).

[Lee83] Lee, D.M., Moody, K.J., Nurmia, M.J., Seaborg, G.T., von Gunten, H.R., Hoffman, D.C., Phys. Rev. C **27**, 2656 (1983).

[Ler87] Leres, R.G., Lawrence Berkeley Laboratory Report LBL-24808 (1987).

[Liu91] Liu, S.-S. and Zhang, F., Science in China **34**, 9, 1120 (1991).

[Lou87] Lougheed, R.W., Moody, K.J., Dougan, R.J., Wild, J.F., Hulet, E.K., Dupzyk, R.J., Henderson, C.M., Gannett, C.M., Henderson, R.A., Hoffman, D.C., Lee, D.M., Summerer, K., Hahn, R.L, Nuclear Chemistry Division FY87 Annual Report, UCAR 10062/87, Lawrence Livermore National Laboratory, 4-2 (1987).

[Lou89] Lougheed, R.W., Hulet, E.K., Wild, J.F., Moody, K.J., Dougan, R.J., Gannett, C.M., Henderson, R.A., Hoffman, D.C., Lee, D.M., in Proceedings of the Conference on 50 Years with Nuclear Fission, National Institute of Standards and Technology, Gaithersburg, 1989 (American Chemical Society, LaGrange Park, 1989), Vol. II, p. 694.

[Lou92] Lougheed, R.W., Hulet, E.K., Wild, J.F., Dougan, R.J., Dupzyk, R.J., Henderson, C.M., Moody, K.J., Glaser, R.E., Hahn, R.L., Sümmerer, K., Bethune, G.R., Report UCRL-JC-109951 (1992).

[Lou94] Lougheed, R.W., Moody, K.J., Wild, J.F., Hulet, E.K., McQuaid, J.H., Lazarev, Yu.A., Lobanov, Yu.V., Oganessian, Yu.Ts., Utyonkov, V.K., Abdullin, F.Sh., Buklanov, G.V., Gikal, B.N., Iliev, S., Mezentsev, A.N., Polyakov, A.N., Sedykh, I.M., Shirokovsky, I.V., Subbotin, V.G., Sukhov, A.M., Tsyganov, Yu.S., Zhuchko, V.E., Proc. Conf. Actinides-93, Santa Fe, NM; J. Alloys Comp. **213/214**, 61 (1994).

[Luk91] Luke, S.J., Gossett, C.A., Vandenbosch, R., Phys. Rev. C **44**, 1548 (1991).

[McM40] McMillan, E.M., and Abelson, P.A., Phys. Rev. **57**, 1185 (1940).

[Mei39] Meitner, L. and Frisch, O.R., Nature **143**, 239 (1939).

[Möl87] Möller, P., Nix, J.R., Swiatecki, W.J., Nucl. Phys. A **469**, 1 (1987).

[Möl94] Möller, P. and Nix, J.R., J. Phys. G: Nucl. Part. Phys. **20**, 1681 (1994).

[Moo83] Moody, K.J., Ph.D. Thesis, University of California, Berkeley (1983).

[Moo92] Moody, K.J., Lougheed, R.W., Wild, J. F., Dougan, R.J., Hulet, E.K., Hoff, R.W., Henderson, C.M., and Dupzyk, R.J., Report UCRL-JC-103830 (1992).

[Moo93] Moody, K.J., Lougheed, R.W., Wild, J.F., Dougan, R.J., Hulet, E.K., Hoff, R.W., Henderson, C.M., Dupzyk, R.J., Hahn, R.L., Summerer, K., O'Kelley, G.D., Bethune, G.R., Nucl. Phys. A **563**, 21 (1993).

[Mül75] Müllen, G. and Aumann, D.C., Nucl. Instr. Meth. **128**, 425 (1975).

[Mün85] Münzenberg, G., Hofmann, S., Folger, H., Heβberger, F.P., Keller, J., Poppensieker, K., Quint, B., Reisdorf, W., Schmidt, K.-H., Schött, H.J., Armbruster, P., Leino, M.E., Hingmann, R., Z. Phys. A **322**, 227 (1985).

[Mün88] Münzenberg, G., Hofmann, S., Hessberger, F.P., Folger, H., Ninov, V., Poppensieker, K., Quint, A. B., Reisdorf, W., Schött, H.-J., Sümmerer, K., Armbruster, P., Leino, M.E., Ackermann, D., Gollerthan, U., Hanelt, E., Morawek, W., Fujita, Y., Schwab, T., Türler, A., Z. Phys. A **330**, 435 (1988).

[Mün89] Münzenberg, G., Armbruster, P., Hofmann, S., Hessberger, F.P., Folger, H., Keller, J.G., Ninov, V., Poppensieker, K., Quint, A.B., Reisdorf, W., Schmidt, K.-H., Schneider, J.R. H., Schött, H.-J., Sümmerer, K., Zychor, I., Leino, M.E., Ackermann, D., Gollerthan, U., Hanelt, E., Morawek, W., Vermeulen, D., Fujita, Y., Schwab, T., Z. Phys. A **333**, 163 (1989).

[Nil69] Nilsson, S.G., et al., Nucl. Phys. A **131**, 1 (1969).

[Nin97] Ninov, V., Abbott, S.A., Gregorich, K.E., McGrath, C.A., LBNL Annual Report LBNL-43071 (1997).

[Nod34] Noddack, I., Angew. Chem. **47**, 653 (1934).

[Oga74] Oganessian, Yu.Ts., Tret'yakov, Yu.P., Il'inov, A.S., Demin, A.G., Pleve, A.A., Tret'yakova, S.P., Plotko, V.M., Ivanov, M.P., Danilov, N.A., Korotkin, Yu.S., Flerov, G.N., JETP Lett. **20**, 265 (1974).

[Oga83] Oganessian, Yu.Ts., *in Proc. Int. School-Seminar on Heavy Ion Physics, Alushta, USSR, 1983*, D7-83-644, Dubna, 55 (1983).

[Ort71] Orth, C.J., Nucl. Sci. and Eng. **43**, 54 (1971).

[Pat89] Patyk, Z., Sobiczewski, A., Armbruster, P., Schmidt, K.-H., Nucl. Phys. A **491**, 267 (1989).

[Pat91] Patyk, Z. and Sobiczewski, A., Nucl. Phys. A **533**, 132 (1991).

[Pat91b] Patyk, Z. and Sobiczewski, A., Phys. Lett. B **256**, 307 (1991).

[Per37] Perrier, C. and Segrè, E., J. Chem. Phys. **5**, 715 (1937); **7**, 155 (1939).

[Per96] Pershina, V., Chem. Rev. **96**, 1977 (1996).

[Pet40] Petrzhak, K.A. and Flerov, G.N., C.R. Acad. Sci. U.S.S.R. **28**, 500 (1940).

[Ple73] Pleasonton, F., Ferguson, R.L., Plasil, F., Bemis, C.E. Jr., Phys. Rev. C **8**, 1018 (1973).

[Poe95] Poenaru, D.N. and Plonski, I.H., Nuclear Decay Modes, Inst. of Phys. Publ., Bristol, England, ed. D.N. Poenaru (1995).

[Pok90] Pokotilovskii, Yŭ.N., Sov. J. Nucl. Phys. **52**, 599 (1990).

[Pyk88] Pykkö, P., Chem. Rev. **88**, 563 (1988).

[Ran76] Randrup, J., Larsson, S.E., Möller, P., et al., Phys. Rev. C **13**, 229 (1976).

[Ray78] Rayleigh, J.W., Proc. London Math. Soc. X, 4 (1878).

[Rut11] Rutherford, E., Phil. Mag. **21**, 669 (1911).

[Sch65] Schmitt, H. W., Kiker. W. E., and Williams, C. W., Phys. Rev., **137**, B837 (1965).

[Sch66] Schmitt, H.W., Neiler, J.H., Walter, F.J., Phys. Rev. **141**, 1146 (1966).

[Sch89] Schädel, M., Brüchle, W., Jäger, E., Schimpf, E., Kratz, J.V., Scherer, U.W., Zimmermann, H.P., Radiochim. Acta **48**, 171 (1989).

[Sch92] Schillebeeckx, P., Wagemans, C., Deruytter, A.J., Barthelemy, R., Nucl. Phys. A **545**, 623 (1992).

[Sea90] Seaborg, G.T. and Loveland, W.D., The Elements Beyond Uranium, John Wiley & Sons, Inc., New York (1990).

[See88] Seeliger, D., Marten, H., Neubert, W., Richter, D., Sov. J. Nucl. Phys. **47**, 403 (1988).

[Smo95] Smolanczuk, R., and Sobiczewski, A., Proc. XV Nucl. Phys. Conf.: Low Energy Nuclear Dynamics, St. Petersburg (Russia) 1995, eds. Yu. Ts. Oganessian, W. von Oertzen, R. Kalpakchieva (World Scientific, Singapore 1995) p. 313.

[Smo95b] Smolanczuk, R., Skalski, J., Sobiczewski, A., Phys. Rev. C **52**, 1871 (1995).

[Smo96] Smolanczuk, R., Skalski, J., Sobiczewski, A., in Proc. Intl. Workshop XXIV on Gross Properties of Nuclei and Nuclear excitations "Extremes of Nuclear Structure", Hirschegg (Austria), eds. H. Feldmeier, J. Knoll, W. Nörenberg (GSI, Darmstadt) p. 35 (1996).

[Smo97] Smolanczuk, R., Phys. Rev. C **56**, 812 (1997).

[Sob66] Sobiczewski, A., Gareev, F.A., Kalinkin, B.N., Phys. Lett. **22**, 500 (1966).

[Sob87] Sobiczewski, A., Patyk, Z., Cwiok, S., Phys. Lett. B **186**, 6 (1987).

[Sob94] Sobiczewski, A., J. Alloys Comp. **213/214**, 38 (1994).

[Sob94b] Sobiczewski, A., Phys. Part. Nucl. **25**, 119 (1994).

[Sob97] Sobiczewski, A., "Predicted Properties of Transactinide Nuclei", *Robert A. Welch Foundation 41st Conference on Chemical Research: The Transactinide Elements*, Houston, October 27-28, 1997.

[Sok89] Sokol', E.A., Zeinalov, Sh.S., Ter-Akopian, At. Energy **67**, 5, 357 (1989).

[Som85] Somerville, L.P., Nurmia, M.J., Nitschke, J.M., Ghiorso, A., Hulet, E.K., Lougheed, R.W., Phys. Rev. C **31**, 1801 (1985).

[Spe82] Spencer, R.R., Gwin, R., Ingle, R., Nucl. Sci. Eng. **80**, 603 (1982).

[Str67] Strutinsky, V., Nucl. Phys. A **95**, 420 (1967).

[Ter59] Terrell, J., Phys. Rev. **113**, 527 (1959).

[Ter81] Ter-Akopian, G.M., Popeko, A.G., Sokol, E.A., Chelnokov, L.P., Smirnov, V.I., Gorshkov, V.A., Nucl. Instr. and Methods **190**, 119 (1981).

[Ter87] Ter-Akop'yan, G.M., Buklanov, G.V., Zeinalov, Sh.S., et al., *Int. Workshop on the Physics of Heavy Ions,* Dubna, JINR Report No. D7-87-68, 212 (1987).

[Tul90] Tuli, J.K., Kinsey, R.R., Martin, M.J., Nucl. Data Sheets **59**, 618 (1990).

[Tul95] Tuli, J.K., "Table of Nuclides", in Handbook of Nuclear Properties (Oxford University Press, 1995), D. N. Poenaru and W. Greiner, Eds. (1995).

[Tür88] Türler, A., Gäggeler, H.W., Jost, D.T., Armbruster, P., Brüchle, W., Folger, H., Hessberger, F.P., Hofmann, S., Münzenberg, G., Ninov, V., Schädel. M., Sümmerer, K., Kratz, J.V., and Scherer, U., Z. Phys. A **331**, 363 (1988).

[Tür98] Türler, A., Dressler, R., Eichler, B., Gäggeler, H.W., Jost, D.T., Schädel, M., Brüchle, W., Gregorich, K.E., Trautmann, N., Taut, S., Phys. Rev. C **57**, 1648 (1998).

[Tür98b] Türler, A., Buklanov, G.V., Eichler, B., Gäggeler, H.W., Grantz, M., Hübener, S., Jost, D.T., Lebedev, V.Ya., Piguet, D., Timokhin, S.N., Yakushev, A.B., Zvara, I., A., J. Alloys Comp. **271-273**, 287 (1998).

[Uni74] Unik, J.P., Gindler, J.E., Glendenin, L.E., Flynn, K.F., Gorski, A., Sjoblom, R.K., in Proc. Third Internatl. IAEA Symp. On Phys. and Chem. Fission, Rochester, New York, 1973, **II**, 19 (IAEA, Vienna 1974).

[Van73] Vandenbosch, R. and Huizenga, J.R., Nuclear Fission, Academic Press, Inc., New York (1973).

[van94] van Aarle, J., Westmeier, W., Esterlund, R.A., Patzelt, P., Nucl. Phys. A **578**, 77 (1994).

[Var91] Varma, R., Mehta, G.K., Choudhury, R.K., Kapoor, S.S., Nayak, B.K., Ramamurthy, V.S., Phys. Rev. C **43**, 1850 (1991).

BIBLIOGRAPHY

[Vio66] Viola, Jr., V.E. and Seaborg, G.T., J. Inorg. Nucl. Chem. **28**, 741 (1966).

[Vio66b] Viola, V.E., Nucl. Data A **1**, 391 (1966).

[Vio85] Viola, V.E., Kwiatowski, K., Walker, M., Phys. Rev. C 31, 1550 (1985).

[von69] von Gunten, H.R., Actinides Rev., **1**, 275 (1969).

[Wag89] Wagemans, C., Schillebeeckx, P., Deruytter, A., Nucl. Phys. A **502**, 287c (1989).

[Wag91] Wagemans, C., The Nuclear Fission Process, CRC Press, Inc., Boca Raton, Florida, p. 35 (1991).

[Wah88] Wahl, A.C., At. Data and Nucl. Data Tables **39**, 1 (1988).

[Wal87] Walsh, R.L., Nucl. Phys. A **469**, 333 (1987).

[Wei86] Weissenberger, E., Geltenbort, P., Oed, A., Gonnenwein, F., Radiat. Eff. **96**, 47 (1986).

[Wie95] Wierczinski, B. and Hoffman, D.C., "Instrumentation for Atom-at-a-Time Chemistry of the Heavy Elements", pp. 171-191, Frontiers in Nuclear Chemistry, Sood, Reddy, Pujari, Eds., Perfect Prints, Thane, India, 1996; LBL-37463 preprint (June 1995).

[Wil76] Wilkins, B.D., Steinberg, E.P., Chasman, R.R., Phys. Rev. C **14**, 1832 (1976).

[Wil90] Wild, J.F., van Aarle, J., Westmeier, W., Lougheed, R.W., Hulet, E.K., Moody, K.J., Dougan, R.J., Koop, E.A., Glaser, R.E., Brandt, R., Patzelt, P., Phys. Rev. C **41**, 640 (1990).

[Wil94] Wild, J.F., Hulet, E.K., Lougheed, R.W., Moody, K.J., Bandong, B.B., Dougan, R.J., Veeck, A.C., J. Alloys Comp. **213/214**, 86 (1994).

[Wu96] Wu, C.-L., Guidry, M., Feng, D.H., Phys. Lett. B **387**, 449 (1996).

[Zum84] Zumbro, J.D., Shera, E.B., Tanaka, Y., Bemis, Jr., C.E., Naumann, R.A., Holhn, M.V., Reuter, W., Steffen, R.M., Phys. Rev. Lett. **53**, 1888 (1984).

[Zva66] Zvara, I., Chuburkov, Y.T., Tsaletka, R., Zvarova, T.S., Shalaevskii, M.R., Shilov, B.V., Sov. At. Energy **21**, 709 (1966).

ERNEST ORLANDO LAWRENCE BERKELEY NATIONAL LABORATORY
ONE CYCLOTRON ROAD | BERKELEY, CALIFORNIA 94720

Prepared for the U.S. Department of Energy under Contract No. DE-AC03-76SF00098